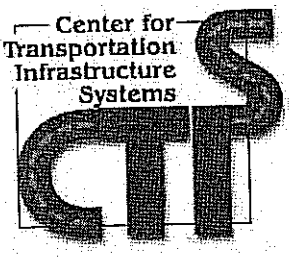

Feasibility of Quantifying the Role of Coarse Aggregate Strength on Resistance to Load in HMA

Research Report 0-5268-1

TxDOT Project Number 0-5268

Conducted for:

Texas Department of Transportation &

Federal Highway Administration

April 2007

Center for Transportation Infrastructure Systems
The University of Texas at El Paso
El Paso, TX 79968
(915) 747-6925

TECHNICAL REPORT STANDARD TITLE PAGE

1. Report No. TX FHWA/TX 06/0-5268-1	**2. Government Accession No.**	**3. Recipient's Catalog No.**
4. Title and Subtitle Feasibility of Quantifying the Role of Coarse Aggregate Strength on Resistance to Load in HMA		**5. Report Date** April 2007 **6. Performing Organization Code**
7. Authors C. Alvarado, E. Mahmoud, I. Abdallah, E. Masad, S. Nazarian, Richard Langford, V. Tandon and J. Button		**8. Performing Organization Report No.** Research Report 0-5268-1
9. Performing Organization Name and Address Center for Transportation Infrastructure Systems The University of Texas at El Paso, El Paso, Texas 79968-0516		**10. Work Unit No.** **11. Contract or Grant No.** Project No. 0-5268
12. Sponsoring Agency Name and Address Texas Department of Transportation Research and Technology Implementation Office P.O. Box 5080, Austin, Texas 78763-5080		**13. Type of Report and Period Covered** Technical Report Sept. 1, 2005 –October, 2006 **14. Sponsoring Agency Code**

15. Supplementary Notes
Research Performed in Cooperation with TxDOT and the Federal Highway Administration
Research Study Title: The Role of Coarse Aggregate Point and Mass on Resistance to Load in HMA.

16. Abstract

The ever-increasing traffic volumes, including increased truck traffic and higher tire pressures, are putting greater stresses on the bituminous pavements which manifest in the form of pavement distresses such as rutting and fatigue cracking. To address these issues, improvements in the hot mix bituminous (HMA) blends are being implemented. The new generation of bituminous pavements such as coarse-graded Superpave mixtures, Stone Matrix Bituminous (SMA) and Porous Friction Course (PFC) rely more on stone-on-stone contact for a stronger coarse aggregate skeleton.

The performance of HMA mixtures is greatly influenced by the properties of the aggregate blends such as gradation and strength; therefore they have a significant and direct effect on the performance of bituminous pavements. It is important to maximize the quality of aggregates to ensure a proper performance of roadways.

Several methods are available to determine aggregate characteristics, but their relationship to field performance, aggregate structure in HMA, and traffic loading needs to be further investigated and defined. Current laboratory protocols do not correlate well with aggregate abrasion, toughness, and strength requirements during handling, construction, and service. Specifications should ensure that aggregate particles possess the necessary strengths to avoid degradation during handling, construction, and trafficing.

In this report, the feasibility of determining the characteristics of the aggregates in multifaceted ways, considering the geological, geotechnical and mix design, is reported. The use of these parameters in a micro-mechanical model to predict the performance is also discussed.

17. Key Words Aggregate Interaction, Aggregate Gradation, new-generation HMA, micromechanical models	**18. Distribution Statement** No restrictions. This document is available to the public through the National Technical Information Service, 5285 Port Royal Road, Springfield, Virginia 22161, www.ntis.gov		
19. Security Classified (of this report) Unclassified	**20. Security Classified (of this page)** Unclassified	**21. No. of Pages** 150	**22. Price**

Form DOT F 1700.7 (8-69)

Feasibility of Quantifying the Role of Coarse Aggregate Strength on Resistance to Load in HMA

By

Cesar Alvarado, MSCE
Enad Mahmoud, MSCE
Imad Abdallah, MSCE, EIT
Eyad Masad, Ph.D., PE
Soheil Nazarian, Ph.D., PE
Richard Langford, Ph.D.
Vivek Tandon, Ph.D., PE
Joe Button, MSCE, PE

Research Project 0-5268

The Role of Coarse Aggregate Point and Mass Strength on Resistance to Load in HMA

Conducted for
Texas Department of Transportation

Research Report TX 0-5268-1

April 2007

Center for Transportation Infrastructure Systems
The University of Texas at El Paso
El Paso, TX 79968-0516

DISCLAIMERS

The contents of this report reflect the view of the authors who are responsible for the facts and the accuracy of the data presented herein. The contents do not necessarily reflect the official views or policies of the Texas Department of Transportation or the Federal Highway Administration. This report does not constitute a standard, a specification or a regulation.

The material contained in this report is experimental in nature and is published for informational purposes only. Any discrepancies with official views or policies of the Texas Department of Transportation or the Federal Highway Administration should be discussed with the appropriate Austin Division prior to implementation of the procedures or results.

NOT INTENDED FOR CONSTRUCTION, BIDDING, OR PERMIT PURPOSES

Cesar Alvarado, MSCE
Enad Mahmoud, MSCE
Imad Abdallah, MSCE
Eyad Masad, Ph.D., PE (96368)
Soheil Nazarian, Ph.D., PE (69263)
Richard Langford, Ph.D.
Vivek Tandon, Ph.D., PE (88219)
Joe Button, MSCE, PE (40874)

ACKNOWLEDGEMENTS

The successful progress of this project could not have happened without the help and input of many personnel of TxDOT. The authors acknowledge Mr. Richard Williammee, P.E., the project PD and Mr. Elias Rmeili, P.E., the project PC for facilitating the collaboration and with TxDOT Districts. They have also provided valuable guidance and input.

Special thanks to the PAs, Dr. K.C. Evans, P.G., Dr. Zhiming Si, P.E., Mr. Jim Black, Mr. Joel Carrizales, and Mr. Josiah Yuen whom have been very supportive on this project and were helpful in finalizing the literature review portion of this report.

ABSTRACT

The ever-increasing traffic volumes, including increased truck traffic and higher tire pressures, are putting greater stresses on the bituminous pavements which manifest in the form of pavement distresses such as rutting and fatigue cracking. To address these issues, improvements in the hot mix bituminous (HMA) blends are being implemented. The new generation of bituminous pavements such as coarse-graded Superpave mixtures, Stone Matrix Bituminous (SMA) and Porous Friction Course (PFC) rely more on stone-on-stone contact for a stronger coarse aggregate skeleton.

The performance of HMA mixtures is greatly influenced by the properties of the aggregate blends such as gradation and strength; therefore they have a significant and direct effect on the performance of bituminous pavements. It is important to maximize the quality of aggregates to ensure a proper performance of roadways.

Several methods are available to determine aggregate characteristics, but their relationship to field performance, aggregate structure in HMA, and traffic loading needs to be further investigated and defined. Current laboratory protocols do not correlate well with aggregate abrasion, toughness, and strength requirements during handling, construction, and service. Specifications should ensure that aggregate particles possess the necessary strengths to avoid degradation during handling, construction, and trafficing.

In this report, the feasibility of determining the characteristics of the aggregates in a multifaceted way, considering the geological, geotechnical and mix design, is reported. The use of these parameters in a micro-mechanical model to predict the performance is also discussed.

TABLE OF CONTENTS

LIST OF FIGURES

LIST OF TABLES

CHAPTER ONE - INTRODUCTION

INTRODUCTION

The ever-increasing traffic volumes, including increased truck traffic and higher tire pressures, are putting greater stresses on the bituminous pavements which manifest in the form of pavement distresses such as rutting and fatigue cracking. To address these issues, improvements in the hot mix bituminous (HMA) blends are being implemented. The new generation of bituminous pavements such as coarse-graded Superpave mixtures, Stone Matrix Bituminous (SMA) and Porous Friction Course (PFC) rely more on stone-on-stone contact for a stronger coarse aggregate skeleton.

The performance of HMA mixtures is greatly influenced by the properties of the aggregate blends such as gradation and strength; therefore they have a significant and direct effect on the performance of bituminous pavements. It is important to maximize the quality of aggregates to ensure a proper performance of roadways.

Several methods are available to determine aggregate characteristics, but their relationship to field performance, aggregate structure in HMA, and traffic loading needs to be further investigated and defined. Current laboratory protocols do not correlate well with aggregate abrasion, toughness, and strength requirements during handling, construction, and service. Specifications should ensure that aggregate particles possess the necessary strengths to avoid degradation during handling, construction, and trafficing.

To address these questions, the characteristics of the aggregates have to be considered in a multifaceted way, considering the geological, geotechnical, mix design and construction. These parameters can be input in a micro-mechanical model to predict the performance. The effects of stress concentration at contact points on coarse aggregates and means of reducing them are also of interest. The geological aspects consist of characterizing the hardness and nature of rock mass. The geotechnical aspects are necessary to optimize the gradation, to consider the shape and size of the aggregates in the mix and to assess the strength of the aggregate mass as whole. A proper HMA mix is needed to ensure the adequate durability, structural capacity and performance after the gradation is optimized.

ORGANIZATION

The work presented within this report represents an analytical and experimental investigation to evaluate the effect of stress concentration at contact points on coarse aggregates that could cause aggregate fracture. Chapter two gives an overview of current and new methods used for measuring the strength, shape and hardness of individual aggregates, and the bulk strength and deformation characteristics of the aggregate skeleton. The focus of Chapter 3 is on the description of the aggregates and mix selection, whereas Chapter 4 describes the geological aspects of the aggregates.

The next five chapters further develop some of the methods discussed in Chapter 2. Chapter 5 describes the tests used to identify and evaluate the toughness and abrasion resistance in aggregates, those to evaluate the aggregate shape characteristics, and those used to evaluate aggregate breakdown. Chapter 6 presents a series of strength and stiffness tests to characterize the aggregate quality which is needed for the micromechanics modeling. Chapter 7 explains a series of methods related to the evaluation of the effect of different aggregate particle characteristics on aggregate interaction and shear strength. Chapter 8 discusses the tests used in this research to characterize the HMA performance such as the Hamburg wheel test, indirect tensile test, dynamic modulus test, and flow test. Chapter 9 explains the micromechanical modeling to describe the behavior of materials considering their grain-to-grain interaction.

In Chapter 10, based on the information gathered in chapters 3 through 9, statistical and other analysis of results are presented. Finally, Chapter 11 discusses the conclusions and recommendations for future work.

CHAPTER TWO - BACKGROUND

An extensive literature review that documented aggregate properties that significantly impact HMA performance was detailed in Technical Memorandum 0-5268-1. Some of the conventional and recently developed aggregates tests as well as the significance of aggregate stone-on-stone interaction were also described in that technical memorandum. Excerpts from that document are included here.

AGGREGATE GRADATION

An aggregate's particle size distribution, or gradation, is one of its most influential characteristics. In HMA, gradation influences almost every important property including stiffness, stability, durability, permeability, workability, fatigue resistance, frictional resistance and resistance to moisture damage. Because of this, gradation is a primary concern in HMA mix design and thus most agencies specify allowable aggregate gradations. Inappropriate selections of aggregate gradation, aggregate properties, and binder grade, type and content are major contributors to rutting and cracking of HMA pavements. The effect of gradation on HMA performance has long been a controversial issue. Strong opinions exist among industry experts as to which gradation type, ranging from fine to coarse to open-graded or stone matrix bituminous gradations, will provide the best performance (Hand et al., 2002).

An aggregate is typically defined as a coarse aggregate if particles are retained on the No. 8 sieve (see Figure 2.1). The coarse aggregates comprise then the portion of the aggregates that has large particle sizes. An aggregate is defined as a fine aggregate if the material passes the No. 8 sieve (see Figure 2.2). That is, the aggregate particles that can fill the voids created by the coarse aggregates in the mixture (Prowell et al., 2005). When a mixture design is composed mainly from the selection of coarse or fine aggregates, the mixture will be defined as coarse- or fine-graded mixture, respectively.

The mixture resistance to permanent deformation is highly dependent on the aggregate structure. Several research studies have agreed that giving more importance to the aggregate gradation would be the solution for pavement rutting (Karakouzian, 1996). Aggregates are expected to provide a strong stone skeleton to resist repeated load applications. Shape, surface texture, angularity and gradation have a great influence on HMA performance. Today, aggregate gradations are commonly evaluated using a "0.45 Power Chart." Since single-sized particles do

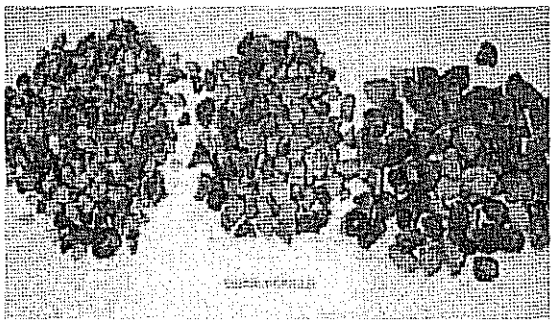

Figure 2.1 - Coarse Aggregate

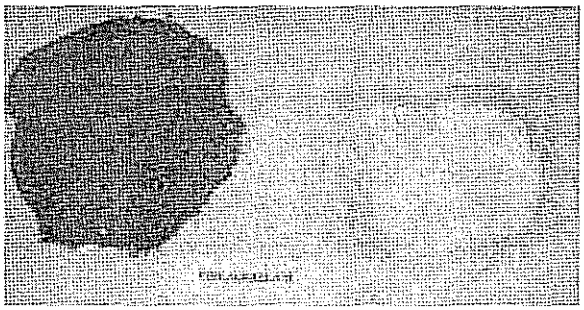

Figure 2.2 - Fine Aggregate

not pack as densely as a mixture of particle sizes, the blending of the aggregates provides a better interlock and good aggregate packing and therefore ensures a strong aggregate structure to be more resistance to pavement distress.

Aggregate gradations can also be described as dense-graded, gap-graded, uniformly-graded and open-graded. Dense-graded aggregates produce low air void content and maximum weight when compacted.

The gap-graded aggregates refer to the gradation that certain intermediate sizes are substantially absent. Stone Matrix Bituminous (SMA) is an example of this type of gradation. These mixtures are characterized by high bituminous contents and fiber additives. The gap-grading of the SMA aggregates results in a more open texture, creating stone-on-stone contact with a higher amount of voids in mineral aggregate (VMA) in the mixtures (Schmiedlin and Bischoff, 2002). Since the strength of SMA relies heavily on the stone-on-stone aggregate skeleton, it is imperative that the mixture be designed and placed with a strong coarse aggregate skeleton (Brown and Haddock, 1997).

Uniformly-graded aggregates refer to a gradation that contains most of the particles in a very narrow size range. In the open-graded mix, the voids are relatively large when the aggregate is compacted. The high air void content and the open structure of this mix promote the effective drainage of rain water, which also minimizes hydroplaning during wet weather. Other benefits of this type of gradation are lower pavement noise and reduced roadway glare during wet weather, which improves the night visibility of pavement markings. Open-Graded Friction Course (OGFC) mix designs are composed of this type of gradation.

Superior Performing Bituminous Pavement (Superpave) is a complete mixture design and analysis system (Chowdhury et al., 2001). In the Superpave gradation, recommendations have been made that encourage the use of coarse-graded mixtures (mixture gradations plotting below the reference zone, a.k.a. restricted zone [BRZ]) rather than fined-graded (above the reference zone [ARZ]) mixtures. The reference zone is an area surrounding the maximum density line adopted to reduce premature rutting. The purposes of the reference zone are to limit the inclusion of large amounts of natural sand that may cause "humps" in the gradation curve and to discourage gradations that lack adequate VMA.

Kandhal and Cooley (2001) determined that the reference zone was an unnecessary requirement when used in conjunction with the other aggregate and volumetric properties specified. Hand et al. (2002) suggested that above the reference zone (ARZ) and through the reference zone (TRZ) mixtures provide slightly better permanent deformation resistance than below the reference zone (BRZ) gradations, contrary to the Superpave specifications.

AGGREGATE SHAPE, ANGULARITY, AND TEXTURE

Masad et al. (2003) indicate that the particle geometry of an aggregate can be fully expressed in terms of three independent properties which influence the rutting potential of HMA: shape (or form), angularity (roundness), and surface texture (see Figure 2.3).

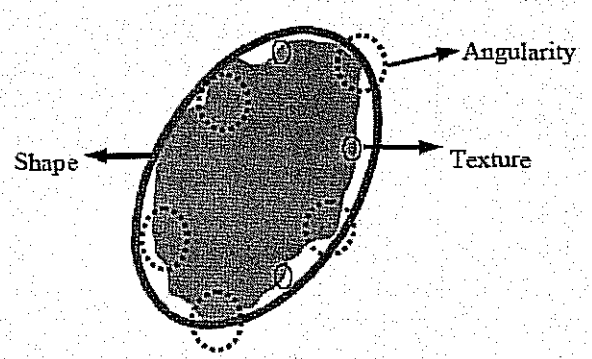

Figure 2.3 - Components of an Aggregate Shape: Shape, Angularity, and Texture (Masad et al., 2003)

Shape or form reflects variations in the proportions of a particle. Angularity reflects variations at the corners, that is, variations applied on the shape. Surface texture is used to describe the surface irregularity. Particle texture plays a major role in influencing the adhesive bond between the aggregate and the binder, while aggregate form influences the anisotropic response of bituminous mixtures. Angular, rough-textured aggregates provide more shear strength and produce higher-quality HMA pavements than rounded, smooth-textured aggregates which tend to produce rut-susceptible HMA mixtures (Masad et al., 2003). When load is applied to the aggregate in a bituminous mixture, the angular, rough-textured aggregates lock tightly together and function as a large, single elastic mass, thus increasing the shear strength of the bituminous mixture. On the other hand, smooth, rounded aggregates tend to slide past each other instead of locking together, and can break under compaction and change aggregate gradation. This change in gradation is detrimental to the performance of a HMA (Masad et al., 2003).

Aggregate shape, angularity, and texture are believed to be key factors affecting the strength of the aggregate structure. Particle shape and angularity have been identified as the second most important parameters after gradation for the performance of HMA (Aho et al., 2001). According to Cheung and Dawson (2002) "roundness and angularity are the major factors affecting ultimate shear strength and permanent deformation." Specifications for aggregate angularity are included in the Superpave mixture design system. Some of the criteria included are coarse aggregate angularity, fine aggregate angularity, and flat and elongated particles.

To evaluate coarse aggregate shape, angularity, and texture, alternative methods have been investigated that combine shape, angularity, and texture into one measure. For this purpose, different laboratory tests have been used including Tex-460-A (ASTM D5821) "Determining Crushed Face Particle Count," ASTM D3398 "Index of Aggregate Particle Shape and Texture," Tex-280-F (ASTM D4791) "Determination of Flat and Elongated Particles," Tex-405-A (AASHTO TP56) "Determining the Percent of Solids and Voids in Concrete Aggregate," and image analysis.

Test methods to describe aggregate angularity have been classified into two categories: direct and indirect (Kandhal et al., 1991). In indirect methods, particle shape and texture are determined based on measurements of bulk properties as in ASTM D3398 "Index of Aggregate Particle Shape and Texture," Tex-405-A "Determining the Percent of Solids and Voids in Concrete Aggregate," Particle Index, and Compacted Aggregate Resistance (CAR) test. Direct methods are defined as those in which particle shape, angularity or texture are measured and described through direct measurement of individual particles. Several new tests based on imaging techniques have been developed to directly measure aggregate size, shape, angularity, and texture. Measurements are made from digital images or laser scans in order to improve testing precision.

Because indirect tests can be time consuming and the results are influenced by the technician experience, direct tests such as the digital systems appear to be a lot more promising. Some of the advantages of digital image techniques include faster results, ability to test larger or smaller sample sizes, less unit testing cost, and minimal technician subjectivity. Several researchers have attempted to use image analysis to measure the Fine Aggregate Angularity (FAA). Masad et al. (2000) developed the automated image analysis to quantify FAA, while Wang and Mohammad (2003) conducted a study on quantification of morphology characteristics of aggregate profile images to evaluated particle size, shape, angularity, and texture. Wilson and Klotz (1996) developed a technique to measure the angularity of fine aggregates in which fine aggregates are spread on a glass plate while a high resolution video camera captures the image of each particle.

PROPERTIES OF AGGREGATES

Aggregates must be tough and abrasion resistant to resist crushing, degradation, and disintegration when stockpiled, placed with a paver, compacted with rollers, and subjected to traffic loadings (Wu et al., 1998). These properties are especially critical for open- or gap-graded bituminous mixtures where coarse particles are subjected to high contact stresses. Aggregate degradation or breakdown of aggregate may result in significant loss of pavement life.

Aggregates are usually manufactured products originating from a source rock which has been blasted, crushed, and divided to give a granular material with acceptable particle size distribution (Wylde, 1976). During production, construction, and during the service life of the road, the aggregates may be subjected to the effects of weather, climate, and a range of mechanical processes which together contribute to the deterioration in its physical condition. Therefore, when the construction of a road is necessary, it is important to obtain a material sufficiently

durable to last the design life of the road in order that its performance is not affected by deterioration or degradation of the material. The term "durable" may be used when describing a road aggregate showing adequate resistance to the particular service conditions. On the other hand, "degradation" refers to the breakdown of aggregate pieces into smaller particles through chemical or physical processes.

Toughness/Abrasion Resistance and Durability/Soundness of Aggregates

Aggregate toughness refers to the property of an aggregate to resist breakdown. Such breakdown can alter the HMA gradation, resulting in a mixture that does not meet the volumetric properties (Prowell et al., 2005). Abrasion refers to the weathering of the aggregates in the pavement structure. Therefore, abrasion resistance is the resistance of an aggregate to wearing. Aggregates lacking adequate toughness and abrasion resistance may cause construction and performance problems. In addition, aggregates must also be resistant to breakdown when subjected to wetting and drying or freezing and thawing. Moreover, water can penetrate the aggregate particles if some degradation of the bituminous mixture has occurred during construction since soft or weak particles that break down during compaction provide convenient access for water. Therefore, raveling, cracking, stripping and, in extreme cases, rutting of bituminous concrete pavement can result from the use of aggregates not resistant to weathering. Aggregate toughness and abrasion resistance are closely related to durability and soundness. Toughness-abrasion resistance is associated with mechanical degradation while durability-soundness is with degradation due to weathering (Wu et al., 1998). Aggregate durability generally composes two categories of tests: those tests that measure aggregate abrasion resistance and breakdown of particles (toughness-abrasion resistance tests) and tests that address aggregate weathering when exposed to freezing and thawing or wetting and drying (durability-soundness tests).

Numerous tests have been developed to identify and evaluate toughness and abrasion resistance in aggregates used in bituminous mixtures. Some of the most common test methods selected for determining such parameters include the Los Angeles (LA) abrasion (Tex-410-A), Micro-Deval abrasion (Tex-461-A), aggregate impact value (AIV) (BS 812-Part-112), and the aggregate crushing value (ACV) (BS 812-Part-110).

Aggregate tests related to durability-soundness have commonly been used to assess the degradation from freezing and thawing as well as from wetting and drying. Two methods for characterizing aggregate soundness and durability are the sodium and magnesium sulfate soundness (Tex-411-A or AASHTO T104) and freezing and thawing soundness (Tex-432-A or AASHTO T103). Since aggregates can deteriorate from wetting and drying or freezing and thawing cycles, the sulfate soundness test simulates the effects of the expansion of water in the aggregate pores during freezing (Prowell et al., 2005). Magnesium or sodium sulfates can be used in the sulfate soundness tests. The soundness test describes procedures to be followed in testing aggregates to determine their resistance to disintegration by freezing and thawing. It furnishes information helpful in judging the soundness of aggregates subjected to weathering.

Wu et al. (1998) concluded that the Micro-Deval tests provided the best correlations with field performance of bituminous mixtures, and recommended it for characterizing aggregate toughness/ abrasion resistance and durability/soundness. Rogers et al. (1991) recommended a number of modifications to the Micro-Deval test for testing fine aggregates in order to replace the sulfate soundness test. Some of the modifications included a smaller sample, smaller charge, less water, and shorter test time. According to Yiping et al. (1998), the Micro-Deval and magnesium sulfate soundness tests (Tex-411-A) provide the best correlation with performance of bituminous mixtures and recommended using them. Wu et al. (1998) suggested magnesium sulfate soundness test over sodium sulfate soundness test and the Micro-Deval test instead of the LA abrasion test. Testing by Senior and Rogers (1991) suggested that the freeze-thaw soundness test was to be preferred because it showed better discrimination than the sulfate test and was more precise.

Hardness of Aggregates

Another important aggregate property includes hardness. Hardness of a rock is the resistance that the surface of an aggregate offers to being broken or exposed to abrasion. In addition, hardness usually implies a resistance to deformation. Hardness is another major component in aggregates for a proper pavement performance. Three general types of hardness measurements are performed. These are scratch hardness, rebound or dynamic hardness, and indentation hardness. Some of the most common hardness tests are the Schmidt hammer test (Tex-446-A), indentation hardness test (ASTM D 785), and the shore hardness scleroscope test (ASTM E 448).

Holmgeirsdottir and Thomas (1998) presented a report about the use of the Shore hardness scleroscope for testing small rock volumes. They suggested that the Shore hardness (SH) might be used for the determinations of the unconfined compressive strengths when the value of SH is less than 60. In that study however, no comparison was done between the Shore scleroscope and any other hardness tests.

Strength of Aggregate

One of the major components in aggregate degradation is the breaking up of the aggregates. The permanence of aggregates depends on their ability to retain their shape after being subjected to mechanical loads and applied disruptive forces (Oztas et al., 1999). Oztas et al. (1999) stated "the stability and response of aggregates to stress depend on the relative importance of different bonding mechanisms. The more strongly the particles in an aggregate are held together, the greater the work that has to be done to break the bonds." The resistance of HMA to rutting is considered the combined resistance (shear strength) of the mineral aggregates and bituminous cement. Aggregates must provide support from traffic loads without deforming excessively (Cheung and Dawson, 2002).

The properties of aggregates can be divided into two groups: exterior and interior characteristics. Exterior features have already been discussed earlier in this chapter and are based on particle size, shape, and angularity. Interior features include density, hardness, durability, and strength.

The strength of an aggregate may be selected as a key factor in providing a qualitative evaluation of the interior quality of aggregates. Traditionally, the coarse aggregate strength is estimated indirectly by well known tests such as the Los Angeles abrasion test, the hardness and soundness tests, the aggregate crushing value test, etc. However, the direct measurement of the tensile and compressive strengths of aggregates is preferred. Numerous test methods related to the evaluation of the effect of different aggregate particle characteristics on the resistance to permanent deformation and shear strength are utilized. Some of these tests include the direct shear test, triaxial compression test, and indirect tensile test.

ASSESSING GRAIN TO GRAIN INTERACTION

If a reasonably well compacted material with good grain-to-grain contact is subjected to shearing, the aggregates have to then displace. Such a displacement results in an initial increase in the volume of a dense specimen. The amount of volume change to some extent is related to the hardness of the aggregates. For very hard aggregates, the aggregates have to roll on top of one another, whereas for the softer aggregates, the rolling can be accompanied by crushing of aggregates. Under normal triaxial tests or direct shear tests of dense specimens, this increase in volume is readily measured. However, to accentuate this behavior, the soil mechanics and particulate mechanics experts rely on high confining pressures for triaxial tests or large normal stresses for the direct shear tests. This dilative behavior of the material can be then used to relate it to the performance of the aggregates in terms of crushing or load resistance within the mix. Vallejo and Chik (2002) studied the evolution of crushing in granular materials and its effect on their mechanical properties. The crushing of a granular material under a combination of compression and shear loads was studied in the laboratory using a ring shear apparatus. The amount of crushing of the material was then evaluated using fractals. A fractal is a geometric pattern that is repeated at ever smaller scales to produce irregular shapes. Fractals are used especially in computer modeling of irregular patterns and structures in nature and in this study fractals were used to evaluate changes in the size distribution in a granular material subjected to varying crushing levels. The changes in the particles size distribution in the material had a large influence on the hydraulic conductivity and the shear strength (Vallejo and Chik, 2002). Oztas et al. (1999) studied the relative strength of individual soil aggregates of different sizes and shapes against crushing forces. The results of that study showed that the strength of the aggregates was directly related to aggregate size and shape. As the aggregate size increased, so did the applied stress required to crush the aggregate. Therefore, the applied mechanical stresses necessary to break up the aggregate depended on the mass, volume, diameter, and geometric mean diameter (Oztas et al., 1999).

The "Locking Point" Design

The Superpave gyratory compaction (SGC) procedure is one of the principal laboratory compaction equipment for bituminous mixture design. The SGC provides an adequate density in the compacted laboratory specimen that approximates the density of the bituminous mixture when subjected to traffic loads and climatic conditions (Brown and Buchanan, 2001). As part of the SGC protocol, a mix design compactive effort or design number of compaction revolutions,

N_{design} was developed to simulate the field density for a given mix achieved at the end of the pavement's life. However, some States have found that N_{design} with SGC for some materials may be excessive due to unnecessary aggregate crushing and problems meeting the optimum bituminous content of the mixes. There is a certain point at which the aggregate structure "locks up", meaning the mixture has been compacted to an optimum point. Beyond such point, the aggregate may degrade and the amount of space available for the binder in a mixture reduces.

A new mix design concept called "locking point" has been adopted by some States to increase the bituminous content in Superpave mixtures. Because there is a great degree of interlocking between the aggregates, it is important to identify the stage at which the mix exhibits such stone-on-stone interlocking during compaction. This point of interlocking, called the "Locking Point," was first defined by Vavrik and Carpenter (1998) for dense graded HMA. The locking point is defined as "the first three gyrations that are at the same height preceded by two gyrations at same height" (Vavrik and Carpenter, 1998). In other words, it is the point beyond which the resistance to compaction increases significantly.

Different specifications exist for the locking point design. The Alabama Department of Transportation defines the locking point as the point where two consecutive gyrations produce no change in the specimen height, whereas the Georgia DOT defines it as "the number of gyrations at which, in the first occurrence, the same height has been recorded for the third time." In other words, the first time the gyratory compactor displays a single height three times in a row, the locking point is the first gyration in which that height occurs. The State of Illinois utilizes the locking point concept and they refer to it as "the first of three consecutive gyrations producing the same specimen height" (Brown and Buchanan, 2001). The concept is used to prevent over-compaction of their design mixes by determining the locking of the mixture and stopping compaction at that level using the locking point as a modification of the N_{design}.

West and James (2005) stated "the rationale of limiting the gyrations to the point where the aggregate has locked together is to reduce the aggregate breakdown." The authors concluded that the locking point concept reduced the amount of compaction and resulted in higher binder contents for their bituminous mixtures.

DISCRETE ELEMENT METHOD

The discrete element method (DEM) is a finite difference scheme, used to study the interaction among assemblies of discrete particles. DEM was introduced by Cundall (1971) and later in 1979 this method was proposed by Cundall and Strack for the simulation of two-dimensional non-continuous materials. Since then, it has been applied to study different types of geotechnical problems such as: the deformation mechanisms in geo-materials, constitutive relations and flow of granular media, and many other problems.

Cundall and Hart (1992) summarized the advancements in discrete element codes. It was proposed that the name discrete element method (DEM) should only apply to codes that allow finite displacements and rotations of discrete objects, including full detachment, and recognize new contacts automatically as the calculation progresses.

The DEM has been mainly utilized as a research tool in many studies in the last few years. In this study a commercially available DEM code called *Particle Flow Code in 2-Dimensions* (PFC2D Version 3.1), developed by Itasca Consulting Group is used. This code includes a user-friendly graphical interface, linear and non-linear contact models, linear and curvilinear boundary conditions.

DEM Principles

The DEM concept is simple in principle; it is based on successively solving law of motion (Newton's second law) and the force-displacement law for each particle. Figure 2.4 represents this concept; an explicit time-stepping scheme is employed to integrate Newton's second law for each particle, given a set of contact forces acing on the particle, which results in the updated particles' positions and velocities. Based on the new positions, the relative displacements of each particle are calculated, and used to calculate the contact forces. The DEM is based upon the idea that the time step chosen is sufficiently small so that during a single time step, disturbances cannot propagate from any particle further than its immediate neighbors, so at all times the forces acting on any particle are determined exclusively by its interaction with particles that it is in contact with.

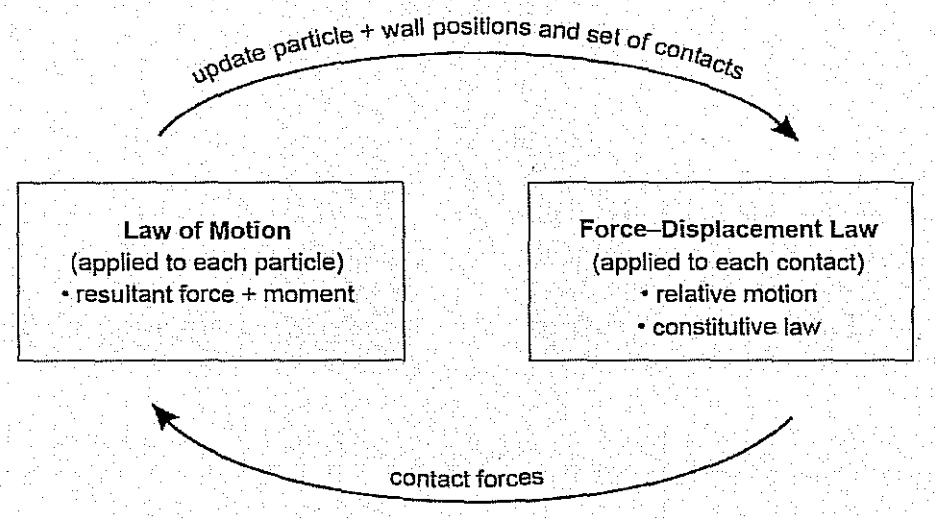

Figure 2.4 - Calculation Cycle in Discrete Element Method (after PFC2D Manual)

In PFC2D, particles are circular (balls). They are allowed to overlap at the contact points, which occur over a very small area (i.e., at a point). The amount of overlap is related to the contact force via the force-displacement law. All overlaps are assumed to be small in relation to particle sizes.

Bonds can be added to the contacts between the particles, to either increase the stiffness of the contact and/or to include a strength parameter above which the bond breaks; PFC2D allows different types of bonds to be assigned. In the absence of bonding, particles slide over each other once the shear force exceeds the friction.

Contact Behavior in PFC2D

The contact behavior in PFC2D is described using up to three models:

1. Contact Stiffness Models,
2. Slip Models, and
3. Bonding Models.

These models are activated for all contacts. A contact between two particles exist whenever the distance between the centers of two adjacent particles is equal to or less than the summation of their radii (i.e., the two particles are just touching or overlapping).

Contact Stiffness Models

The contact stiffnesses relate the contact forces and relative displacement in the normal and shear directions (normal and shear stiffness). The linear contact model is the simplest stiffness model (Figure 2.5). An effective normal and shear contact stiffness is calculated from the particles' stiffnesses assuming that they act in series,

$$K^n = \frac{k_n^{[A]} k_n^{[B]}}{k_n^{[A]} + k_n^{[B]}} \tag{2.1}$$

$$k^s = \frac{k_s^{[A]} k_s^{[B]}}{k_s^{[A]} + k_s^{[B]}} \tag{2.2}$$

where, k_s : shear stiffness, k_n : normal stiffness, k^n : effective normal stiffness, k^s : effective shear stiffness, and A & B: ball designation.

Another contact stiffness model supported by PFC2D is the Hertz-Mindlin Contact Model, but this model is not compatible with any type of bonding.

Slip Model:

This model is an essential property between two elements in contact. It provides no normal strength in tension and allows slipping to occur by limiting the shear force. It is defined by the friction coefficient at contact (dimensionless)

Bonding Models:

These models allow bonding between particles at contacts as summarized in Figure 2.6. The two basic models are contact-bond model, and parallel-bond model.

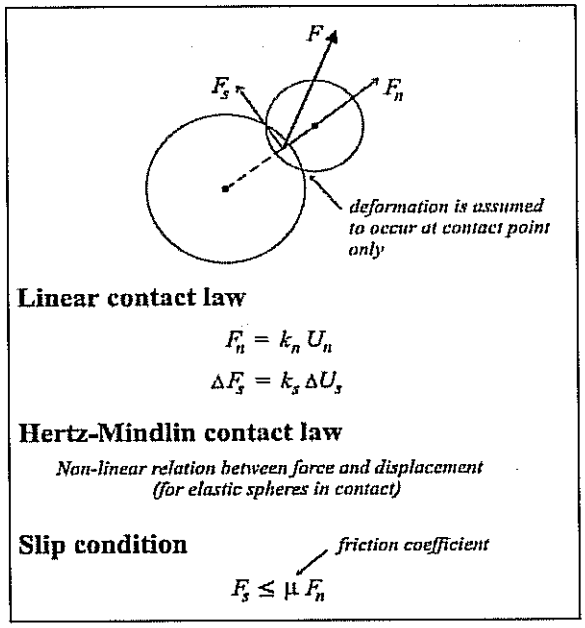

Figure 2.5 - Linear Contact Model in the Discrete Element Code PFC2D (after PFC2D Manual)

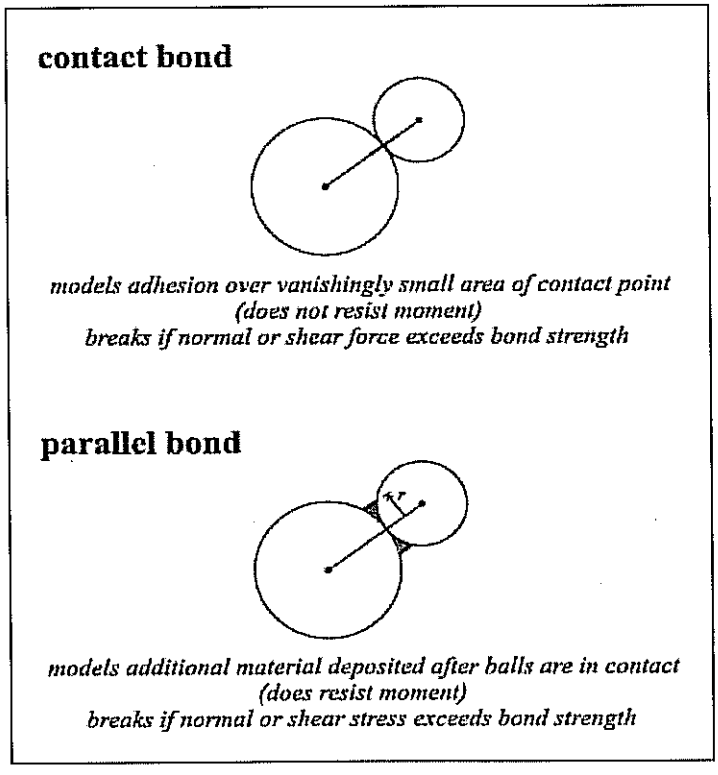

Figure 2.6 - Contact Bonds and Parallel Bonds in PFC2D (after PFC2D Manual)

A more detailed explanation of the parallel contact model can be seen in Figure 2.7. The contact bond acts as a point adhesion between the two particles. It does not resist any moment and will break if normal or shear force exceed the bond strength. The parallel bond between the particles is not at a point, but covers a defined area; this model resists moment, and will also break if normal or shear force exceeds the bond strength.

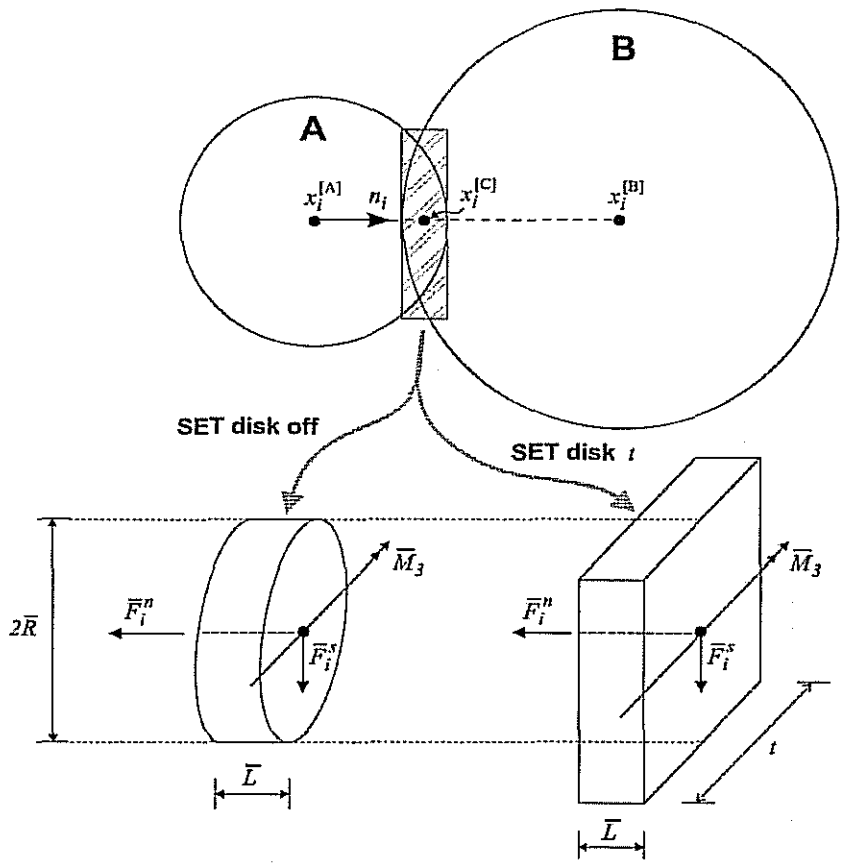

Figure 2.7 - Parallel Bond Model in PFC2D (after PFC2D Manual Version 3.1)

Alternative models:

Several alternative models are implemented in PFC2D and can be used depending on the complexity of contact behavior. These different models are:

- Simple Viscoelastic
- Simple Ductile
- Displacement-Softening
- Hysteretic Damping Model
- Burgers Model
- Viscous Damping Contact Model.

Model Geometry

The model geometry in PFC2D is defined using an arrangement of circle elements (i.e., balls), which can be either defined directly by the user or created using the built-in generation algorithms of the software. Using the built-in generation algorithms, the location of the particle is chosen at random. If the newly generated particle is found to overlap a previously generated one, another location is randomly selected. The number of trials to fit each particle is controlled by the user, with a default value of 20,000. This technique makes it impossible to describe materials of known geometry, but it is useful in describing materials with random particle distributions. The other way to describe the geometry is to generate several particle arrangements by defining their radii, x, and y coordinates. Generally for this case, the user can write a code using the built-in programming language (FISH), instead of individually defining each ball.

Boundary and Loading Conditions

As mentioned above, the basic components in PFC2D are circular particles (balls). Both forces and velocities can be applied to a ball or a set of balls to load the model. By default, balls are not fixed when created. Walls are used as the boundaries of the discrete element model. The walls are defined by specifying their end-points. In accordance to the order in which the end-points are entered, only the left side of each wall is active. Walls do not interact with one another, but interact with balls. Intersecting walls produce no problems, as no interaction will occur. By default, walls are fixed when created but can be given a translational and/or an angular velocity. Forces cannot be directly prescribed for walls because the equation of motion is not solved for them. In order to apply stresses, a numerical servo-control mechanism can be used in which the wall velocity is updated at each cycle to meet the targeted stress level.

CHAPTER THREE - AGGREGATES AND MIX SELECTION

PHILOSOPHY

The main object of this study is to evaluate the effect of stress concentration at contact points on coarse aggregates that could cause aggregate to fracture. Three aggregate types were selected from three TxDOT districts: granite, a hard limestone, and a soft limestone. These aggregates are commonly used in TxDOT paving and their performance histories are well known. For each of these three aggregate sources, three mix types were chosen: Porous Friction Course (PFC), Superpave-C, and Coarse Matrix High Binder (CMHB-C). A total of nine mixes were used in this study for three aggregate sources and three mix types as shown in Table 3.1. The same bituminous binder (PG 76-22) was used for all mixes to minimize the impact of the binder properties on the results.

GRADATION AND AGGREGATE SELECTION CRITERIA

The gradation for each mix type was selected to be in the middle of the gradation band specified by TxDOT. Although the gradation needs to be adjusted depending on mix design, this step was taken to make sure that an average estimate of crushing can be obtained for each mix type. The average gradation curves for each mix type are illustrated in Figure 3.1. These gradations differ from one another to provide different grain-to-grain contact. The PFC is a coarse, gap-graded mixture with a high percentage by weight of coarse aggregates. It is composed of 89% aggregates larger than a No. 8 sieve. In contrast, Superpave-C is a fine-graded mixture. It consists of 35% coarse aggregates and 65% fine aggregates. The CMHB-C mix is a coarse-graded mixture that is composed of 63% coarse aggregates and 37% fine aggregates.

Since the main focus of this study is to evaluate the effect of stress concentration at contact points on coarse aggregates that could cause aggregate fracture, only coarse aggregates (Retained No. 8) from different sources were used while the fine portion (Passing No. 8) was obtained from one source only.

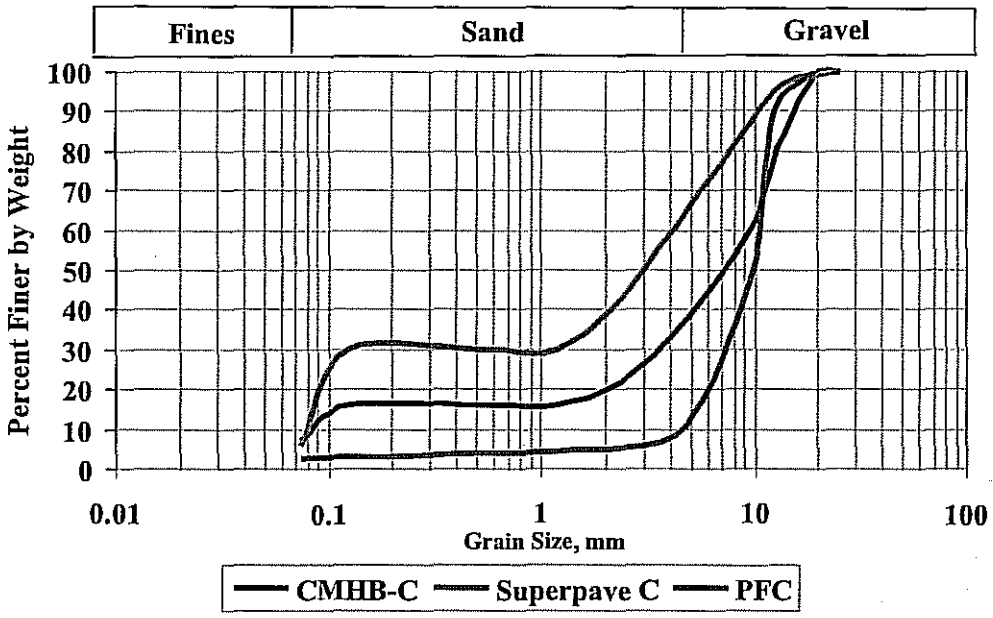

Figure 3.1 - Project Gradations

Table 3.1 - Selection of Aggregates and Mixtures

Aggregate Source	Mix Type
Hard Limestone	CMHB-C
	Superpave-C
	PFC
Granite	CMHB-C
	Superpave-C
	PFC
Soft Limestone	CMHB-C
	Superpave-C
	PFC

TRADITIONAL TESTS TO CHARACTERIZE MIXES AND AGGREGATES

An important issue to address is the criteria for selecting aggregates for use in HMA such that the aggregates can resist degradation due to the high contact stresses during compaction and traffic loading. The results of numerous tests, including the Los Angeles abrasion and Micro-Deval tests, currently specified by TxDOT to evaluate such degradation resistance in aggregates were obtained. Table 3.2 contains a summary of the results obtained from the TxDOT database and measured for this project.

The angularity, shape, and texture of the aggregate particles have a significant effect on the performance of HMA mixtures by controlling the mixture's strength and rutting resistance. Consequently, the results of the aggregate imaging system (AIMS) used to measure the shape characteristics of the aggregates are also provided in Table 3.2.

Table 3.2 - Summary Results of Tests to Characterize Aggregates

Source	Test Procedure		Hard Limestone	Granite	Soft Limestone
TxDOT	Los Angeles % Wt. Loss - Bituminous	Tex-410-A	23	34	34
	Mg Soundness – Bituminous*	Tex-411-A	6	13	41
	Mg Soundness - Stone**		5	10	29
	Polish Value	Tex-438-A	21	28	25
	Micro-Deval % Wt. Loss - Bituminous	Tex-461-A	11.4	9.6	19.7
	Fine Aggregate Acid Insolubility	Tex-612-J	5	92	2
TTI	Micro-Deval %Wt. Loss	Tex-461-A	15	8.8	20.4
	Texture Before Micro-Deval	AIMS procedure	193	221	80
	Texture After Micro-Deval		95	187	36
	Angularity Before Micro-Deval		2323	2791	2195
	Angularity After Micro-Deval		1730	2491	1671

*Using HMAC Application Sample Size Fractions
**Using Other Applications Sample Size Fractions

MIX DESIGN

The mix design for the three mix types was developed using Tex-241-F and Tex-204-F. All mixes were designed using the Superpave Gyratory Compactor (SGC) regardless of mix types. The mixing, curing and compaction temperatures were selected as per Tex-241-F. The target air void contents for CMHB-C and Superpave-C were 4% and for PFC mixes were 20%. For PFC mixtures, 1% lime and 0.4% fiber was added, as specified in Tex-241-F. The job mix formula (JMF) for each of the nine mixes is summarized in Table 3.3. The bituminous content varied from 4% to 7.1%. For each coarse aggregate type, the Superpave mixes had the lowest bituminous content whereas the PFC had the highest. The CMHB-C mix designs do not meet the TxDOT specifications of 15% VMA. Similarly, the dust proportion of 0.6 to 1.2 was not met for some of the mixes. Since the gradations of the mixes were fixed for this study, the desired VMA or dust proportions could not be achieved.

SPECIMEN PREPARATION

All HMA mixes were prepared using a Pine Instrument Co. Superpave Gyratory Compactor (SGC) with the same compactor parameters such as the angle of gyration, vertical pressure, and rotational speed. Two different sets of bituminous specimens were prepared for this project at two different compactive efforts. First, the samples were compacted to achieve a nominal air void content of 7%, as specified in the TxDOT specifications. This generally occurred around 50 to 75 gyrations. Secondly, another set of lab specimens was compacted to 250 revolutions. Such

Table 3.3 - Mix Design for all Materials

Property	Hard Limestone			Granite			Soft Limestone		
	CMHB-C	Superpave-C	PFC	CMHB-C	Superpave-C	PFC	CMHB-C	Superpave-C	PFC
Binder Grade	PG 76- 22								
Binder Content,%	4.2	4.0	5.1	5.3	4.8	6.6	5.8	5.2	7.1
Sieve Size, in. (Sieve No.)	Percent Passing, %								
1	100	100	100	100	100	100	100	100	100
0.750 (3/4)	99	99	100	99	99	100	99	99	100
0.492 (1/2)	78.5	95	90	78.5	95	90	78.5	95	90
0.375 (3/8)	60	92.5	47.5	60	92.5	47.5	60	92.5	47.5
0.187 (No. 4)	37.5	77.5	10.5	37.5	77.5	10.5	37.5	77.5	10.5
0.0929 (No. 8)	22	43	5.5	22	43	5.5	22	43	5.5
0.0469 (No. 16)	16	30	5	16	30	5	16	30	5
0.0234 (No. 30)	-	-	4.5	-	-	4.5	-	-	4.5
0.0117 (No. 50)	-	-	3.5	-	-	3.5	-	-	3.5
0.0029 (No. 200)	7	6	2.5	7	6	2.5	7	6	2.5
Maximum Specific Gravity	2.554	2.572	2.555	2.471	2.520	2.469	2.450	2.515	2.445
Aggregate Bulk Specific Gravity	2.696	2.715	2.673	2.601	2.655	2.526	2.587	2.653	2.527
Binder Specific Gravity	1.02								
Air Voids at N_{design} = 100,%	4.0	4.0	20	4.0	4.0	20.0	4.0	4.0	20.0
VMA at N_{design} = 100, %	12.7	12.7	27.2	13.7	13.2	27	14.3	13.7	28
VFA at N_{design} = 100,%	70.2	68.5	26.4	69.7	69.9	25.8	72.5	70.9	28.8
Effective Bituminous Content, %	3.7	3.6	3.7	4.1	3.9	3.6	4.5	4.1	4.2
Dust Proportion, %	1.7	1.5	0.5	1.3	1.3	0.4	1.2	1.2	0.4

variation in the compactive effort or number of gyrations was important to evaluate the potential of crushing in the aggregates.

Once compacted, the specimens were tested to characterize the HMA performance utilizing the Hamburg wheel tracking device (HWTD) test, indirect tensile test (IDT), dynamic modulus test, and flow time test. After testing, the aggregate breakdown was examined. Samples compacted to the nominal 7 % air voids and to 250 gyrations were heated and broken down. The bituminous was then burned from the aggregates using an ignition oven according to Tex-236-F and a sieve analysis was performed on each mix.

CHAPTER FOUR - GEOLOGICAL ASPECTS OF AGGREGATES

HARD LIMESTONE QUARRY

The hard limestone Quarry is operated by Vulcan Materials Inc and located in Brownwood, Texas. The quarry has a large surface area, but only a 25-40 ft thick layer of acceptable limestone. The quarry floor is a thick shale that underlies the limestone and the top is soil that forms the surficial outcrop of the limestone. The Limestone is generally pale gray. Soil processes have tinged the upper 1-3 ft of limestone a tan or orange color. The entire unit thins and pinches out within half a mile in the northeastern part of the quarry, being replaced by a dark gray shale unit that is not mined.

Four slightly different layers were noted and specimens were collected from each. Figure 4.1 illustrates the layers sampled. The top of the outcrop is approximately 25 ft above the quarry floor. The lowest layer (unit 1) is a dark gray lime mudstone. This is pure limestone, but composed of microscopic crystals that allow the rock to break with smooth curving fractures. The basal layer is approximately 1 ft thick, but above this, thin shale (clay) partings separate the lime mud into layers 3-6 in thick. The layers gradually thicken and become lighter upward until they transition into unit 2.

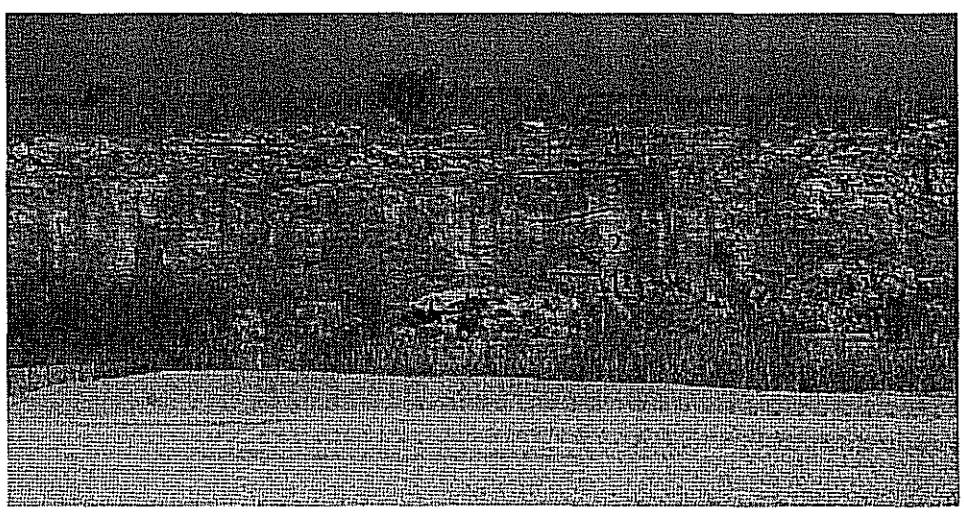

Figure 4.1 – Hard Limestone Quarry

Unit 2 is a lighter gray lime mud, thicker bedded and more widespread than unit 1. Most of the unit is composed of a 3 ft thick bed of the mud. The entire unit thins and disappears to the northeast, although it continues farther than unit 1. Unit 3 is a grainstone; a limestone composed of large crystals that essentially acted as sand grains when the limestone was deposited. Fossils are common in this unit, the most common being crinoid stems. This unit is darker grey than the underlying lime mud and is continuous throughout the quarry. It forms the base of the quarried interval in the northeastern part of the quarry. The layers in the unit are 0.5 ft to 1 ft thick and pinch and swell in the quarry wall. Unit 4 is a sandy limestone with quartz sand grains interspersed with the limestone grains. The unit is generally tan in color from overlying soil. It is resistant to erosion and the bed holds up the hill in which the quarry is developed. Layers are 0.5 to 2 ft thick. Beds of concentrated fossils are evident in the middle of the layer. Crinoid stems are the most common.

GRANITE QUARRY

The granite quarry is located in El Paso, TX at the McKelligon Canyon plant operated by CEMEX. It exposes a fractured and faulted edge of granite mass. The granite is essentially uniform and, except for alteration along fractures, is granite with ¼ to ½ inch crystals of potassium feldspar, plagioclase feldspar, quartz and amphibole minerals. There is greenish and yellowish hydrothermal alteration along some of the fractures, but it does not penetrate into the wall rock of the fractures. The uppermost rock is weathered and weakened by the overlying soils. Several samples were collected to document the slight variations present. The main pink granite, the darker granite that forms patches on the north and south walls (Figure 4.2) and a sample of the hydro-thermally altered material were sampled for testing.

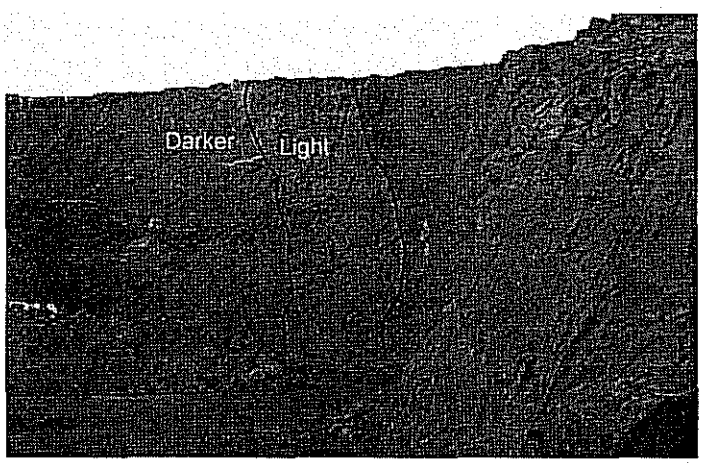

Figure 4.2 - South Wall of the Granite Quarry

SOFT LIMESTONE QUARRY

The soft limestone quarry is operated by Martin Marietta Materials and located at the Beckman plant near San Antonio, TX. The quarried section is at least 150 ft thick. The interval currently being quarried and the interval sampled for this study is the lower 80 ft of the section (Figure

4.3). The entire quarry consists of 10 layers of thick limestone separated by thin layers of tan and red shale. Several caves, filled with red sand and mud are evident in the quarry walls. There are also many fractures that show red and tan muds and where the limestone has been dissolved.

Three types of limestone are evident and were sampled (Figure 4.4). The basal part of some layers is composed of a limestone, containing numerous mollusk fossils. This layer is formed of interlocked crystals $^{1}/_{16}$ in. to ½ in. in diameter. The second rock type makes up the bulk of each layer. This layer is a light beige colored lime mudstone. This is pure limestone, but composed of microscopic crystals that allow the rock to break with smooth curving fractures. This limestone contains numerous large irregular open cavities, called vugs, which are lined with large calcite crystals. The upper part of each layer is a yellowish sandy limestone that contains scattered quartz grains intermixed into the limestone The interval forms more distinct layers and varies internally more than the underlying layers.

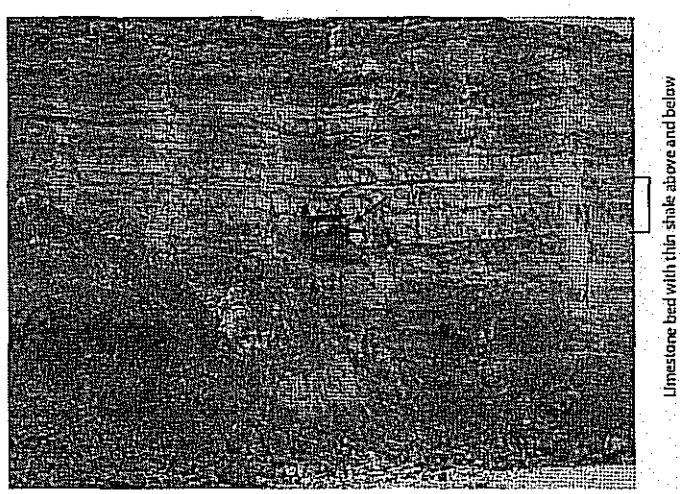

Figure 4.3 - Soft Limestone Quarry

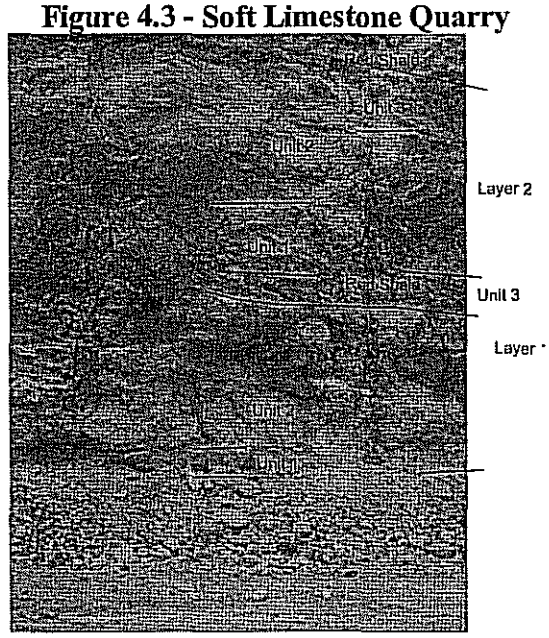

Figure 4.4 - Detail Showing Units for Layers in Soft Limestone Quarry

PETROGRAPHIC ANALYSIS

Hard Limestone Quarry

Samples from units 2 and 3 were studied together. These form the bulk of the quarried limestone shown in Figure 4.1. Unit 2 is a lighter gray lime packstone-wackestone with small fossils, thicker bedded and more widespread than unit 1 in the quarry. Figure 4.5 illustrates an 8 in. polished slab of Unit 2 material showing the void filling texture and the fossils floating in a mud matrix. In polished slabs and thin sections, the unit is composed of fossils that have been micritized. The open interiors of the fossils were filled with void filling calcite spar. The original rock matrix is dominantly filled with lime mudstone.

There is very little evident porosity, accounting for the hard nature of the limestone. Almost all the porosity is molds where fossil fragments have been dissolved. A photomicrograph of the middle of unit 2 in Figure 4.6 shows the typical lack of porosity in this formation. Light colored areas in the figure are filled fossil fragments. Dark matrix in the figure is lime mud (micrite). The arrow points to a blue ring in the center which is a pore that formed through dissolution of a brachiopod spine. Letters "M" indicate some of the molds filled with coarsely crystalline calcite. The field of view is 1.2 mm. The only visible pore is a mold around a brachiopod spine in the center of the photo. The fossil fragments have been replaced with calcite spar and the matrix between them is composed of micrite, (calcite mud). The field of view from Figure 4.6 is 0.8 mm. The sample is composed of 45% micrite and 30% spar that fill the molds. Another 13% is micritized shells and 10% spar filling irregular vuggy pores. The remaining 2% is filled with fossil molds.

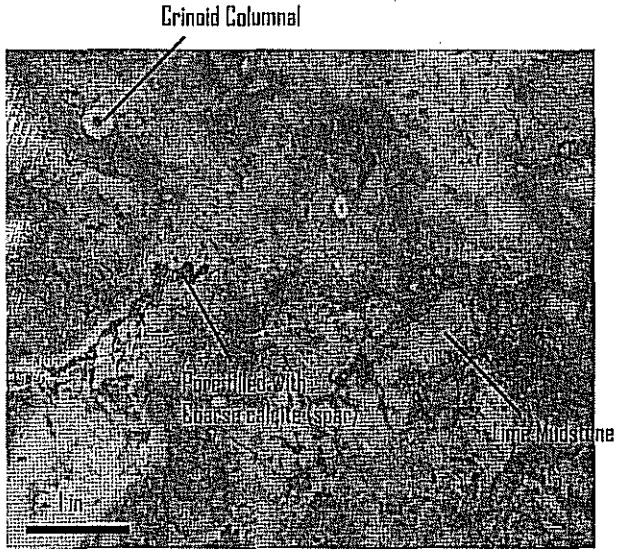

Figure 4.5 - Polished Slab of Unit Two from the Hard Limestone Quarry

Figure 4.6 - Photomicrograph of the Interior of Unit 2

Unit 3 is a grainstone/packstone; a limestone composed of large crystals that essentially acted as sand grains when the limestone was deposited. Fossils are common in this unit, the most common being crinoid stems brachiopods and fusulinids. This unit is darker grey than the underlying lime mud and is continuous throughout the quarry. It forms the base of the quarried interval in the northeastern part of the quarry. The layers in the unit are 0.5 ft to 1 ft thick and pinch and swell in the quarry wall.

The petrography supports the macroscopic interpretation. Diverse fossils are cemented with lime mud and spar creating a dense limestone without microscopically visible pores as shown in Figure 4.7. The vuggy pore filled with blue epoxy is large, but because these are rare, they make up only 1% of the sample. The laminar of coarser and finer grained material in this unit will probably make it less brittle than the underlying micrite. About 37% of the sample is micrite while 22% is micritized fossil fragments. However, in contrast to unit 2, only 11% of the sample is sparry mold fill, whereas 28% is interstitial spar that fills the spaces between the fossils. Another 1.1% is unaltered bioclasts. The photomicrograph of unit 3 (Figure 4.7) shows micritized fossils cemented together by calcite spar. The field of view from Figure 4.7 is 1.2 mm.

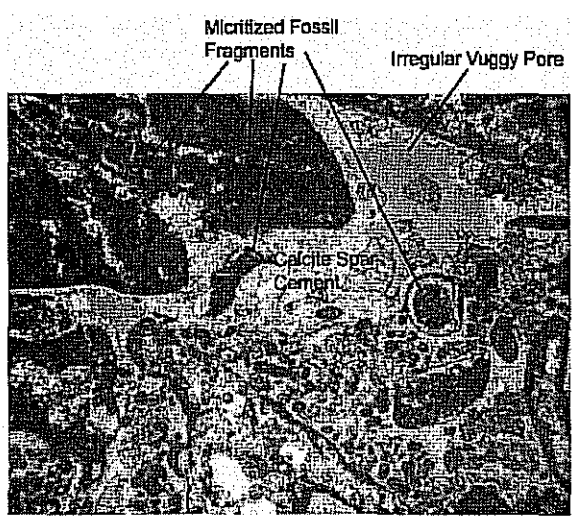

Figure 4.7 - Photomicrograph of Unit 3

Granite Quarry

All the granite samples showed fracturing and filling of fractures with what is probably hematite and clay, followed by quartz (Figures 4.8 and 4.9). The sample shown in Figure 4.8 is 10 inches across. The dark lines shown in the figure are fractures. The granite selected as being darker and more fractured exhibited denser and more frequent fracturing. The granite was dominantly composed of large crystals (up to 0.8 in. in cross section) of microcline potassium feldspar. Microcline composed 59 to 63 percent of the two thin sections. Quartz crystals formed 9 to 17 percent of the samples, being lower in the more highly fractured sample. Plagioclase formed less than 2 percent of each sample and hornblende formed 1 percent of the slides. Alteration products formed 15 to 20 percent of each slide. In the less highly disturbed sample, fractures filled with iron-oxide and shattered grains formed 17 percent of the sample. In the more highly fractured sample, almost all the grains were fractured with hairline, iron-oxide filled cracks (Figure 4.9). However, these only formed 6 percent of the sample. Quartz filled fractures formed another 6 percent of the sample and clay filled fractures formed 3 percent of the sample. Thus, 15 percent of the sample was fracture fill. An additional 6 percent of the sample was composed of iron oxide alteration in irregular vugs and 2 percent was open porosity. The field of view is 1.2 mm

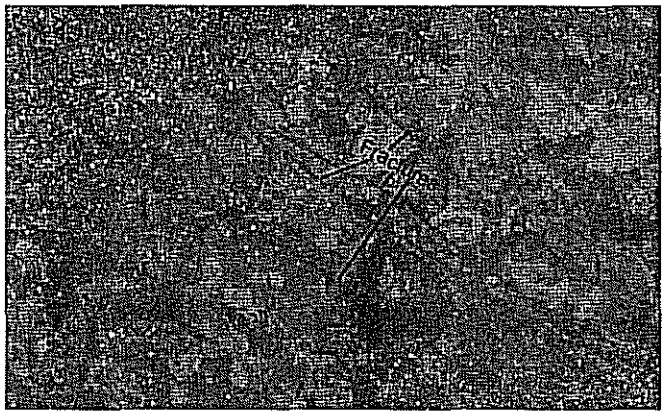

Figure 4.8 - Polished Slab of Granite

Figure 4.9 - Photomicrograph of a Large Fractured Microcline

Soft Limestone Quarry

The soft limestone quarry exposed repeated layers of limestone, each containing two units. The basal part of some layers is composed of lime sandstone, containing numerous mollusk fossils. The layer is formed of interlocked crystals $^{1}/_{16}$ in. to ½ in. in diameter. Unit 1 forms the lowest 1-2 ft of the sampled unit (see Figure 4.4).

Petrographically, unit 1 is a pure limestone (Grainstone in Dunham classification scheme), with abundant mollusk and algae fossils as well as peloidal grains (Figure 4.10). The fossils had been micritized and the matrix is coarse grained calcite spar. The only porosity present was large irregular late stage dissolution pores shown as darker spots. Micritized fossils form 55% of the sample whereas un-micritized fossil clasts form 15 % of the sample. Coarse Spar cement forms 19 percent of the samples while Peliods forms 6.6 percent of the sample. Porosity forms only 2.6 percent of the thin section in contrast to the overlying unit 2.

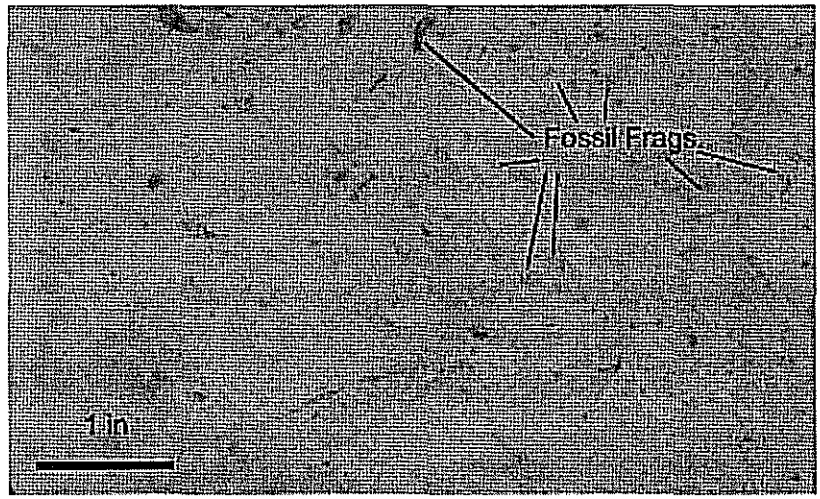

Figure 4.10 - Polished Slab of Unit 1 in the Soft Limestone Showing the Abundant Fossils

Figure 4.11 shows the photomicrograph of unit 1 showing the abundant fossils separated by sparry cement. The photo is 0.8 mm across and the isolated pores are stained blue. The field of view is 1.2 mm. Letters show features described in texts. Letters "f" show some of the visible fossil fragments; letters "c" show coarse calcite spar cement, and letters "p" show porosity filled with blue stained epoxy.

The second rock type makes up the bulk of each layer. This layer is a light beige colored lime mudstone with a few scatted fossils (Mudstone in the Dunham classification scheme). This is pure limestone, but composed of microscopic crystals that allow the rock to break with smooth curving fractures (Figures 4.12 and 4.13).

Petrographically, the limestone shows abundant micro-porosity where small calcite crystals had been dissolved. Large irregular vugs are also present. However, the most important porosity is the lenticular fracture pores that crosscut the sample (Figures 4.12 and 4.13). In Figure 4.12, the Fractures appear as lighter colored lines. This rock is probably the weakest of the entire sample because of the porosity at all scales. The slab illustrated in Figure 4.12 is 10 inches across while

the field of view in Figure 4.13 is .03 inches. In Figure 4.13, porosity appears as blue stained epoxy. Micro-porosity appears as tiny blue spots. Fractures are blue lines that cross the slide. The field of view is 1.2 mm. Porosity forms a total of 19 percent of the sample, with 11% of this being micro porosity and 8 percent of the slide being large solution widened fractures and vugs. Micrite forms 67 percent of the sample and small patches of pores form 12 percent of the samples. Biotic clasts make up 0.5 percent of the slide and small oxide spots, probably altered pyrite grains, make up 2.5% of each sample.

Figure 4.11 - Photomicrograph of Unit 1 with Abundant Fossils

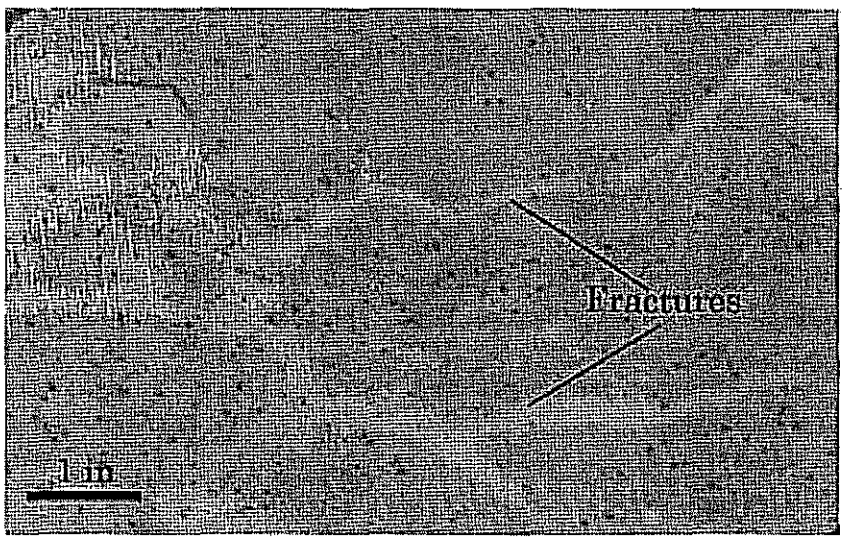

Figure 4.12 - Polished Slab of Unit 2 Showing Fractures and Vuggy Porosity Widened by Solution

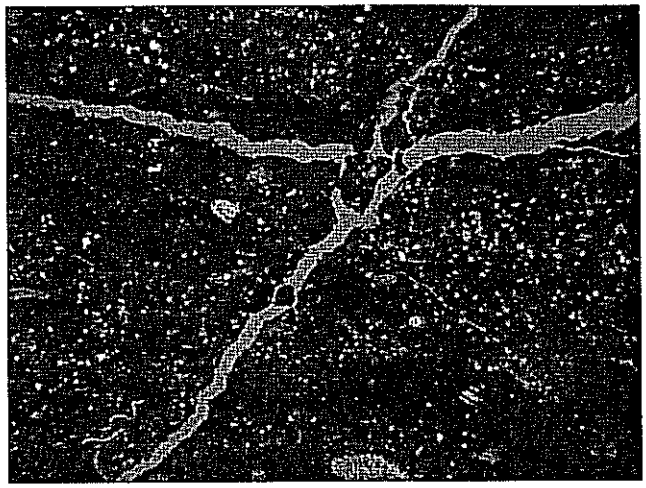

Figure 4.13 - Photomicrograph Showing Solution Widened Fractures and Micro Porosity due to Dissolution of Grains in the Dark Micrite

CHAPTER FIVE - CHARACTERIZATION OF AGGREGATES

INTRODUCTION

A lack of practical methods for measuring the aggregate structure in HMA has led to limited understanding of how factors such as aggregate shape, mix design, and compaction influence the aggregate structure. This lack of understanding has led to the development of design methods that tended to overemphasize the need for superior aggregate properties, rather than the development of innovative design methods to accommodate a wide range of aggregate properties.

Numerous tests to identify and evaluate the toughness and abrasion resistance in aggregates used in bituminous mixtures are summarized in Chapter 2. Some of the most common test methods include the Los Angeles (LA) abrasion (Tex-410-A) and Micro-Deval abrasion (Tex-461-A). A number of alternative tests have been used to assess the aggregate breakdown throughout the European Union. Some of these test methods, such as aggregate crushing value, ten percent fines value, and aggregate impact value, are included in the British Standards 812 and described in detail below.

AGGREGATE IMPACT VALUE (AIV)

The Aggregate Impact Value (British Standard 812-Part 112) provides a measure of the resistance of aggregates to impact. To conduct the test, a specimen is compacted into an open steel cup (Figure 5.1). The sample is subjected to a number of vertical impacts from a dropped weight. This action breaks the aggregate to a degree which is dependent on the vertical impact resistance of the material.

As part of the procedure, a portion of the material is dried in the oven at a temperature of 220°F. The material is cooled to room temperature before thoroughly sieving sufficient quantity of material passing the 1/2 in. sieve and retained on the 3/8 in. sieve to fill the cylindrical steel cup. The material is placed in a 4-in. diameter cylindrical steel cup to a height of 2 in., and compacted by 25 strokes of a tamping rod before attaching it to the impact device. Once the cup is firmly attached in position on the base of the device, the material is then subjected to 15 vertical impacts from a 30-lb metal hammer, each being delivered at an interval of not less than 1 second

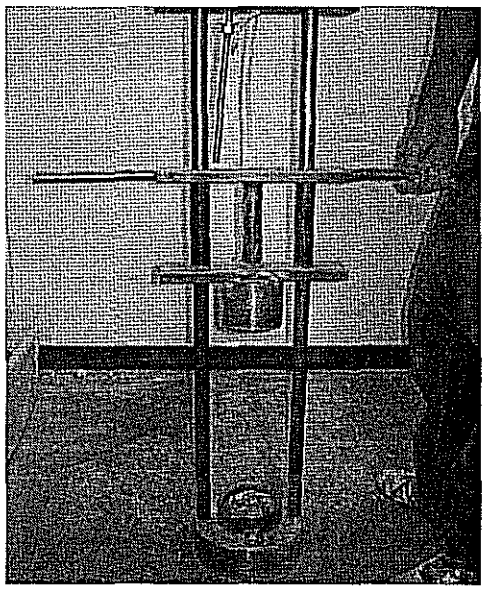

Figure 5.1 - Aggregate Impact Value Machine

from a vertical distance of 15 in. Following the impacts, the crushed aggregate is then removed from the steel cup and weighed to record its mass. A sieve analysis is performed afterwards and the material passing the No. 8 sieve is weighed and recorded. The aggregate impact value (AIV) is then determined as a percentage using the following equation:

$$AIV = (M2 / M1) \times 100 \tag{5.1}$$

where *M2* is the mass of the crushed material passed on the No. 8 sieve and *M1* is the mass of the total material after crushing. Traditionally, a dry AIV of 20 is assumed as the borderline between acceptable and unacceptable aggregates.

The AIV tests can also be performed on aggregates soaked for 24 hours before testing. The AIV values for tests on the three aggregates in dry and soaked conditions are summarized in Table 5.1. Under the dry condition, the hard limestone exhibits very good resistance to crushing. Surprisingly, the granite is prone to crushing under impact in a manner similar to the soft limestone. This can be explained with the large embedded crystals in the granite aggregates. Under the soaked condition, the three aggregates behave similarly. This indicates that the aggregates may not be as durable when they are exposed to water.

Table 5.1 - Aggregate Impact Values for Aggregates Used in this Study

Aggregate Type	Dry AIV		Soaked AIV	
	Mean, %	COV, %	Mean, %	COV, %
Hard Limestone	13	*5*	31	*1*
Granite	29	*6*	35	*2*
Soft Limestone	28	*7*	34	*2*

Tests on triplicate specimens exhibit a maximum COV of 7% for the dry AIV and 2% for the soaked AIV, indicating that the tests are fairly repeatable.

AGGREGATE CRUSHING VALUE (ACV)

The Aggregate Crushing Value Test (British Standard 812-Part 110) provides a measure of the resistance to crushing under gradually applied compressive loads by a compression testing machine (Figure 5.2). This action crushes the aggregate to a degree which is dependent on the crushing resistance of the material. This degree is evaluated by a sieve analysis on the crushed aggregate and is taken as a measure of the aggregate crushing value (ACV).

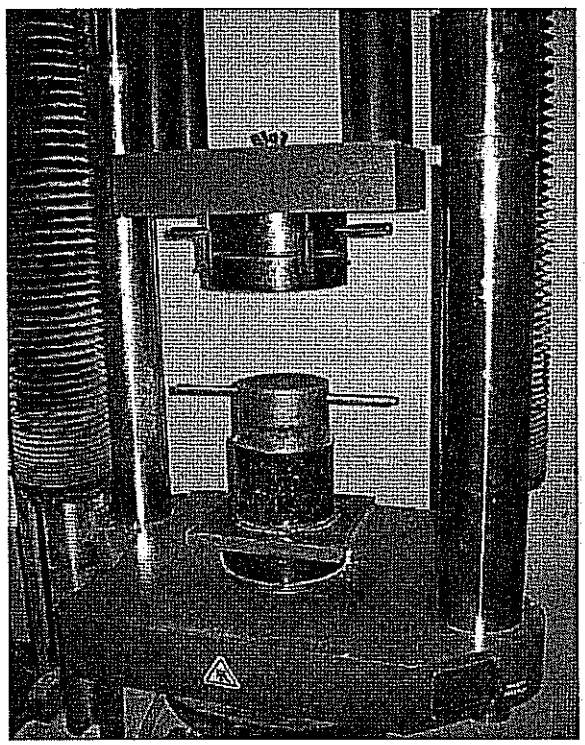

Figure 5.2 - Aggregate Crushing Value Apparatus

A part of the procedure for this test method is very similar to the AIV test method. A portion of the material is dried in the oven at a temperature of 220°F. The material is cooled to room temperature before sieving it on the 1/2 in. and 3/8 in. sieves. The material is then used to fill a 6-in. diameter by 5-in. high steel cylinder in three equal layers, each tamped 25 times. Once the material is compacted, the sample is then subjected to a standard loading of 90,000 lb applied through a freely moving plunger by a compression testing machine. The load is applied over a period of 10 minutes. The load is then released and the crushed material is removed and weighed to determine the mass of aggregates (*M1*). The material is subjected to sieve analysis and the mass of the fractions passing the No. 8 sieve is recorded as *M2*. The aggregate crushing value (ACV) is expressed as a percentage using the following equation:

$$ACV = (M2 / M1) \times 100 \qquad (5.2)$$

To quantify the behaviors of aggregates under loading, the load and deformation of the specimen was monitored during loading. The stress-strain curve was then developed for each test. An example is shown in Figure 5.3. The stress strain curve can be approximated by two lines. The slope of the line at lower strains, termed "Compacting Modulus," can be interpreted as the resistance to compaction. The slope of the line at higher strains, termed "Crushing Modulus," is related to the resistance to crushing.

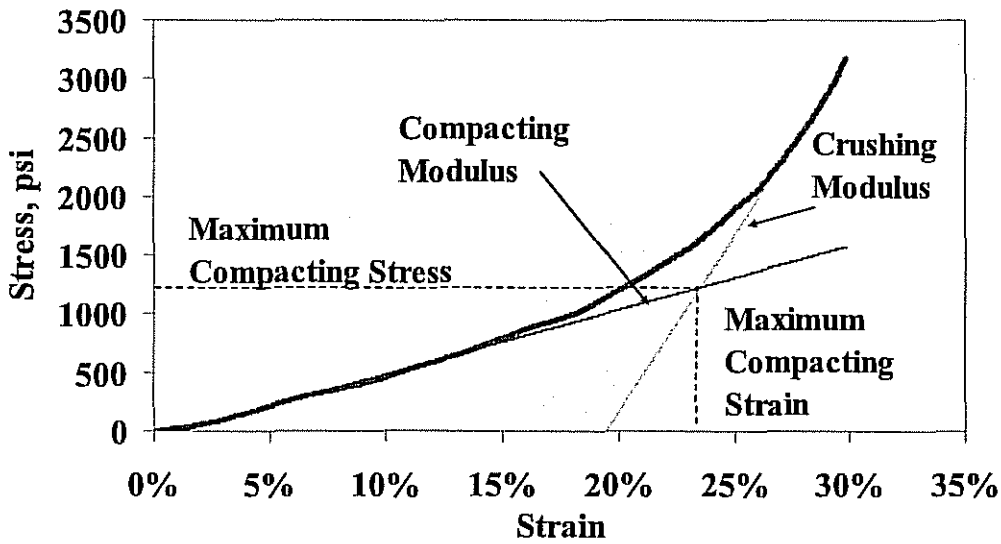

Figure 5.3 - Typical Results for the ACV Test

The stress at the intercept of these two lines, termed "Maximum Compacting Stress," corresponds to the maximum stress that should be applied to the material to minimize the crushing of the aggregates during compaction. In our opinion, the maximum compacting stress should be related to the energy that the compactors apply to the fresh mat during compaction.

The strain at the intercept of the two lines is termed "Maximum Compacting Strain." This parameter can be conceptually used to estimate the volume change anticipated in the aggregates if the compaction energy is limited to the maximum compacting strain. This parameter can be potentially used to estimate the number of passes needed to achieve the desired air voids in the bituminous mixture.

The ACV values for the three aggregates are reported in Table 5.2. The hard limestone exhibits the least amount of crushing, followed by the granite and the soft limestone. These tests seem to be reasonably repeatable with a maximum COV of 13%.

The compacting modulus, crushing modulus, maximum compacting stress and maximum compacting strain values for the three aggregates are also shown in Table 5.2. From the compacting moduli, the hard limestone will be more resistant to compaction, followed by the granite and the soft limestone.

From the crushing modulus, the hard limestone with a crushing modulus of 26 ksi is more resistant to crushing than the granite and soft limestone. All three aggregates demonstrate a reduction of about 20% in the volume if the load is limited to the maximum compacting strain.

Table 5.2 - Results from Aggregate Crushing Value Tests on Aggregates

Aggregate Type	ACV, %	Compacting Modulus, ksi	Crushing Modulus, ksi	Maximum Compacting Stress, psi	Maximum Compacting Strain, %
Hard Limestone	22 *(1%)**	6.8 *(9%)*	26.0 *(3%)*	1371 *(2%)*	20 *(9%)*
Granite	27 *(13%)**	4.9 *(7%)*	27.2 *(6%)*	1008 *(11%)*	20 *(5%)*
Soft Limestone	32 *(2%)**	4.1 *(30%)*	31.5 *(4%)*	988 *(25%)*	23 (5%)

** Numbers in the parentheses are the coefficients of variation from triplicate tests.*

TEN PERCENT FINES VALUE (TFV)

The protocol for conducting the TFV tests is identical to the ACV with one exception. The applied load is reduced to the approximate load required to achieve the maximum compacting stress. The force is then released and the crushed material in the cylinder is sieved through the No. 8 sieve. The weight of the fraction passing the sieve is measured. The empirical relationship to obtain the force that yields ten percent fines value (TFV) is:

$$F = 14*f/(m + 4) \tag{5.3}$$

where F is the force (in kN) required to produce 10% of fines for each test specimen, f is the maximum force applied to produce the required penetration (400 kN, 90,000 lbs), and m is the weight of material passing the No. 8 sieve from the ACV test.

The TFV values from the hard limestone, granite and soft limestone were 9%, 12%, and 10%, respectively (see Table 5.3). The stresses corresponding to the required forces from Equation 5.3 are also shown in Table 5.3. These stresses are about 150 psi to 500 psi more than the maximum compacting stress reported in Table 5.2. This indicates that if the applied stress is limited to close to the maximum compacting stress, the amount of crushing of the aggregates should be minimal.

Table 5.3 - Results from Ten Percent Fines Value Tests on Aggregates

Aggregate Type	Stress for 10% Fines, psi	TFV	
		Mean, %	COV, %
Hard Limestone	1531	9	*0*
Granite	1362	12	*5*
Soft Limestone	1419	10	*6*

SHAPE CHARACTERISTICS USING AIMS

AIMS is a computer automated system that includes a lighting table where aggregates are placed in order to measure their physical characteristics (shape, angularity and texture) through image processing and analysis techniques. It is equipped with an auto-focus microscope and a digital camera (Figure 5.4), and is capable of analyzing the characteristics of aggregates sizes retained on sieve #100 (0.15 mm sieve) up to aggregates retained on the 1 in. sieve (25.4 mm sieve). A coarse aggregate sample is placed on specified grid points, while a fine aggregate sample is spread uniformly on the entire tray. Texture is measured by analyzing gray scale images captured at the aggregate surface using the wavelet analysis method (Chandan et al. 2004). The surface irregularities manifest themselves as variations in gray-level intensities that range from 0 to 255. Large variations in gray-level intensity mean a rough surface texture, whereas a smaller variation in gray-level intensity means a smooth particle. The wavelet transform analyzes the image as a two dimensional signal of gray scale intensities, and it gives a higher texture index for particles with rougher surfaces. It takes about 10 minutes to analyze the texture of a coarse aggregate sample that consists of 56 particles. AIMS measures the aggregate angularity by analyzing black and white images of aggregate particles. Angularity is analyzed using the gradient and radius methods. The gradient method measures the angle of the orientation of gradient vectors at boundary segments from a reference direction (θ) and the summation of the magnitude of difference of these values ($\Delta\theta$) for the gradient angularity index. The direction of the gradient vector changes rapidly at sharp corners of the image, but it changes slowly along the outline of rounded particles. In the radius method the angularity index is measured as the difference between the particle radius in a certain direction to that of an equivalent ellipse. The shape of the aggregate is described by 2D form (form index) and 3D form (sphericity). The form index uses incremental change in the particle radius and is expressed by the following equation:

$$\text{Form Index} = \sum_{\theta=0}^{\theta=360-\Delta\theta} \frac{\left|R_{\theta+\Delta\theta} - R_{\theta}\right|}{R_{\theta}} \tag{5.4}$$

where R_θ is the radius of the particle at an angle of θ; and $\Delta\theta$ is the incremental difference in the angle. Sphericity is quantified using the three dimensions of the particle; the longest dimension (d_L), the intermediate dimension (d_I), and the shortest dimension (d_s) in the following equation:

$$\text{Sphericity} = \sqrt[3]{\frac{d_s . d_I}{d_L^2}} \tag{5.5}$$

Al-Rousan (2004) gives detailed background information about AIMS operations and analysis methods. AIMS provides measurements on all particles in an aggregate sample, so the results are presented by cumulative distribution functions as shown in Figure 5.5.

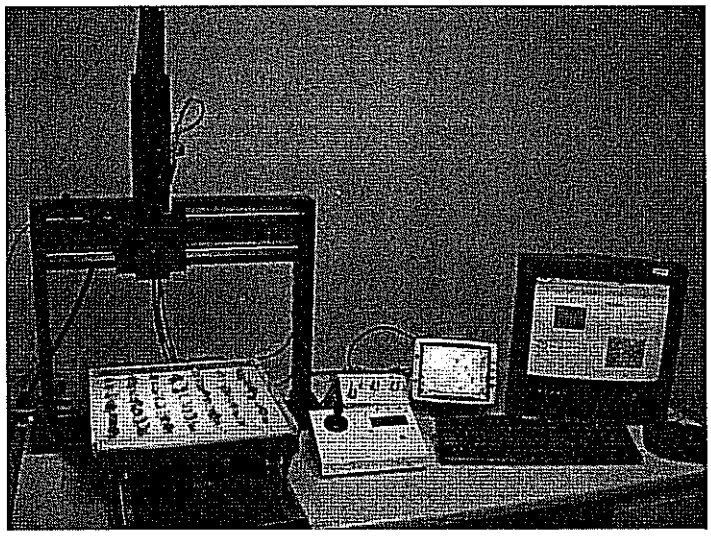

Figure 5.4 - Aggregate Imaging System (AIMS)

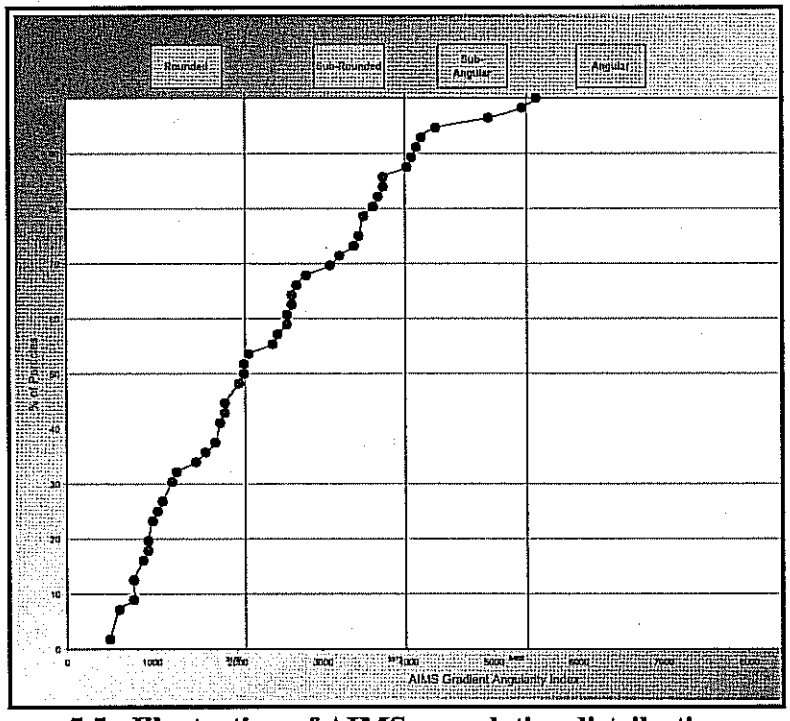

Figure 5.5 - Illustration of AIMS cumulative distribution results

AIMS was used to characterize the form, texture and angularity of the three aggregates. Three different sizes from each aggregate were characterized as shown in Table 5.4. These three sizes are required for the Micro-Deval test. The aggregate impact value and aggregate crushing value test use the aggregate size of passing 1/2 in. sieve and retained on 3/8 in. sieve.

AIMS provides three different parameters for aggregate shape characterization: texture, angularity, and sphericity. Figure 5.6 shows the angularity results for each of the sizes in Table 5.4. A high angularity index indicates a higher aggregate angularity. The granite has the highest angularity, followed by the hard limestone and then the soft limestone.

Table 5.4 - Aggregate Sizes Used for Characterization

Passing	Retained
12.5 mm (1/2 in.)	9.5 mm (3/8 in.)
9.5 mm (3/8 in.)	6.3 mm (1/4 in.)
6.3 mm (1/4 in.)	4.75 mm (No. 4)

Aggregate texture is plotted in Figure 5.7. A higher texture index means that the aggregate has more texture. The soft limestone is the least textured (smoother), and the granite has the highest texture. Finally, the sphericity of the aggregates is plotted in Figure 5.8. A higher sphericity index indicates a more spherical shape, while a low value corresponds to more flat/elongated aggregates. The granite has the lowest sphericity index among the three aggregate, while hard limestone is slightly more spherical than the soft limestone.

The shape characteristics were also measured on the aggregates after the aggregate crushing test and aggregate impact test. As shown in Figure 5.9, there was no consistent trend in the change in aggregate angularity. This could be attributed to the fact that all three aggregates were crushed as received in the laboratory prior to the crushing and impact tests.

Texture results were also inconsistent for both the granite, and the soft limestone among the three different sizes (Figure 5.10). However, the texture of the hard limestone increased after the impact test. The sphericity results plotted in Figure 5.11 show that the sphericity index increased after each of the crushing and impact tests in most of the cases indicating that particles become less flat/elongated and more equi-dimensional.

ABRASION USING MICRO-DEVAL

The Micro-Deval test was conducted in this study according to Tex-461-A. Coarse aggregate breakage, abrasion and polishing take place in this test through the interaction among aggregate particles and between aggregate particles and steel balls in the presence of water (Cooley and James, 2003). This interaction between aggregates and steel balls in the Micro-Deval jar induces more tumble action than impact (Meininger, 2004). Sieve analysis is conducted after the Micro-Deval test in order to determine the weight loss in the coarse aggregate sample as the material passing the sieve number 16 (1.18 mm). Figure 5.12 shows a schematic of interaction between aggregates and steel balls in the presence of water in the Micro-Deval. The wet conditions in the Micro-Deval test give it the ability to simulate the field condition of aggregates better than the dry state in the Los Angeles test (Rogers, 1998).

In the TxDOT Tex-461-A procedure, 1500 ± 5g of aggregates used in bituminous mixes is blended according to the proportions shown in Table 5.5. The aggregate sample is saturated in 2000 ± 500 mL of tap water at temperature of 20 ± 5 °C for at least 1 hour, and then the sample and the water are placed in a 5-litre Micro-Deval jar with a small steel balls charge of 5000 ± 5 g (Figure 5.13). The Micro-Deval machine provides a rotation rate of 100 ± 5 rpm for 105 ± 1 minute for bituminous aggregate (Figure 5.14). Once the machine stops, the aggregate is washed on a set of two sieves (No. 4 and No. 16). The material passing sieve No. 16 is discarded, and the remaining aggregates are oven dried to a constant weight at 110 ± 5 °C.

a) 3/8 in.

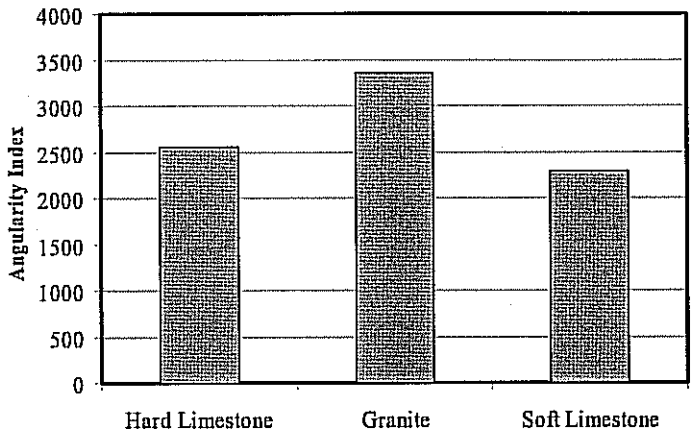

b) 1/4 in.

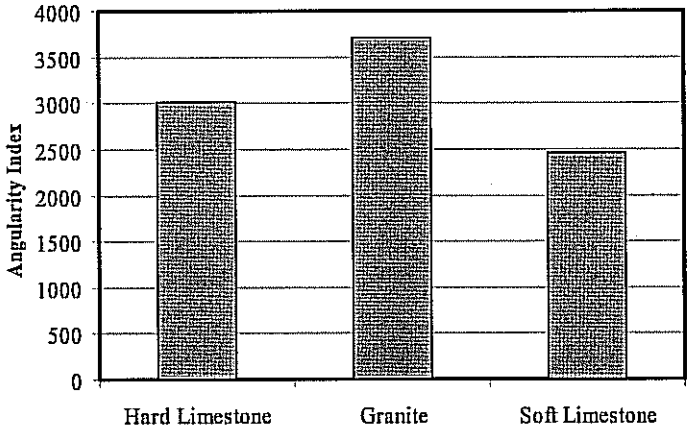

c) No. 4.

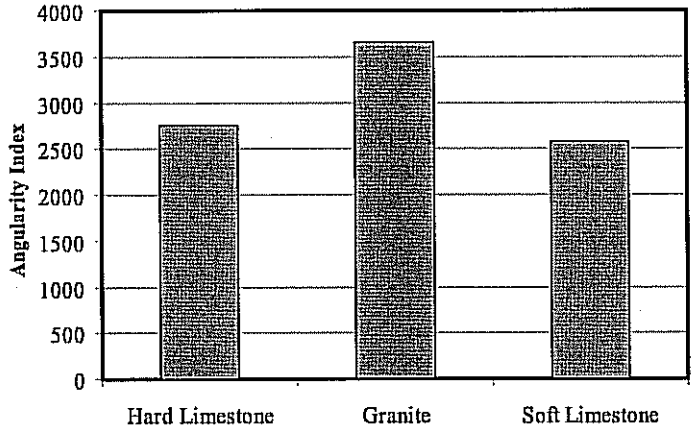

Figure 5.6 - Aggregates Gradient Angularity

a) 3/8 in.

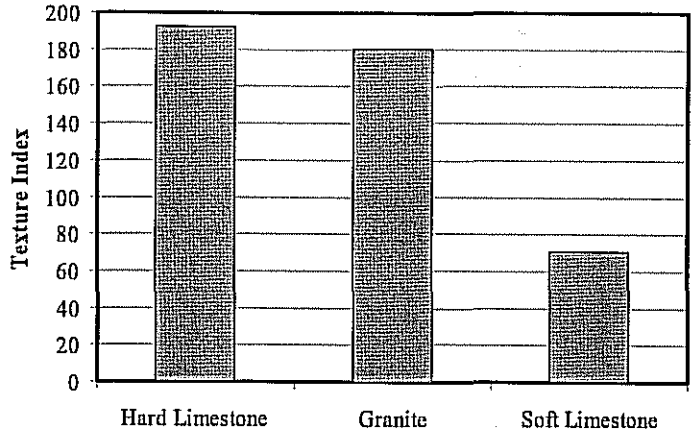

b) 1/4 in.

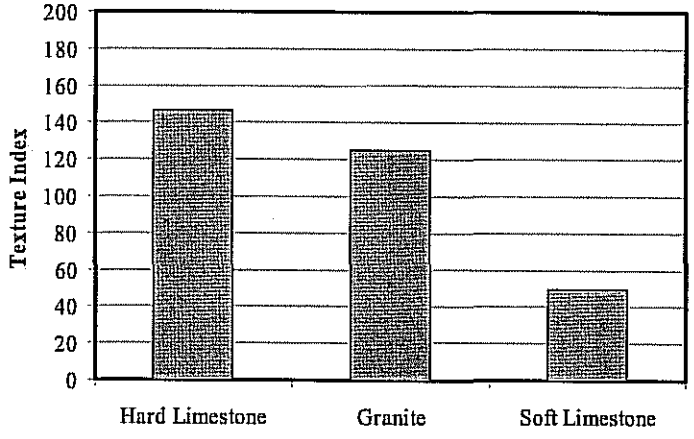

c) No. 4.

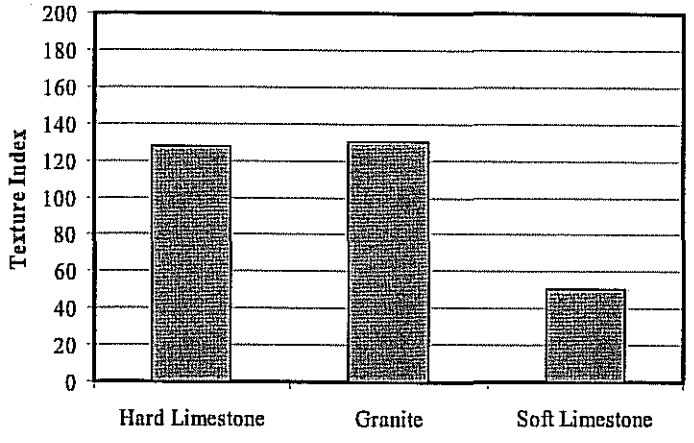

Figure 5.7 - Aggregates Texture Index

a) 3/8 in.

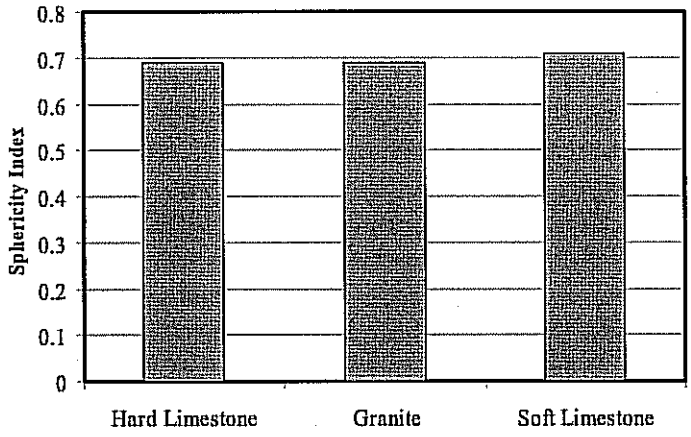

b) 1/4 in.

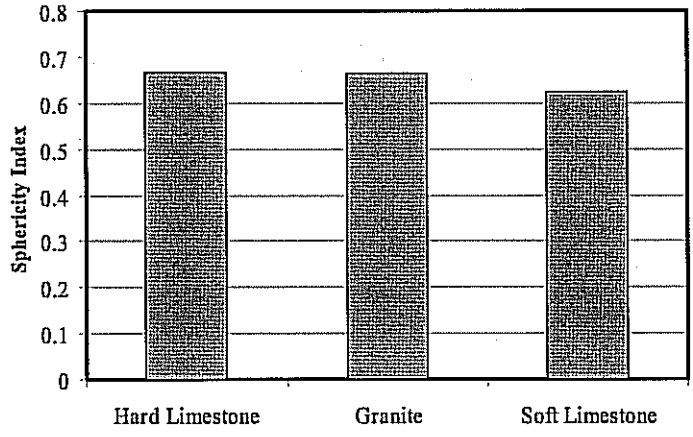

c) No. 4.

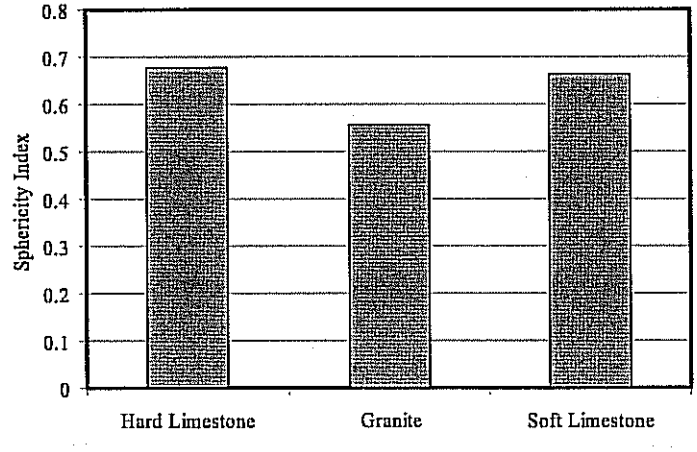

Figure 5.8 - Aggregates Sphericity Index

a) 3/8 in.

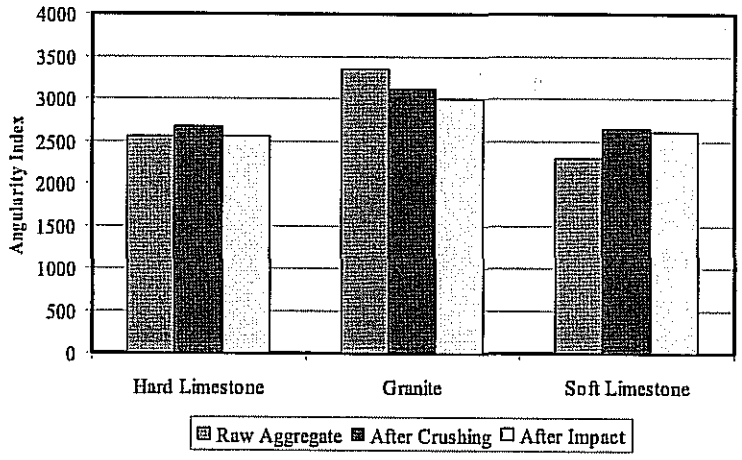

b) 1/4 in.

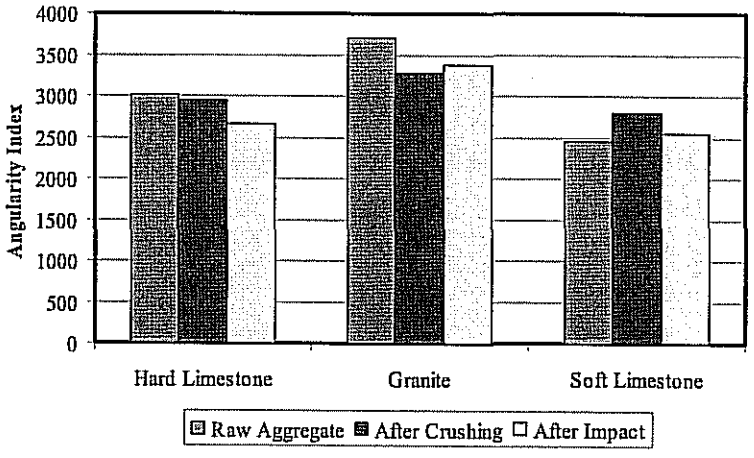

c) No. 4.

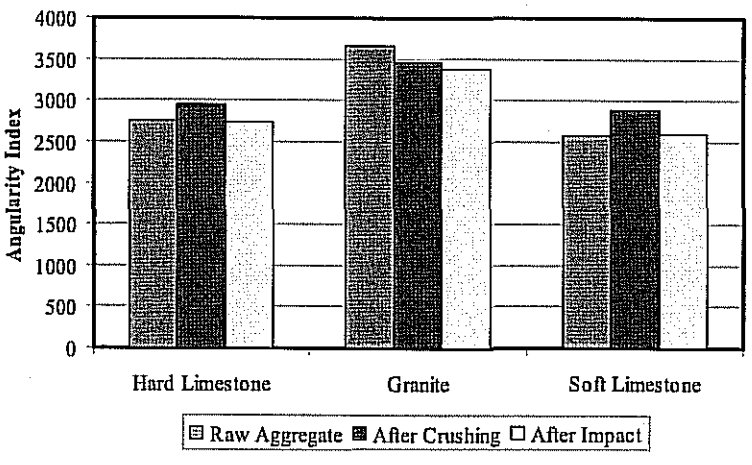

Figure 5.9 - Gradient Angularity Change after Aggregate Impact Value and Aggregate Crushing Value Tests

a) 3/8 in.

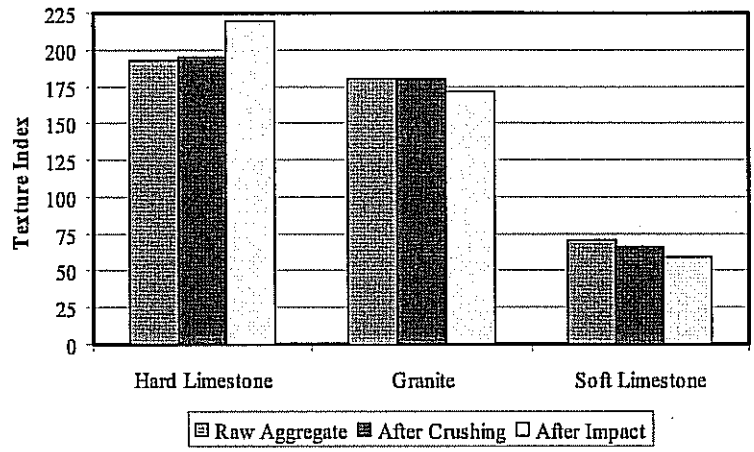

b) 1/4 in.

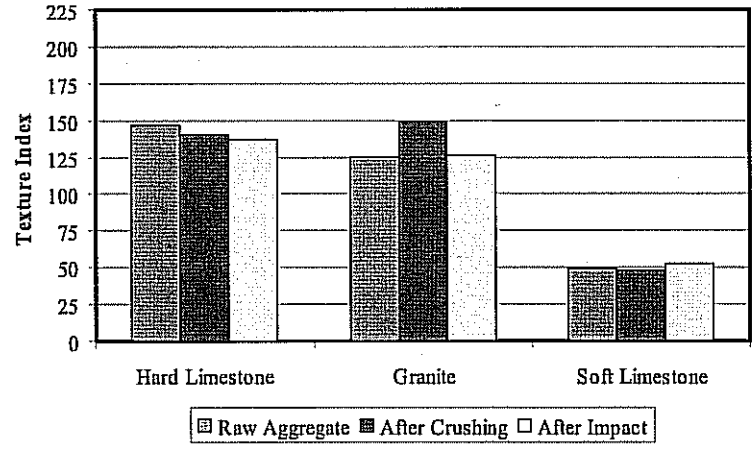

c) No. 4.

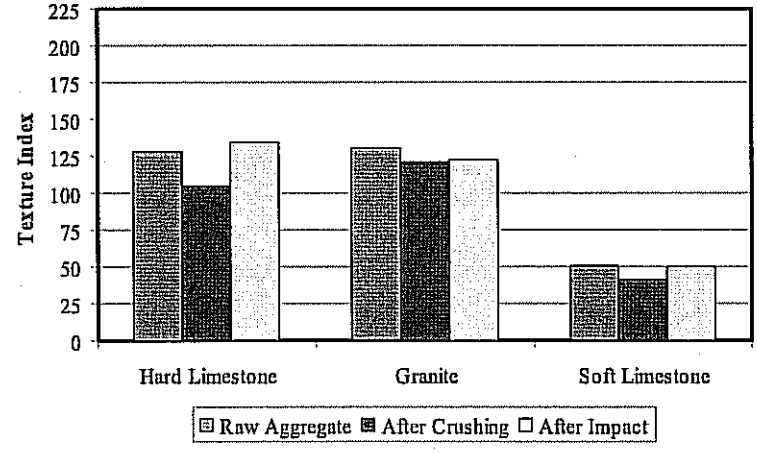

Figure 5.10 - Texture Index Change after Aggregate Impact Value and Aggregate Crushing Value Tests

a) 3/8 in.

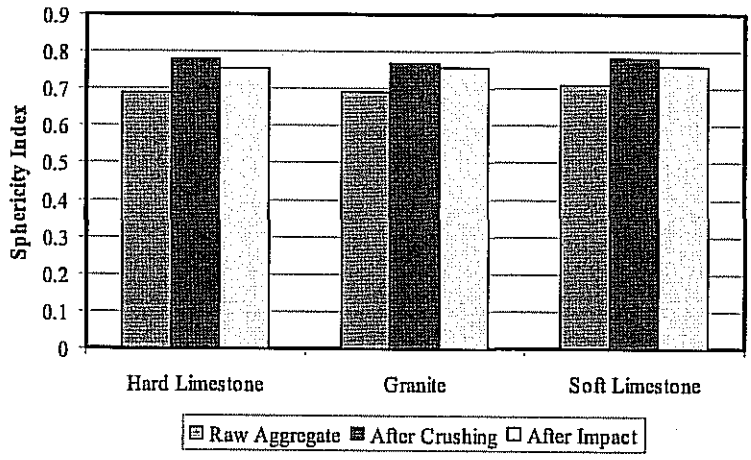

b) 1/4 in.

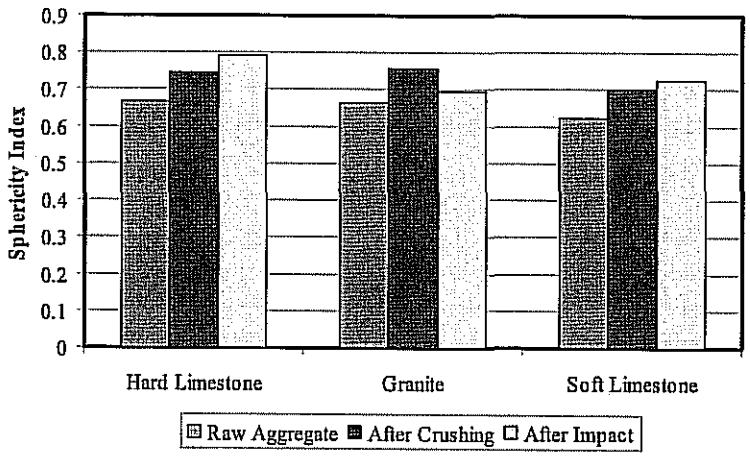

c) No. 4.

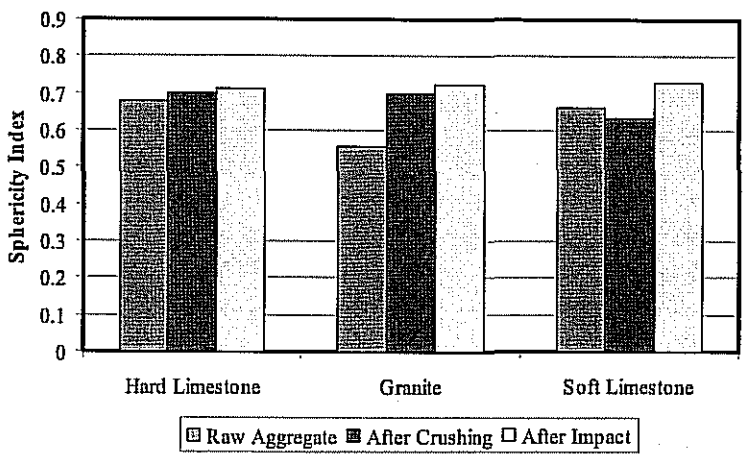

Figure 5.11 - Sphericity Index Change after Aggregate Impact Value and Aggregate Crushing Value Tests

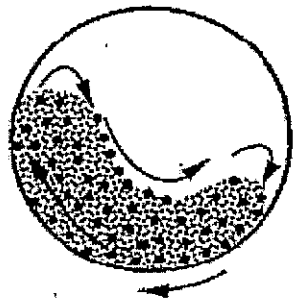

Figure 5.12 - Interaction between Aggregates and Steel Balls in Micro-Deval

The weight of the sample is measured before and after the test, and the percent loss is calculated as follow:

$$\text{Micro} - \text{Deval Weight Loss}\,(\%) = \frac{\text{Weight Before Test - Weight After Test}}{\text{Weight Before Test}} \times 100 \qquad (5.6)$$

The Micro-Deval results for the aggregate used in this study can be found in Table 3.2 from Chapter 3.

Table 5.5 - Gradation of Micro-Deval Sample According Tex-461-A for Bituminous Aggregates

Passing	Retained	Weight, g
12.5 mm (1/2 in.)	9.5 mm (3/8 in.)	750
9.5 mm (3/8 in.)	6.3 mm (1/4 in.)	375
6.3 mm (1/4 in.)	4.75 mm (No. 4)	375

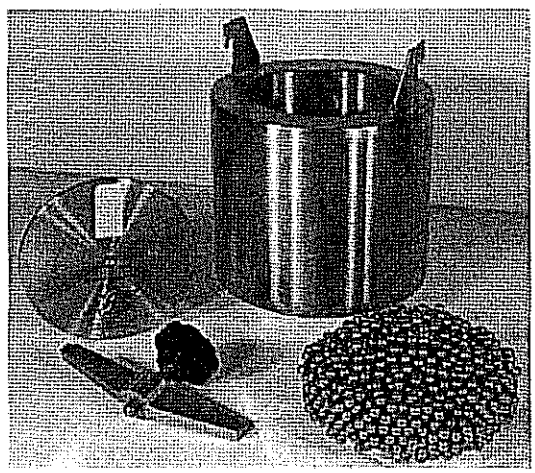

Figure 5.13 - Micro-Deval jar and Steel Balls (Gilson Company website)

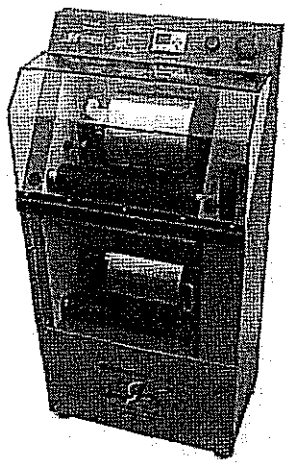

Figure 5.14 - Micro-Deval Machine (Gilson Company website)

The weight losses for the three aggregates from the standard Micro-Deval test are shown in Table 5.6.

Table 5.6 - Weight Losses from the Standard Micro-Deval Tests

Aggregate	Weight Loss,%
Hard Limestone	15.0
Granite	8.8
Soft Limestone	20.4

The soft limestone had the highest Micro-Deval weight loss, while the granite had the least weight loss. The aggregates were characterized using AIMS after the Micro-Deval test. Figures 5.15 and 5.16 show comparisons of angularity and texture respectively. The average indices of the three sizes were used in this comparison. The three aggregates lost some of their shape and texture. Both the soft and hard limestone aggregates lost considerable amount of texture, which was not the case for the granite. The three aggregates lost comparable percentages of angularity.

The method developed by Mahmoud (2005) was used to characterize the resistance of the three aggregates to polishing. In this method, the aggregate texture was measured after different polishing times in the Micro-Deval, and the results are shown in Figure 5.17. The texture versus polishing time is expressed using the relationship:

$$Texture(t) = a + b \times e^{-ct} \tag{5.7}$$

Where Texture (t) is the aggregate texture index at time t in minutes, a represents the terminal texture, (a + b) represents the initial texture, and c is a parameter that quantifies the rate of loss of texture. These parameters for the three aggregates are shown in Table 5.7. The hard limestone had an initial texture slightly less than the granite. However, the hard limestone lost considerable value of texture compared with the granite.

Table 5.7 - Equation Parameters for the Three Aggregates

Aggregate	a	b	c
Granite	178.69	39.02	0.01254
Hard Limestone	83.53	119.93	0.01987
Soft Limestone	39.13	37.46	0.02505

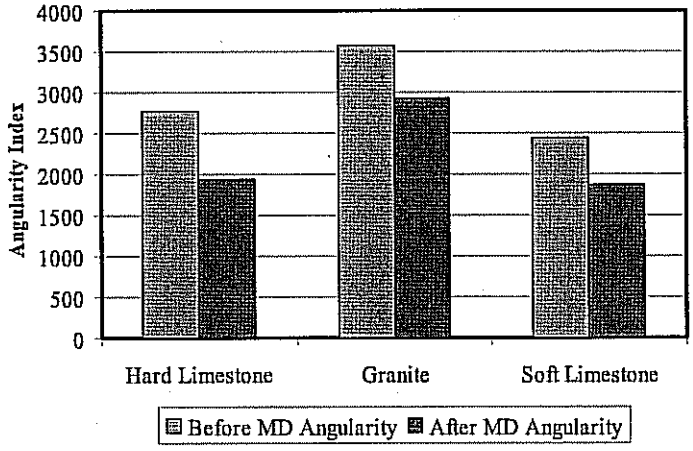

Figure 5.15 - Gradient Angularity Change in Micro-Deval

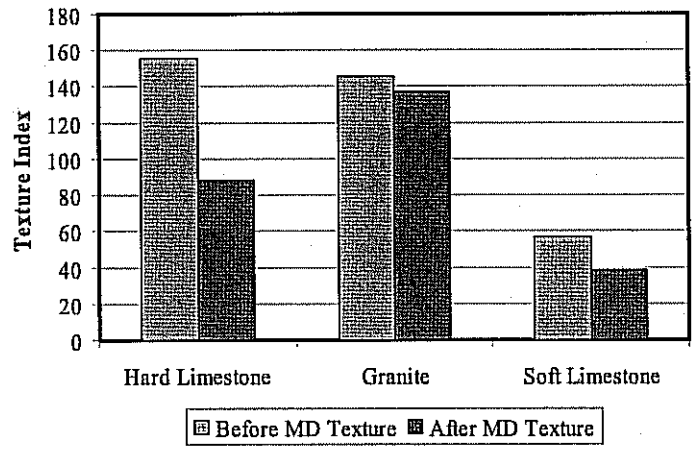

Figure 5.16 - Texture Index Change in Micro-Deval

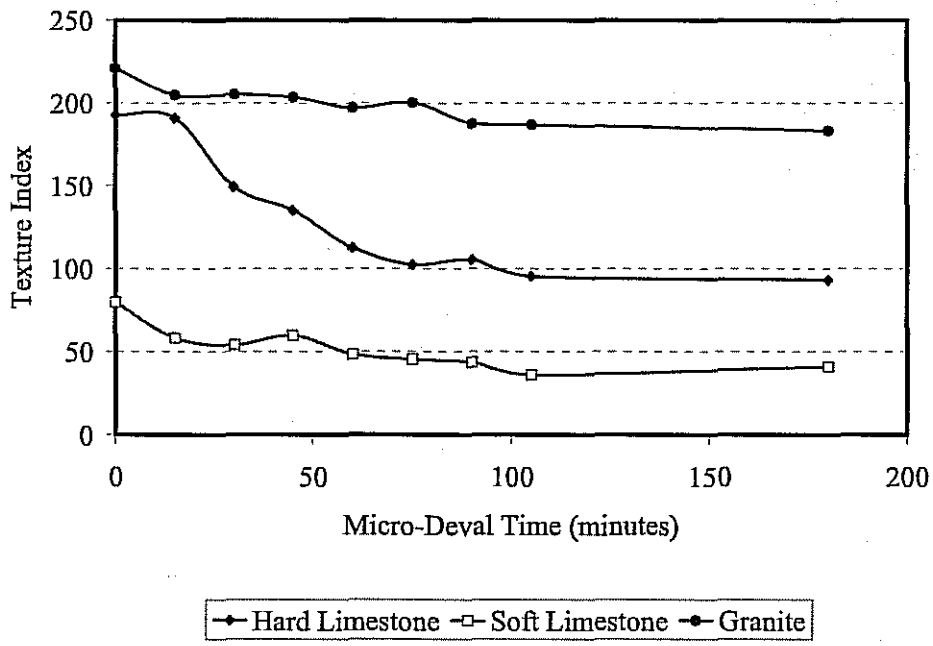

Figure 5.17 - Aggregate Texture as Function of Micro-Deval Time for all Mixes

Figures 5.18 through 5.20 show the percentage change of aggregate passing sieve size 3/8". The granite had more gradation change than the other two limestone aggregates. This finding agrees with the results of the ACV test which showed that the San Antonio limestone had a higher crushing modulus. Also, the soft limestone had more crushing than the hard limestone in all the cases. Cases with negative or zero change are considered as a result of the variability in the sieve analysis measurements. The results in Figures 5.18 through 5.20 indicate that some aggregates undergo breakage and crushing during the compaction, which may alter the produced mix design compared with the original laboratory design.

The difference in aggregate structure plays an important role in determining the forces that individual aggregates are subjected to within the mix structure. These forces can exceed the strength of aggregates in one structure but remain below the strength in a different structure. Testing aggregates does not provide sufficient information about the performance of an aggregate in a certain mix type or structure. Measuring the change in aggregate gradation due to compaction can be used in addition to tests on aggregates as a tool to investigate the influence of aggregate structure on crushing. Even if aggregates do not meet the allowable values based on aggregate tests, they can still be used if the change in gradation is minimized to acceptable limits. On the other hand, aggregates that meet the requirements of aggregate tests should still be evaluated for possible degradation in the mix, and should be avoided if proven to be susceptible for breakage.

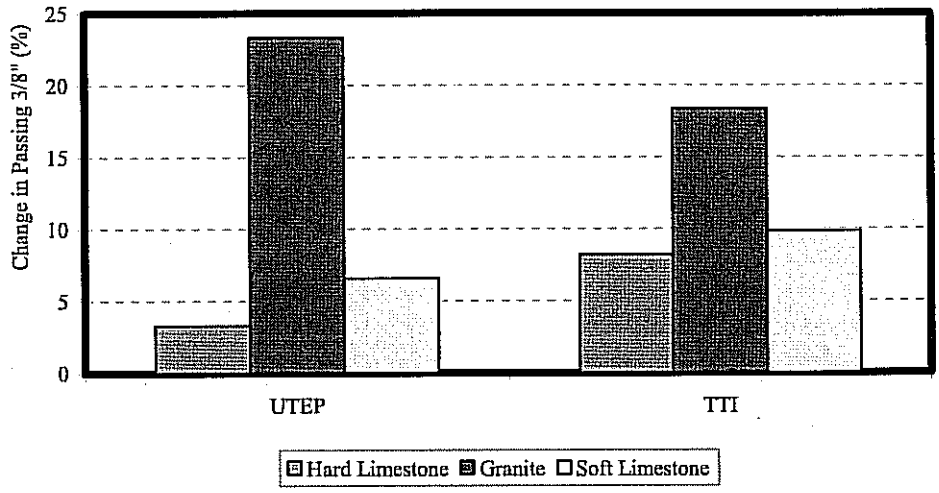

Figure 5.18 - Percentage Change of Aggregate Passing sieve size 3/8 in (CMHB-C)

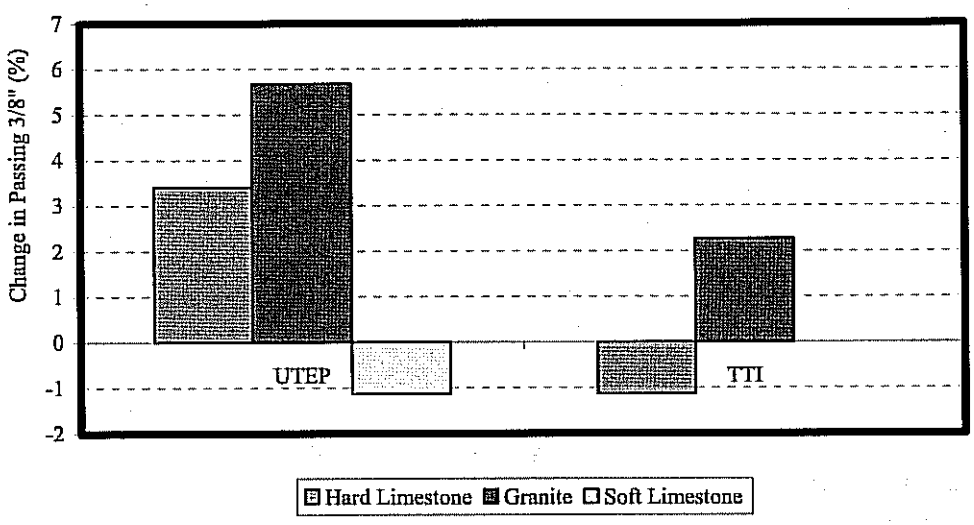

Figure 5.19 - Percentage Change of Aggregate Passing sieve size 3/8 in (Superpave-C)

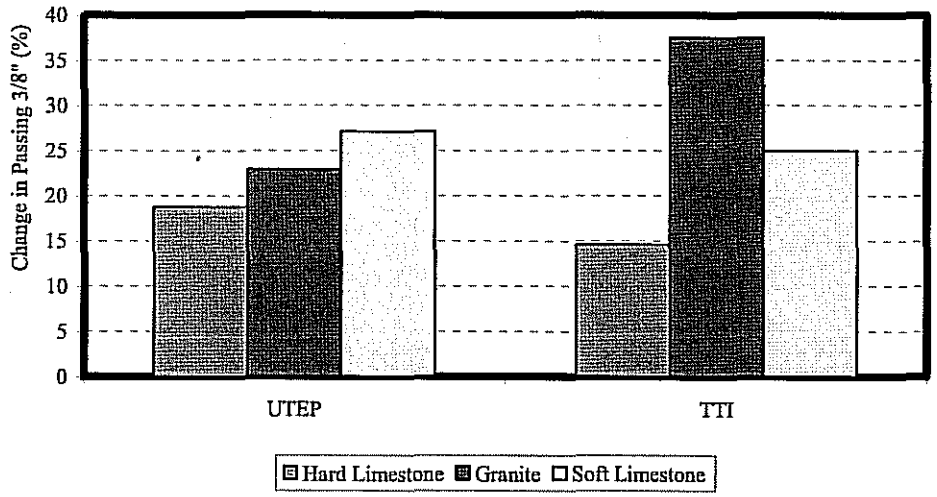

Figure 5.20 - Percentage Change of Aggregate Passing sieve size 3/8 in (PFC)

COMPRESSION TESTING OF INDIVIDUAL AGGREGATE PARTICLES

A single aggregate particle crushing was also performed. Fifty-six particles passing 0.5 in. sieve size and retained on sieve size 3/8" from each aggregate source were tested positioned vertically, and another fifty-six particles were tested positioned horizontally as shown in Figure 5.21. The averages of the results for each aggregate are shown in Figure 5.22 while Figures 5.23 and 5.24 show the distributions of results.

The vertically aligned aggregates had a higher resistance to load than the horizontally aligned ones. This is attributed to the fact that the aggregates were trimmed to have a flat surface for the vertical test. Cumulative distributions for the vertical and horizontal results are shown in Figures 5.25 and 5.26. The main trend in both figures is the fact that the hard limestone aggregates have higher percentages at higher ranges, as opposed to soft limestone aggregates which have higher percentages at lower ranges. These distribution data along with each individual aggregate result will be used to introduce variability of the aggregate properties in DEM; this will be done by calibrating aggregate properties for each single particle to match the experimental results.

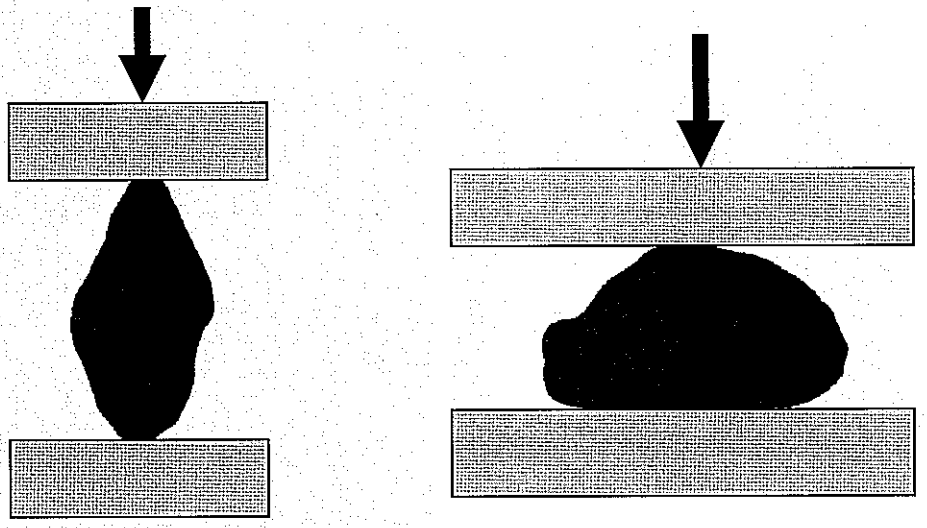

a) Vertically aligned aggregate b) Horizontally aligned aggregate

Figure 5.21 - Single Aggregate Crushing Set-up

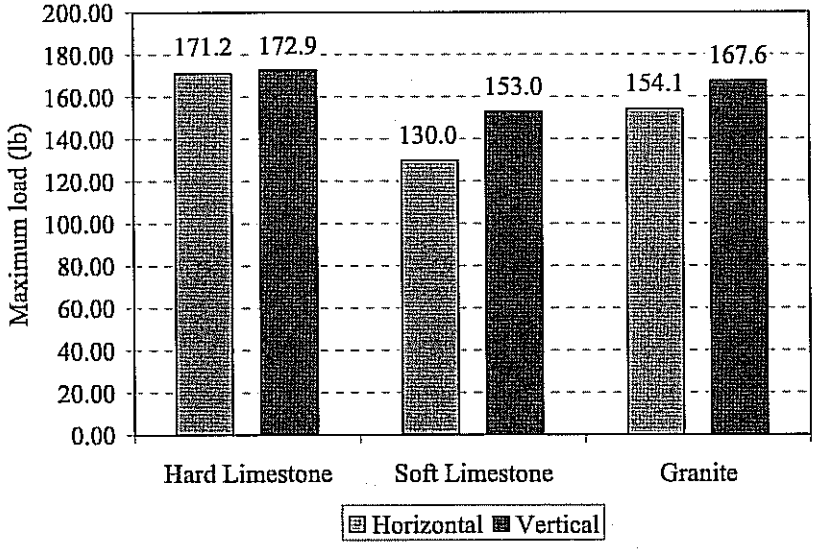

Figure 5.22 - Single Aggregate Crushing Results

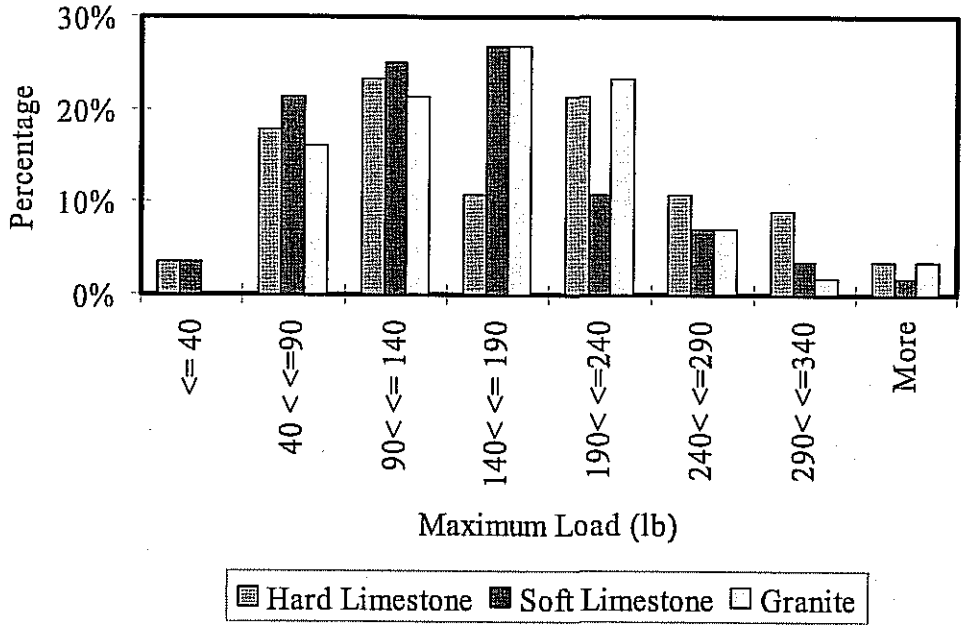

Figure 5.23 - Single Aggregate Crushing Results Distribution (Vertical)

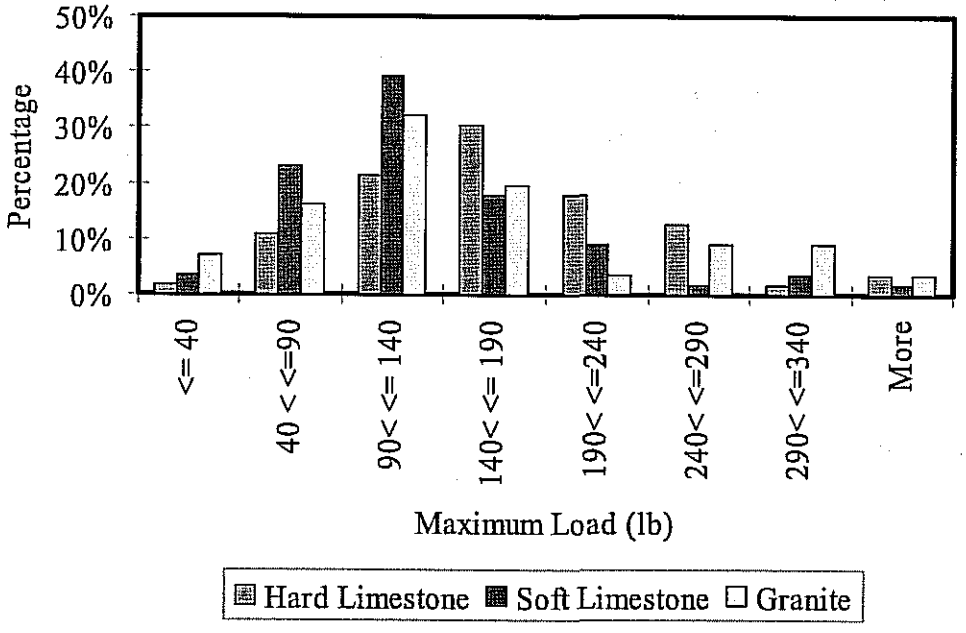

Figure 5.24 - Single Aggregate Crushing Results Distribution (Horizontal)

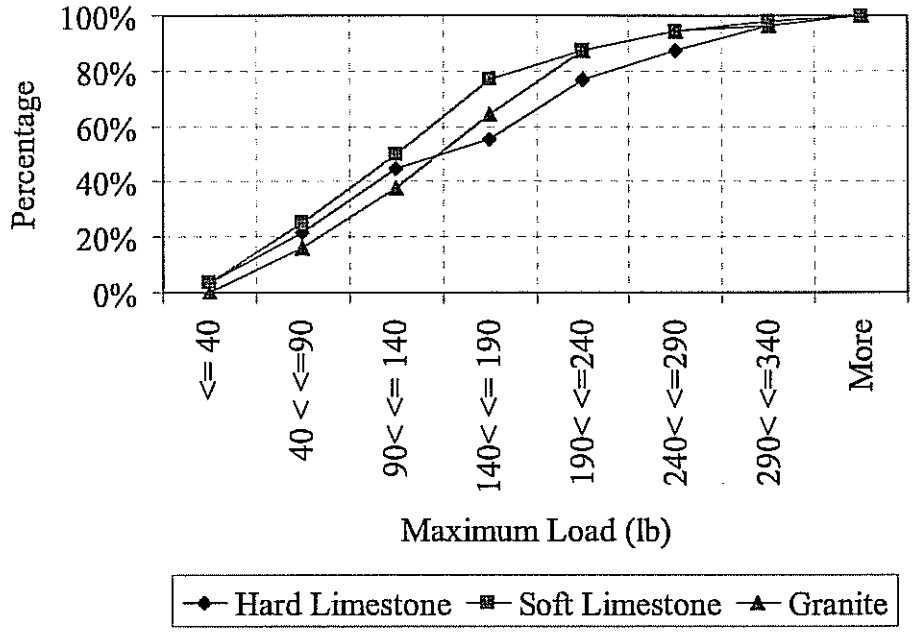

Figure 5.25 - Single Aggregate Crushing Cumulative Distribution (Vertical)

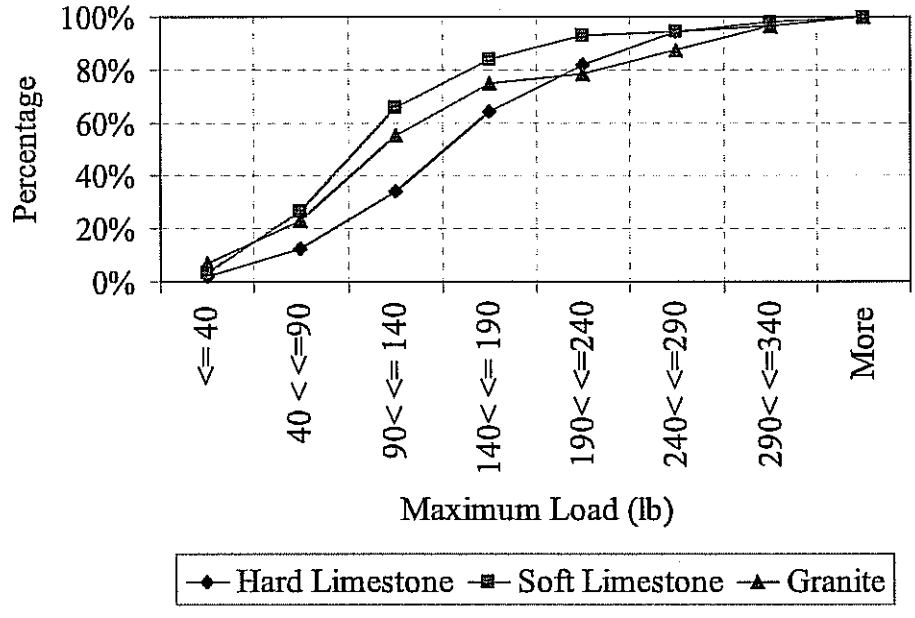

Figure 5.26 - Single Aggregate Crushing Cumulative Distribution (Horizontal)

CHAPTER SIX - PROPERTIES OF ROCK MASSES

INTRODUCTION

A series of strength and stiffness tests were carried out on specimens retrieved from bulk rock samples to characterize the aggregate quality from the properties of its original rocks. This information was needed for the micromechanics models as well. A brief description of each test process is presented in this chapter.

SPLITTING TENSILE TEST

The splitting tensile tests on cores from rock masses retrieved from quarries were carried out to determine the potential tensile crushing strength of the aggregates. In this study, cylindrical rock specimens were tested following a protocol similar to Tex-421-A. Split tensile strength is a measure of a material's ability to resist a diametric compressive force.

Rock core samples were first extracted from bulk rocks and cut to 2.3-in. diameter by 2-in. height. The samples' dimensions were intentionally kept smaller than standard so that the specimen can be forced to fail in a crushing mode similar to an aggregate. Each sample was then placed and centered with its axis placed horizontally between the platens of a compression-testing machine as shown in Figure 6.1. Once in place, a continuously increasing compressive load was applied to the test specimen until splitting or rupture occurred. This load was applied at a nominal constant rate of loading of 250 psi per minute such that failure would occur within 1 to 10 min. of loading. At least 2 to 3 specimens were tested to obtain an average value when possible. Because of its internal structure, it was impossible to obtain adequate number of cores from the soft limestone.

As shown in Table 6.1, the average tensile strengths were about 1400 psi, 1050 psi and 700 psi for the hard limestone, granite and soft limestone, respectively. The typical coefficient of variation for this test seems to be about 20%, which is reasonable given the variability in the rock specimens.

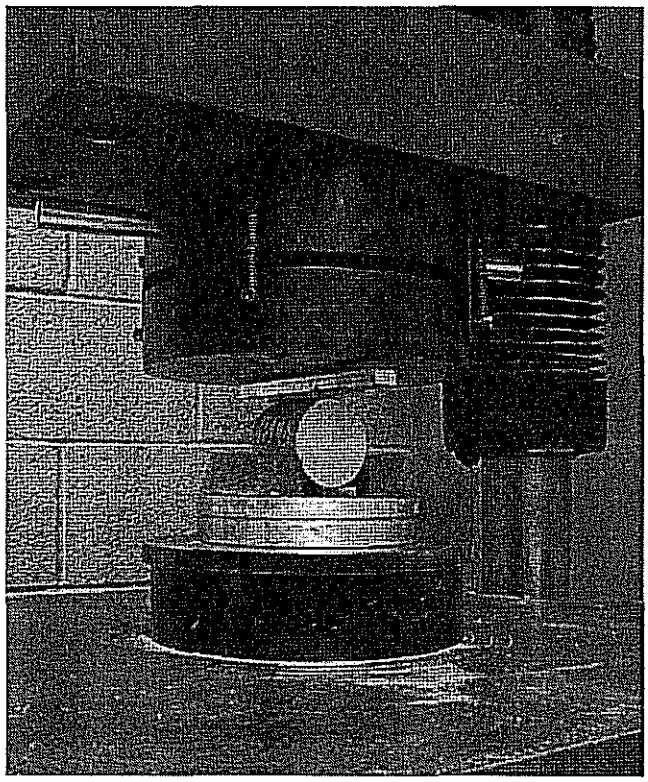

Figure 6.1 - Indirect Tensile Test

Table 6.1 - Summary Results of IDT and Compressive Strength Tests

Material	Strength, psi	
	Compressive	Tensile
Hard Limestone	10427 *(38%)**	1412 *(20%)*
Granite	14034 *(7%)**	1062 *(23%)*
Soft Limestone	6970 *(8%)**	682 *(-)***

** - Numbers in the parentheses are the coefficient of variation from triplicate tests.*
** - only one specimen was tested for the soft limestone

COMPRESSIVE STRENGTH TEST

For the purpose of this project, cylindrical rock specimens were tested in a similar manner to Tex-418-A to determine the unconfined compressive crushing strength of the drilled rock cores. Rock cores similar to those for the indirect tensile tests extracted from bulk rocks were used. Each sample was then placed and centered in the compression-testing machine as shown in Figure 6.2. Once in place, the load was then continuously increased on the specimen until crushing failure occurred. The average values of 2 to 3 samples were taken to obtain a representative compressive strength.

Table 6.1 also includes the results from the compressive strength tests. Contrary to the indirect tensile strength test results, the granite was the strongest in compression with a value of about 14,000 psi, followed by the hard limestone with strength of about 10,000 psi. The weakest rock was still the soft limestone with strength of about 7,000 psi.

One significant finding of this study is that both the compressive and tensile properties of rocks are needed in order to judge the potential crushing of aggregates. For example, even though the granite is considered as a very strong aggregate, it did not fare as well as the hard limestone in crushing and impact tests described in Chapter 5. This can be explained by the fact that the tensile strength of the granite is lower than the hard limestone because of the coarse crystals embedded in the rock mass.

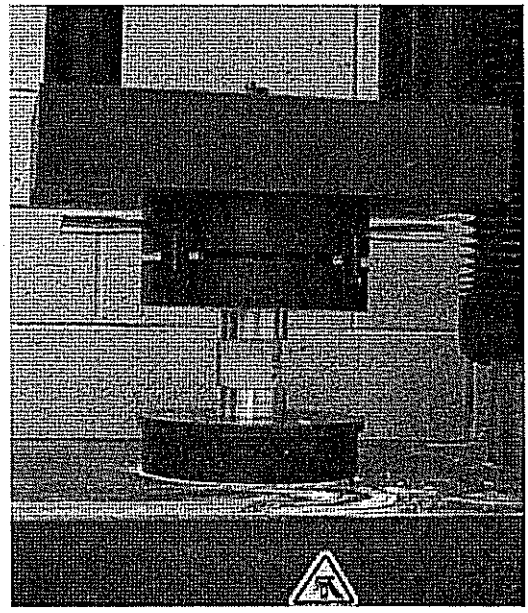

Figure 6.2 - Compressive Strength Test

SCHMIDT HAMMER

A Schmidt hammer was also used to estimate the rock compressive strength. The Schmidt hammer test (Tex-446-A), consists of a spring-loaded mass that is released against a plunger when the hammer is pressed onto a hard surface. The plunger impacts the surface and the mass recoils; the height of piston rebound is called the rebound number (R) and is measured either by a sliding pointer or electronically.

To operate, the impact plunger is placed perpendicular to the surface of the rock and pressure is applied until the plunger is fully depressed as shown in Figure 6.3; the hammer will then release. The pushbutton on the hammer is then pressed to lock the impact plunger after every impact in order to read the rebound value R indicated by the pointer on the hammer. Scale pointer reading gives rebound value in percent of the forward movement of the hammer mass. Each surface should be tested with at least 8 to 10 impacts. The individual impact points must be spaced at least 0.8 inches apart. Once the average of the 8-10 rebound values is determined, a calibration

curve is used to determine the average compressive strength based on the average rebound value R (see Figure 6.4).

The compressive strengths obtained from this method are shown in Table 6.2. The compressive strengths are surprisingly close to those obtained from the compression tests in Table 6.1. Since this method can be used both in the laboratory and in the field, and since little sample preparation is required to perform the test, the rebound test may be an excellent test for characterizing the quality of rock masses in compression.

Figure 6.3 - Schmidt Hammer Test Method

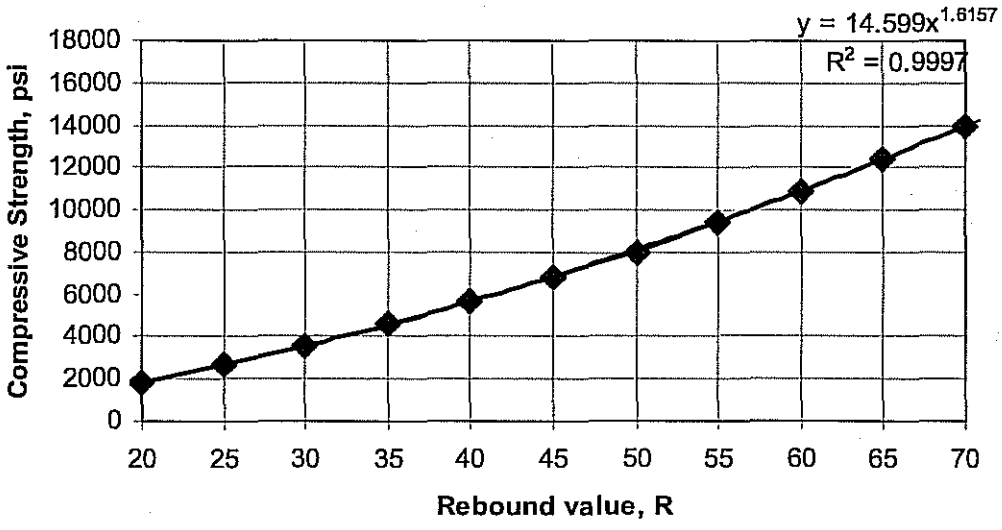

Figure 6.4 - Conversion Curve for the Schmidt Hammer Test

Table 6.2 - Summary Results of the Schmidt Hammer Test

Material	Rock Sample	Rebound Number after 10 trails	Average Rebound Number	Compressive Strength, psi**	
				Schmidt Hammer Test	Compressive Strength Test
Hard Limestone	1	54	56 *(4%)**	9719	10427
	2	57			
	3	57			
Granite	1	65	64 *(2%)**	12034	14034
	2	64			
	3	62			
Soft Limestone	1	52	46 *(16%)**	6994	6970
	2	38			
	3	47			

** - Numbers in the parentheses are the coefficient of variation from triplicate tests.*

*** - According to the manufacturer, the average compressive strength is subjected to a ±1000 psi dispersion*

MODULUS OF ROCK

Young's modulus, sometimes referred to as modulus of elasticity, is the measure of a material's resistance to strain and is an extremely important characteristic of a material's stiffness. Seismic and ultrasonic methods can be used to nondestructively estimate such characteristics. Nondestructive testing (NDT) techniques based on seismic and ultrasonic testing are used to estimate the modulus of most very stiff materials because of its ease and repeatability. Two such methods were used here to determine the modulus of rock mass.

Free-Free Resonant Column

The Free-Free Resonant Column (FFRC, Tex-147-E, draft) consists of an instrumented hammer, an accelerometer, and a waveform analyzer. The basic operational principle is to induce an excitation at one end of the specimen and monitor the response of the specimen at the other end. The specimen is placed on its sides on a sheet of Styrofoam insulation, and an accelerometer is affixed to one end of the sample. As shown in Figure 6.5, a hammer instrumented with a load cell is used to lightly tap the other end to generate and measure compression wave velocity in the specimen. The computer display of the measured wave response shapes as shown in Figure 6.6 is used to determine the Young's modulus based on the sample mass and dimensions.

The moduli determined for the three rocks used in this study are included in Table 6.3. These tests were performed on 2.3 in. diameter cores from rock masses before they were cut for compressive or tensile strength tests. The hard limestone exhibited an average modulus of about 10,000 ksi and granite a modulus of about 7,500 ksi. Once again, the granite is less stiff because of the large crystals embedded within the rock. An intact specimen could not be retrieved from the soft limestone.

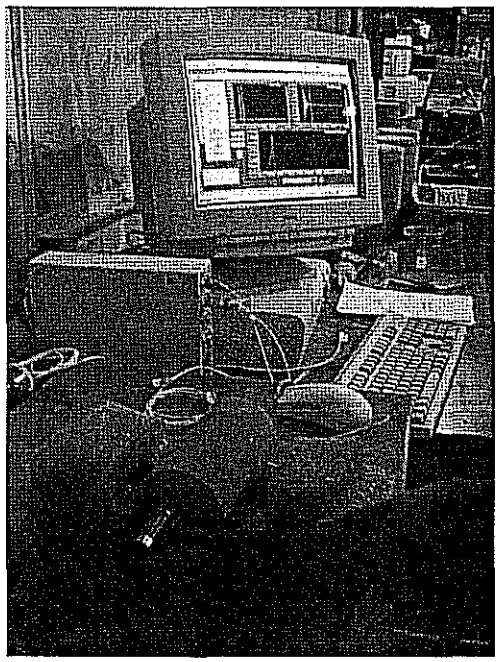

Figure 6.5 - Free-Free Resonant Column

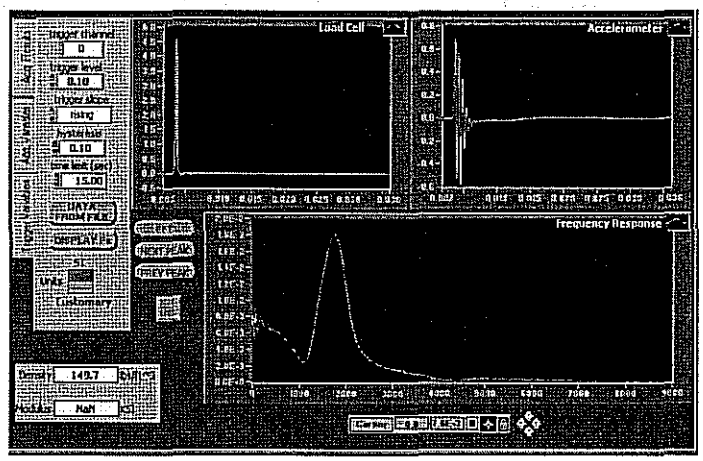

Figure 6.6 - Computer Display of FF-RC Results

Ultrasonic Testing

Ultrasonic testing (Tex-254-F, draft) is a NDT method that is used to obtain the properties of materials by measuring the time of travel of stress waves through a solid medium. The time of travel of a stress wave can then be used to obtain the speed of sound or acoustic velocity of a given material. The velocity of an ultrasonic pulse through a material is a function of the elastic modulus and density of the material.

The V-meter is an ultrasonic device that measures the travel time of compressive waves by means of electric impulses. In this device, a transmitting transducer is securely placed on the top face of the specimen as shown in Figure 6.7. The transducer is connected to the built-in high-voltage electrical pulse generator of the device. The electric pulse transformed to mechanical vibration is coupled to the specimen. A receiving transducer is then placed on the bottom face of the specimen, opposite the transmitting transducer. The receiving transducer, which senses the propagating waves, is connected to an internal clock of the device. The clock automatically displays the travel time of the compression wave. By dividing the length of the specimen by the travel time, the compression wave velocity and as such modulus of the material is determined. In this case, the two opposite faces of each rock mass was made smooth using a band saw. No coring is required for this test. About ten tests were carried out on each rock mass.

Table 6.3 includes the moduli measured with the ultrasonic device. The average moduli for the hard limestone, granite and soft limestone are about 10,500 ksi, 7,000 ksi and 5,500 ksi. Once again, the FFRC and ultrasonic moduli of the granite and hard limestone are quite similar. Based on this study, the ultrasonic device may be a more versatile tool for determining the moduli of rock masses.

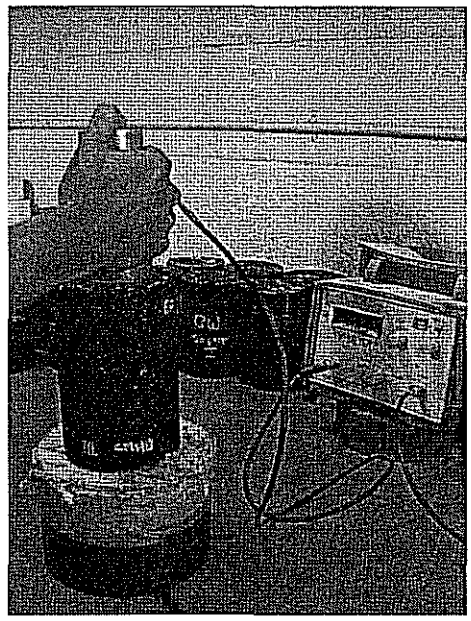

Figure 6.7 - V-Meter Test Set up

Table 6.3 - Results of V-Meter and FFRC Tests

Material	Modulus, ksi	
	FFRC	V-Meter
Hard Limestone	10299 *(6%)**	10328 *(13%)**
Granite	7440 *(15%)**	6686 *(6%)**
Soft Limestone	*(-)***	5473 *(11%)**

** - Numbers in the parentheses are the coefficient of variation from triplicate tests.*
*** - no FFRC was obtained for this specimen*

CHAPTER SEVEN - CHARACTERIZATION OF AGGREGATE INTERACTION

INTRODUCTION

The coarse aggregate strength is traditionally estimated indirectly by well known tests including the Los Angeles abrasion test, the hardness and soundness tests, the aggregate crushing value test, etc. Although these indirect test methods provide some information about the aggregate quality, there is still a need to characterize the interaction within the aggregates. The direct shear test and the triaxial compression test methods were utilized to evaluate this interaction. The results of these tests are particularly of interest in calibrating the micro-mechanics models described in the future chapters.

DIRECT SHEAR TEST

The procedure specified in ASTM D3080 was used to perform the direct shear tests. The sample used for this test was air dried and placed in a direct shear box as shown in Figure 7.1. A 6-in. diameter direct shear test box was retrofitted into a conventional device for use with larger and coarser aggregate materials used in this project.

The procedure to conduct this test included drying enough material in the oven at a temperature of 220°F and then letting it cool to room temperature. The coarse portion of the material was then placed in the mold of the direct shear device in three layers, and each layer was rodded 25 times to ensure compaction. Each specimen was subjected to sieve analysis before and after testing to determine the crushing of aggregates due to compaction and shearing. Normal stress was first applied to the sample. Shear stress was gradually increased until the sample failed in shear along a predefined horizontal plane with a horizontal speed of 0.05 in/min.

Triplicate tests were performed on the coarse aggregates at a normal stress of 20 psi. Since the goal was to study the interaction of the aggregates, tests were repeated for the CMHB-C, Superpave-C and PFC separately. Figure 7.2 illustrates typical results for this test method. The horizontal stress-horizontal strain curve and the variation in vertical strain with horizontal strain for each specimen were developed. Relevant information, such as the peak strength, horizontal strain at peak strength, the maximum vertical expansion, and the vertical strain at peak strength, was extracted to evaluate the grain-to-grain strength of the mixtures. These parameters are summarized in Table 7.1.

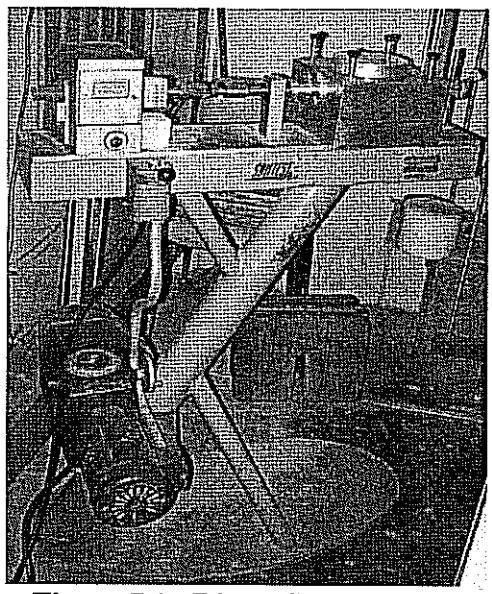

Figure 7.1 - Direct Shear Device

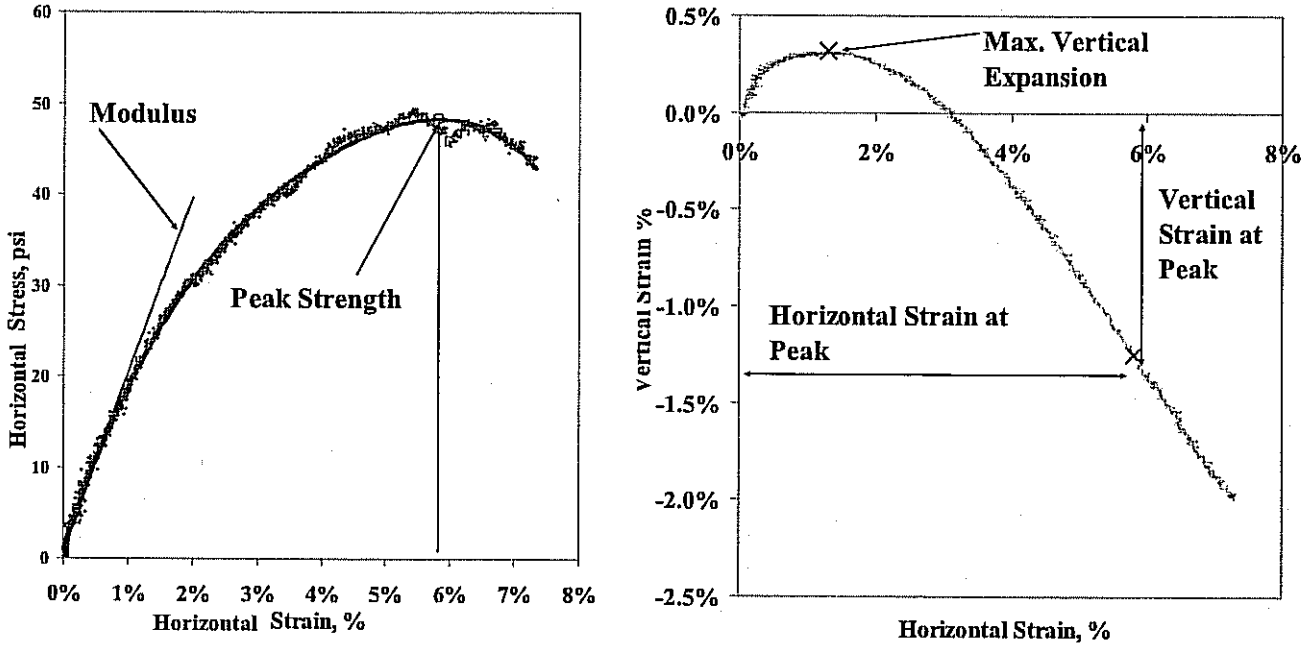

a) Horizontal Stress vs. Horizontal Strain Plot **b) Vertical Strain vs. Horizontal Strain**

Figure 7.2 - Typical Results from Direct Shear Tests

The nine mixes yielded similar dry unit weights, ranging from 90 pcf to 95 pcf (see Table 7.1). The PFC mixes from all three aggregate sources yielded unit weights that were 2 to 3 pcf less than the other two mixes because of the uniformity in the coarse aggregate gradation.

Table 7.1 - Summary Results for the Direct Shear Test

Aggregate Source	Mix Type	Dry Unit Weight, pcf*	Modulus, psi	Peak Strength, psi	Strain at Peak Strength, %		Max. Vertical Expansion, %	Φ
					Horizontal	Vertical		
Hard Limestone	CMHB-C	92 *(0%)*	2207 *(15%)*	55 *(4%)*	6.5 *(10%)*	1.6 *(20%)*	0.3 *(16%)*	70°
	Superpave-C	93 *(1%)*	1699 *(8%)*	45 *(6%)*	6.5 *(9%)*	1.3 *(36%)*	0.4 *(6%)*	67°
	PFC	90 *(1%)*	1827 *(5%)*	50 *(7%)*	6.0 *(3%)*	1.0 *(38%)*	0.3 *(10%)*	68°
Granite	CMHB-C	94 *(0%)*	1907 *(13%)*	44 *(5%)*	6.6 *(10%)*	0.8 *(53%)*	0.4 *(10%)*	66°
	Superpave-C	94 *(0%)*	1717 *(5%)*	40 *(7%)*	6.4 *(10%)*	0.7 *(42%)*	0.5 *(19%)*	63°
	PFC	91 *(0%)*	1856 *(4%)*	43 *(5%)*	6.0 *(10%)*	0.9 *(22%)*	0.3 *(14%)*	65°
Soft Limestone	CMHB-C	94 *(1%)*	1924 *(5%)*	46 *(2%)*	5.8 *(3%)*	1.6 *(39%)*	0.3 *(44%)*	67°
	Superpave-C	95 (1%)	2037 *(17%)*	45 *(10%)*	6.4 *(10%)*	1.7 *(6%)*	0.2 *(27%)*	66°
	PFC	92 *(4%)*	1873 *(4%)*	48 *(2%)*	7.0 *(9%)*	1.0 *(40%)*	0.5 *(27%)*	67°

** - Numbers in the parentheses are the coefficient of variation from triplicate tests.*

The absolute values of the moduli obtained from the direct shear tests are generally not considered reliable because of the size and rigid boundaries of the shear box and because of high strains applied to the specimen. However, they may provide some relative information with regard to the initial shear resistance to the applied loads. The range in the measured moduli is reasonably small varying from about 1,700 psi to about 2,200 psi (see Table 7.1). For the granite and the hard limestone, the Superpave-C mixes exhibit the lowest moduli. But for the soft limestone, the PFC mix exhibits the lowest modulus.

The peak strengths for the nine blends vary from 40 psi to 55 psi (see Table 7.1). The hard limestone generally provides the highest peak strength, while the granite the lowest. For the hard limestone, the impact of gradation on the peak strength is pronounced. The Superpave-C mix for the hard limestone exhibits the lowest peak strength, since the Superpave-C gradation contains smaller particles causing the least amount of grain-to-grain contact. The CHMB-C mix with hard limestone provides the most resistance to shearing due to a good interlocking between the aggregates. The PFC with hard limestone, which practically contains a coarse aggregates matrix, has the lowest peak strength, perhaps because of the lack of fines to form a stable internal structure.

The peak strengths of the three mix types for the soft limestone are similar, since they vary between 45 psi and 48 psi. In this case, the lack of strength of the aggregates dominates the peak strength, with the gradation having a secondary effect on the peak strength of the blends. In other words, the individual aggregates "break" instead of resisting the external shearing forces.

The peak strengths of the three mix types for granite provides a pattern that is similar to the hard limestone. However, the variation in peak strength between the three mix types is only about 4 psi. The granite aggregates were stronger than hard limestone in compression, but were weaker in tension. Therefore, the gradation affects the strength of the mix when the grain-to-grain interaction is in compression. But due to weak aggregate tensile strength, the breakage may dominate when the grain-to-grain interaction is in tension.

In general, the peak strength of a blend is impacted by the gradation and the strength of the coarse aggregates. Both parameters should be considered together in quantifying the strength of a blend. We will revisit this interaction in Chapter 9 when the micro-mechanical models are described.

During shearing, a densely-compacted specimen first exhibits a vertical expansion followed by a vertical contraction, as shown in Figure 7.2b primarily due to the reorientation and crushing of aggregates. The initial expansion occurs because of the "rolling" of the individual particles on top of each other. These values are similar for the three aggregate sources. At this point, the maximum expansion strain may not be a parameter that can be used to quantify the interaction of aggregates.

The vertical contraction at higher horizontal strains may be due to the crushing of aggregates or densification due to the reorientation of the aggregates. These values are fairly similar and not very repeatable (see COV values for this parameter in Table 7.1).

The angles of internal friction obtained from the direct shear tests are also included in Table 7.1. The trend is very similar to that from the peak strength. However, it may be easier to use the angle of internal friction than strength in day-to-day operations of TxDOT.

The percent aggregates passing the No. 8 sieve after the compaction and shearing are shown in Table 7.2. The crushing of aggregates is minimal indicating that higher vertical loads should be applied in the future. Higher vertical loads during testing will accentuate the breakage of the aggregates by restricting the reorientation of them.

Table 7.2 - Sieve Analysis after Compaction and Shearing

Material	Type	Avg. Percentage Passing No. 8 Sieve, %	COV, %
Hard Limestone	CMHB-C	0.6	*4*
	Superpave-C	0.8	*8*
	PFC	0.8	*4*
Granite	CMHB-C	0.7	*13*
	Superpave-C	0.8	*19*
	PFC	0.7	*9*
Soft Limestone	CMHB-C	0.9	*5*
	Superpave-C	1.2	*10*
	PFC	1.1	*1*

TRIAXIAL TEST

For a standard triaxial test, in accordance with Tex-143-E, several 6-in. diameter by 8-in. high samples were prepared at the optimum moisture content and then compacted. The set up is shown in Figure 7.3. The specimens are encased in two rubber membranes, placed between two porous stones, and allowed to mature for at least 24 hours before testing. Each sample is then tested in compression in the triaxial cell under an increasing load of 1% strain per minute while the stress-strain diagram of material is recorded. The results from different confining pressures can be used to draw the Mohr circles and develop the Mohr-Coulomb failure surface to evaluate the optimal stress ratios that the material can handle before experiencing failure as illustrated in Figure 7.4. The end results of the test are the angle of internal friction, cohesion and the classification.

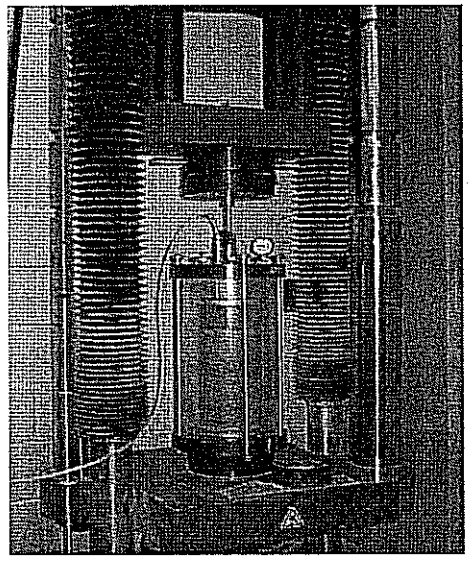

Figure 7.3 - Schematic of Triaxial Compressive Tests

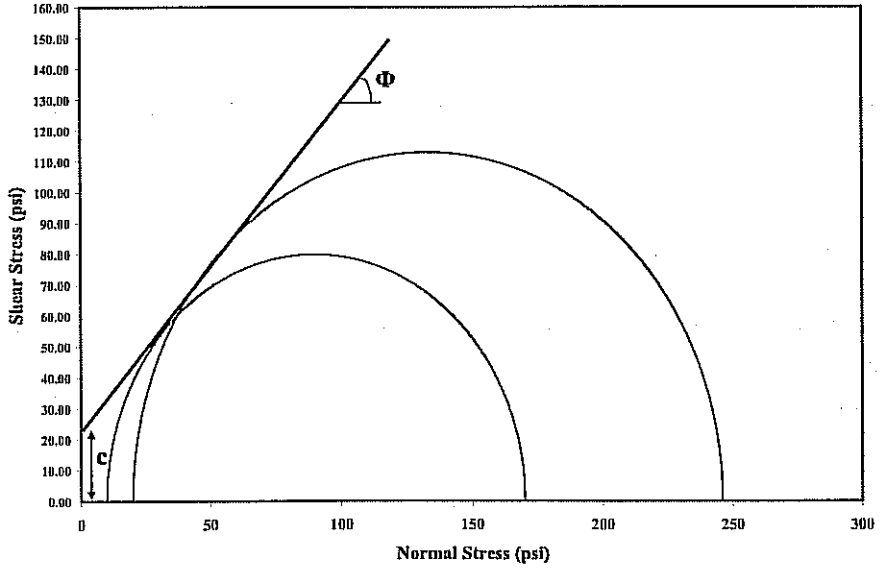

Figure 7.4 - Typical Mohr Diagram

Typical results for this test are provided in Figure 7.5. Strength parameters, such as the peak strength, residual strength, modulus and strain at peak strength were measured. Triaxial tests could not be carried out on the PFC mixes. Since the PFC blend simply contains almost all coarse aggregates, the specimens were not stable when removed from the mold. More advanced sampling processes may be needed in the future.

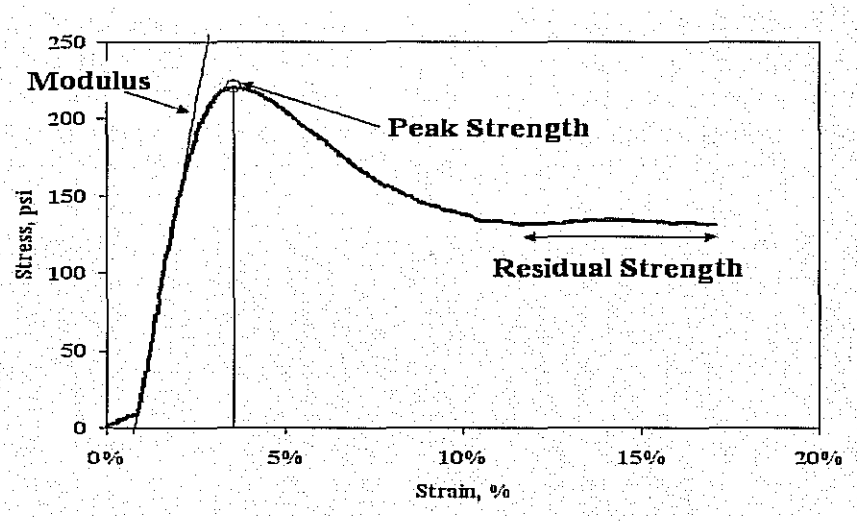

Figure 7.5 - Typical Results for the Triaxial Test

The variations in the dry unit weights for different mixes are included in Table 7.3. These specimens were prepared as per Tex-113-E using a drop hammer. As such, these unit weights are greater than those reported in Table 7.1 for direct shear tests. The specimens for the direct shear tests were prepared using the rodding technique. The Superpave-C mixes consistently yielded higher dry unit weights as compared to the CMHB-C mixes. This occurs because of the finer gradation associated with the Superpave-C mixes. Even though the moduli from these tests are reported in Table 7.3, their validity as a parameter is in doubt and is not considered any further.

The peak strengths were higher for the Superpave-C mixes as compared to the CMHB-C gradations for all three aggregate sources. For the Superpave-C mixes, the hard limestone exhibited the highest shear strength with the granite providing the lowest. For the CMHB-C mixes, the hard limestone's peak strength was less than the other two aggregates.

Because of high strains involved during the construction of a mat, the residual strengths are better indicators of the behavior of a material. For all CMHB-C mixes, the residual and peak strengths are close to one another. On the contrary, large reductions in the residual strengths are observed for the Superpave-C mixes. This indicates that the coarse aggregate skeletons of the CMHB-C mixes are more stable than the Superpave-C mixes. As such, the Superpave-C mixes rely more on the binder properties than the CMHB-C mixes.

The cohesions and angle of internal frictions are also reported in Table 7.3 for completeness. The angles of internal friction in this table are different than those in Table 7.1 for direct shear tests simply because the densities were different as discussed above. The trends are hard to.

Table 7.3 - Summary Results for Triaxial Compression Test

Material	Type	Dry Unit Weight, pcf	Modulus, psi	Peak Strength, psi	Residual Strength, psi	Strain at Peak Strength, %	Cohesion, psi	Angle of Internal Friction
Hard Limestone	CMHB-C	145 *(2%)**	6953	149 *(13%)**	130 *(23%)**	5.5	23	40°
	Superpave-C	152 *(2%)**	10945	241 *(6%)**	155 *(2%)**	4.5	7	59°
Granite	CMHB-C	134 *(0%)**	11670	186 *(5%)**	159 *(24%)**	4.0	11	53°
	Superpave-C	146 *(3%)**	12286	208 *(9%)**	138 *(4%)**	3.2	22	49°
Soft Limestone	CMHB-C	142 *(1%)**	15955	198 *(3%)**	178 *(1%)**	4.9	12	54°
	Superpave-C	150 *(1%)**	9344	226 *(2%)**	148 *(5%)**	4.3	17	53°

** - Numbers in the parentheses are the coefficient of variation from triplicate tests.*

interpret because the results from only two confining pressures of 10 psi and 20 psi were available. In the future, more confining pressures should be used.

CHAPTER EIGHT - STIFFNESS AND STRENGTH OF MIXES

COMPACTIVE EFFORTS

Two different compactive efforts for preparing the lab specimens were used. A set of specimens was compacted to achieve a nominal in-place air void content of 7% (20% for PFC) while another set was prepared to 250 revolutions to evaluate the potential of crushing in the aggregate due to compaction. Once compacted, the lab specimens were tested to characterize the HMA performance using the Hamburg wheel tracking device, indirect tensile test, dynamic modulus test, and flow test.

The number of revolutions to achieve the locking point was also investigated. The numbers of revolutions to lock points and to achieve the in-place air void contents for all mixes are shown in Table 8.1. For the Superpave-C mixes (the finest mixes), about 25 gyrations were needed to achieve 7% air voids for the soft limestone and granite mixes, while about 50 gyrations were needed for the hard limestone mixes. About 44 to 49 gyrations were needed to achieve 7% air voids for the CMHB-C mixes (the intermediate gradation). For the PFC mixes (the coarsest mix) about 70 to 95 gyrations were needed to achieve air voids of 20%. Therefore, as the mixes got coarser in gradation more effort was needed to achieve the desired air voids (densities). None of the mixes required more gyrations that their corresponding locking points. After 250 gyrations, the air void contents were about 3% to 5% less than the corresponding nominal air void contents.

Table 8.1 – Number of Gyrations for Nominal In-place Air Voids, Locking Point

Material	Mix Type	Number of Gyrations to In-place Air Voids*	Number of Gyration to Locking Point	Average Air Void Content after 250 Gyrations, %
Hard Limestone	CMHB-C	44	124	5.2
	Superpave-C	50	99	4.0
	PFC	70	130	17.0
Granite	CMHB-C	49	127	2.8
	Superpave-C	25	94	3.5
	PFC	85	151	17.7
Soft Limestone	CMHB-C	48	125	2.1
	Superpave-C	24	86	4.6
	PFC	94	163	15.7

*** 7% for CMHB-C and SuperPave-C and 20% for PFC**

X-Ray CT

X-Ray CT is used to investigate the air void distribution within each sample; this tool helps in knowing how the air void changes with the height as well as comparing the air void between different mixes. Figures 8.1 through 8.3 show the air void distribution with height in the three mixes, for the hard limestone, soft limestone, and the granite aggregates, respectively. The PFC mix has the higher air voids for the three aggregates, while the CMHB-C and Superpave-C both have comparable air void distributions. This agrees with the original mix design. To compare the effect of aggregate on the air void distribution for each mix, Figures 8.4, 8.5, and 8.6 are generated (Superpave-C, CMHB-C, and PFC), and it shows that each of the three mixes were consistent within the different aggregate types. At each height, an X-Ray image is analyzed to obtain the area of air voids at that specific height; the calculated air void divided by the cross sectional area of the image gives the percent air void for that image i.e. air void content at that specific height. .

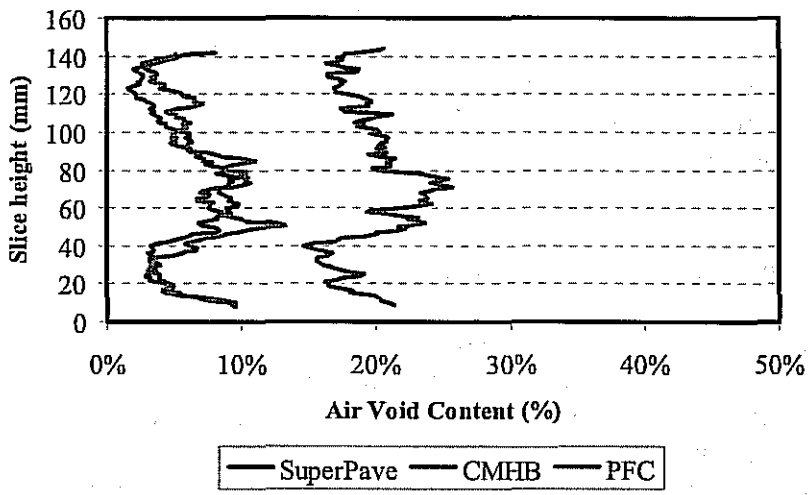

Figure 8.1 - Air Void Distribution among the Three Mixes (Hard Limestone)

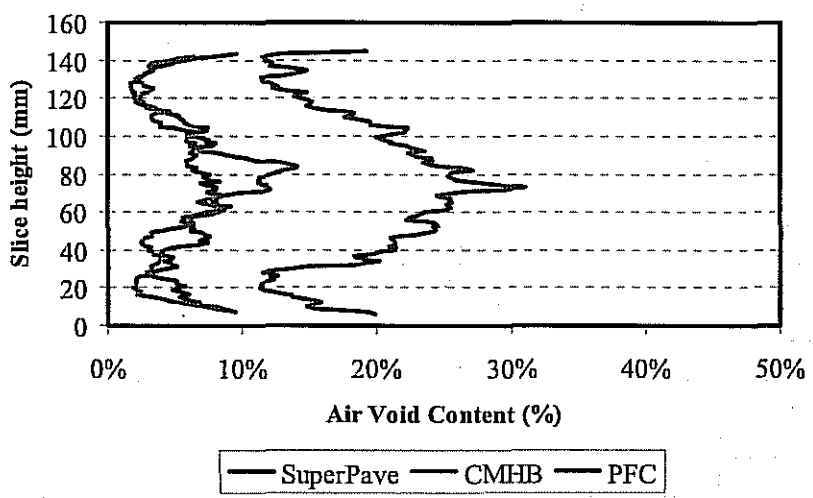

Figure 8.2 - Air Void Distribution among the Three Mixes (Soft Limestone)

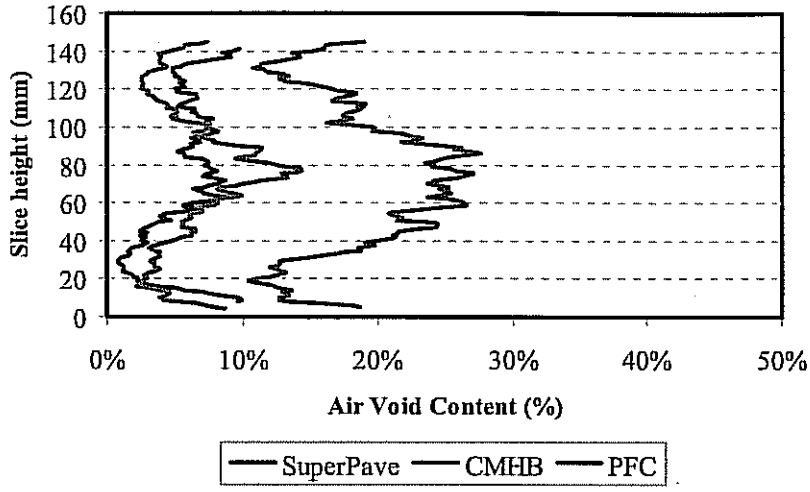

Figure 8.3 - Air Void Distribution among the Three Mixes (Granite)

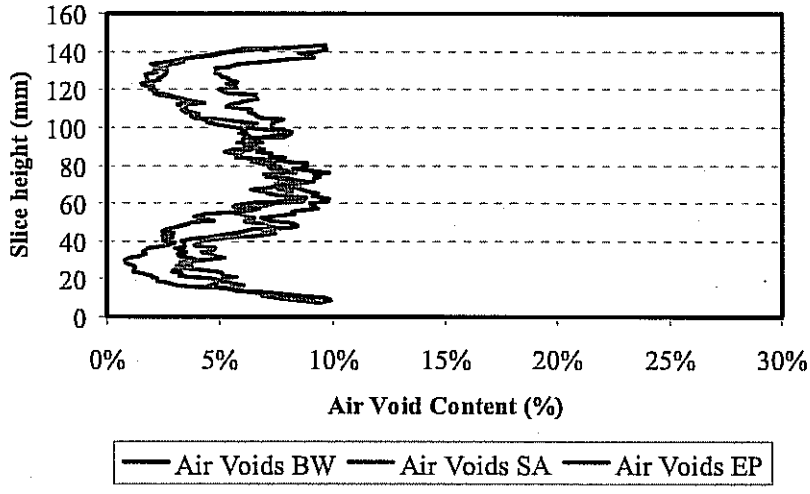

Figure 8.4 - Air Void Distribution among the Three Aggregates (Superpave-C)

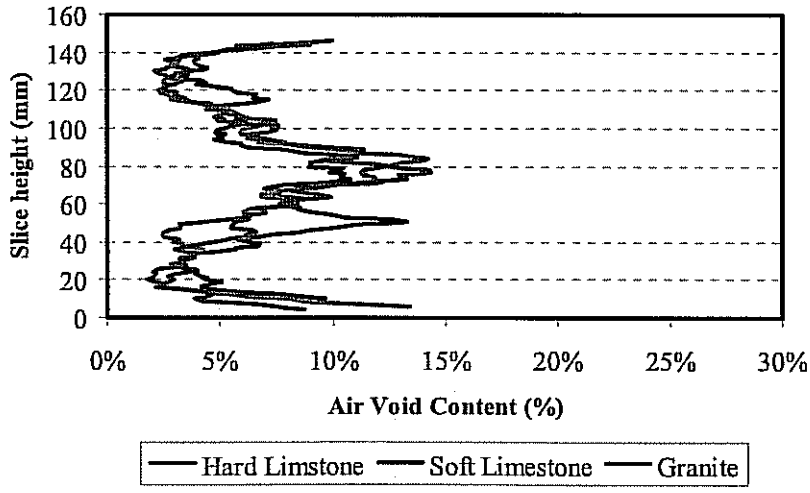

Figure 8.5 - Air Void Distribution among the Three Aggregates (CMHB-C)

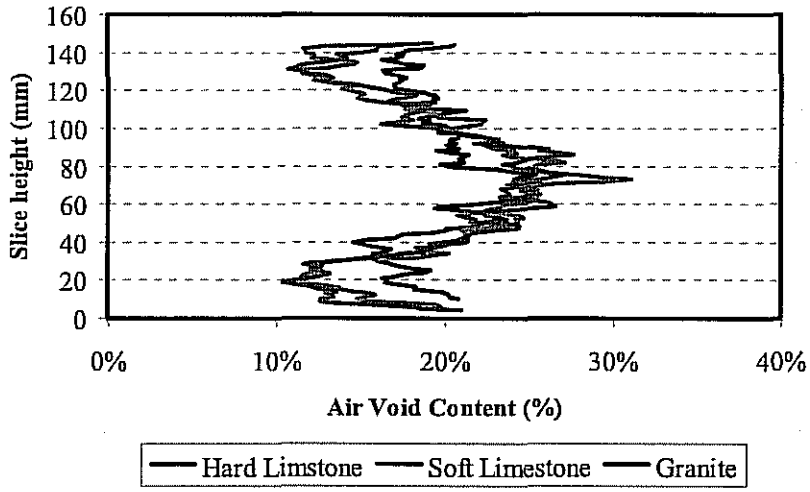

Figure 8.6 - Air Void Distribution among the Three Aggregates (PFC)

Crushing Resistance to Mixing

Measurements were conducted to determine the resistance of aggregates to degradation due to HMA compaction in the Superpave gyratory compactor. Specimens from each mix were compacted to about in-place air void and to 250 revolutions. The ignition oven was used to burn the bituminous, and sieve analysis was performed on the aggregates. Gradations of the compacted specimens to nominal in-place air voids and to 250 gyrations were compared to the original gradations. The results are shown in detail in Table 8.2. However, some of the results at 250 gyrations were not consistent. The shaded area demonstrates the sieves where most of the change in gradation occurs for the three mix designs. Figure 8.7 illustrates the sieve analyses for PFC mix with soft limestone. For the specimens prepared to achieve the nominal in-place air voids, the gradation is finer than the original gradation. Further compaction to 250 gyrations caused even more aggregate crushing yielding a finer gradation. Similar results were found in the sieve analyses of the remaining mixtures.

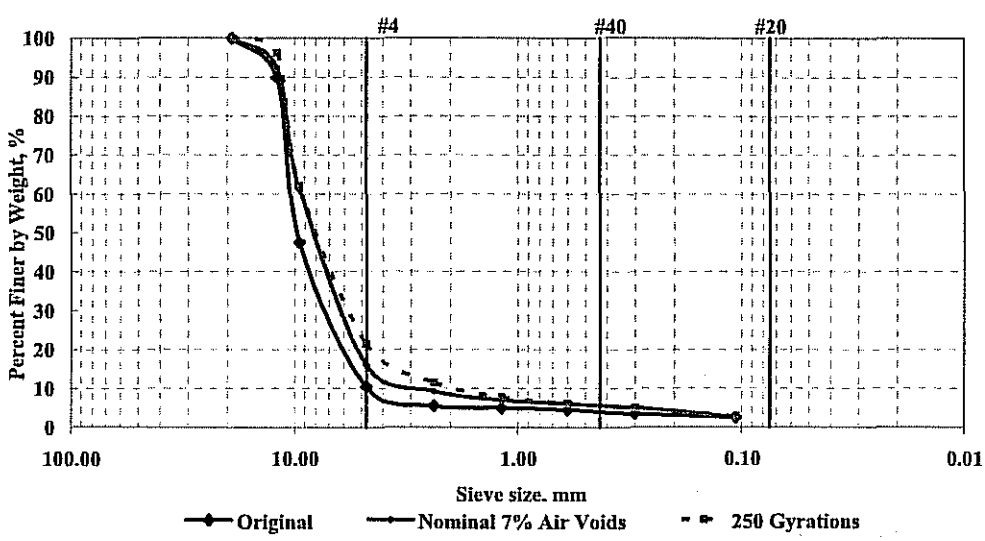

Figure 8.7 - Aggregate Gradation Change after Compaction for Soft Limestone PFC

Table 8.2 - Aggregate Crushing Analysis for all Mixes

a) CMHB-C

Sieve No.	Hard Limestone			Granite			Soft Limestone		
	Original Gradation	Nominal 7% Air Voids	250 Gyrations	Original Gradation	Nominal 7% Air Voids	250 Gyrations	Original Gradation	Nominal 7% Air Voids	250 Gyrations
	Percent Passing, %			Percent Passing, %			Percent Passing, %		
3/4"	100	100	100	99	100	98	100	100	100
1/2"	79	81	83	79	89	82	79	85	90
3/8"	61	63	61	60	74	66	61	65	66
#4	38	38	39	38	45	47	38	40	40
#8	22	25	25	22	28	30	22	25	25
#16	16	18	17	16	19	20	16	18	16
#30	16	16	15	16	16	18	16	16	14
#50	16	15	15	16	15	16	16	15	13
#200	7	7	6	7	7	7	7	7	5

b) Superpave-C

Sieve No.	Hard Limestone			Granite			Soft Limestone		
	Original Gradation	Nominal 7% Air Voids	250 Gyrations	Original Gradation	Nominal 7% Air Voids	250 Gyrations	Original Gradation	Nominal 7% Air Voids	250 Gyrations
	Percent Passing, %			Percent Passing, %			Percent Passing, %		
3/4"	100	100	100	99	100	98	100	100	100
1/2"	96	97	96	95	98	97	96	98	96
3/8"	88	91	89	88	93	92	88	87	92
#4	66	72	68	65	71	73	66	65	71
#8	43	52	50	43	48	50	43	45	50
#16	30	37	35	30	33	34	30	30	35
#30	30	35	34	30	31	32	30	28	33
#50	30	33	32	30	30	31	30	27	31
#200	6	10	8	6	10	9	6	8	9

c) PFC

Sieve No.	Hard Limestone			Granite			Soft Limestone		
	Original Gradation	Nominal 20% Air Voids	250 Gyrations	Original Gradation	Nominal 20% Air Voids	250 Gyrations	Original Gradation	Nominal 20% Air Voids	250 Gyrations
	Percent Passing, %			Percent Passing, %			Percent Passing, %		
3/4"	100	100	100	100	100	100	100	100	100
1/2"	90	91	93	90	89	90	90	92	96
3/8"	48	57	56	48	59	69	48	61	62
#4	11	22	21	11	25	31	11	16	21
#8	6	11	12	6	12	17	5	9	11
#16	5	8	8	5	8	10	5	7	8
#30	4	6	7	5	6	7	4	6	6
#50	3	5	5	4	4	5	3	5	5
#200	3	2	3	3	2	3	2	3	3

The unit weights of the samples compacted to the nominal in-place air void contents are compared to the ones prepared to 250 revolutions in Figure 8.8. The unit weights of the samples compacted to 250 gyrations are greater than those compacted to the in-place air voids. The soft limestone showed a higher increase in density for the CMHB-C and Superpave-C mixes as compared to the other mixes with a 6% and 9% increase, respectively. On the other hand, the unit weights of the PFC mixes with hard limestone and soft limestone increased by 8%.

HAMBURG WHEEL TRACKING DEVICE TEST

The Hamburg Wheel Tracking Device (Tex-242-F), as shown is Figure 8.9, measures the combined effects of rutting and moisture damage by rolling a steel wheel across the surface of a bituminous concrete test specimen that is immersed in hot water. The measurements are customarily reported as the depth of maximum deformation versus the number of wheel passes. The specimens used for this test are 6 in. in diameter and 2.4 ± 0.1 in. in height at an air void content of 7 ± 1%. Two trimmed, cylindrical specimens compacted in the gyratory compactor are arranged in a series to provide the required path length for the wheels. A total number of passes of 20,000 was selected as per Tex-242-F because a PG 76-22 binder was used. The maximum allowable rut depth is 0.5 in. Figure 8.10 shows a typical example of permanent deformation response. A polynomial is fitted to data for demonstration purposes here.

The trend lines of the variations in maximum deformation with the number of load cycles for CMHB-C and Superpave-C mixes compacted to 7% nominal air void content are shown in Figure 8.11. The PFC mixes were not tested because they are not specified in the TxDOT specifications, and because our past experience has shown that the specimens fail this test. The results are summarized in Table 8.3. The mixes with granite deformed the least after 20,000 cycles and the soft limestone the most. The Superpave-C mixes with granite and hard limestone rutted less than 0.5 in while the Superpave-C mixes from soft limestone deformed by slightly more than 0.5 in. (marginally failed). The CMHB-C mix with soft limestone also marginally failed. Again the mixes with granite performed the best, and with the soft limestone the worst.

The trend lines for specimens prepared with the CMHB-C and Superpave-C mixes compacted to 250 gyrations are shown in Figure 8.12 and their corresponding results are summarized in Table 8.3. Specimens prepared from CMHB-C mixes to 250 revolutions showed similar results as those specimens prepared at 7% air void contents. Once again, the CMHB-C-mixes with hard limestone and granite met the requirements while the soft limestone rutted more than 0.5 in. All specimens from the Superpave-C mixes deformed significantly more than those specimens prepared at air void contents of 7%, and failed the TxDOT requirements. This indicates that the CMHB-C specimens (intermediate gradation) were not as sensitive to increases in compaction efforts, but the Superpave-C mixes are quite prone to rutting when they were compacted to denser states.

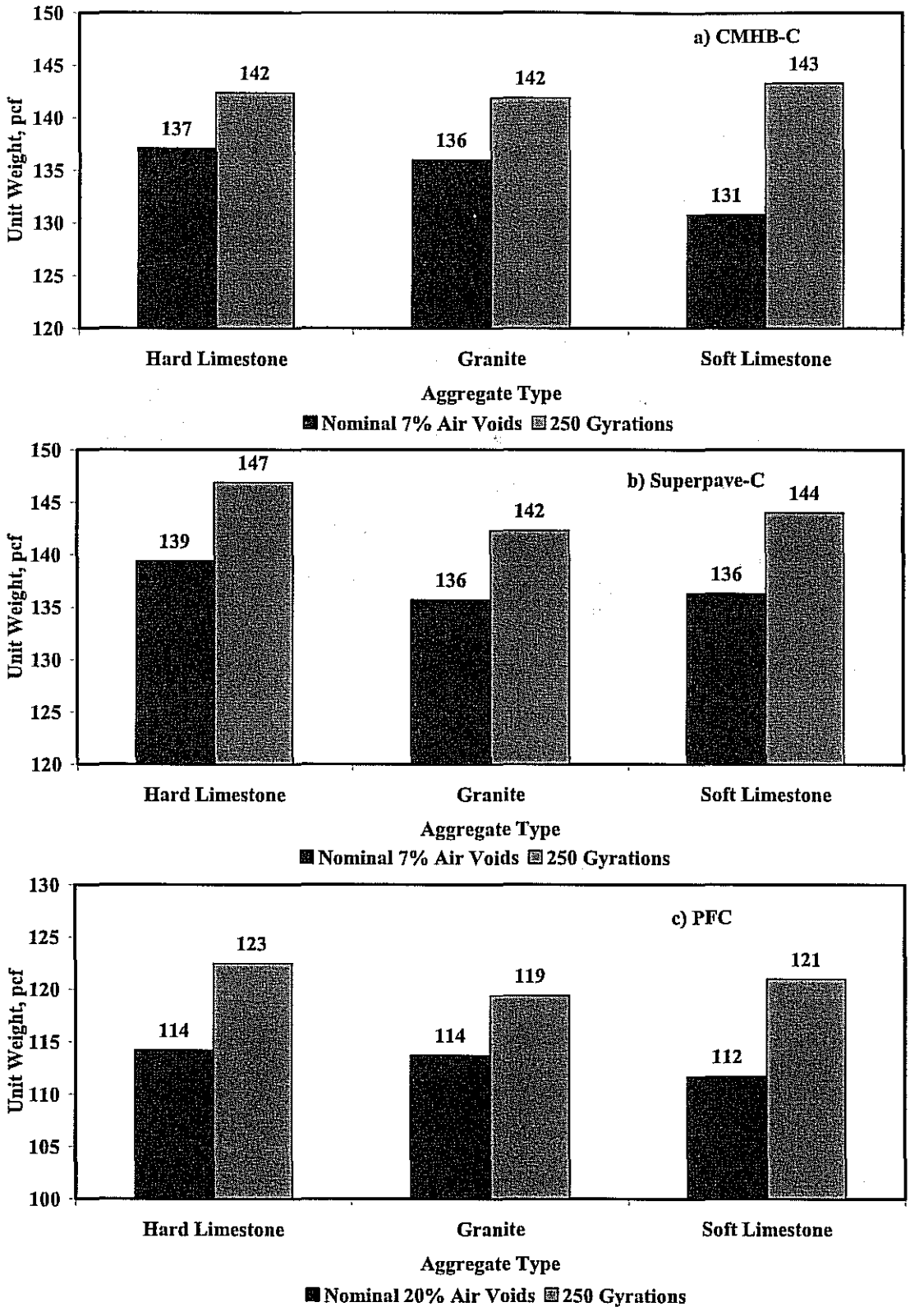

Figure 8.8 - Unit Weights for both Compaction Levels for all Mixes

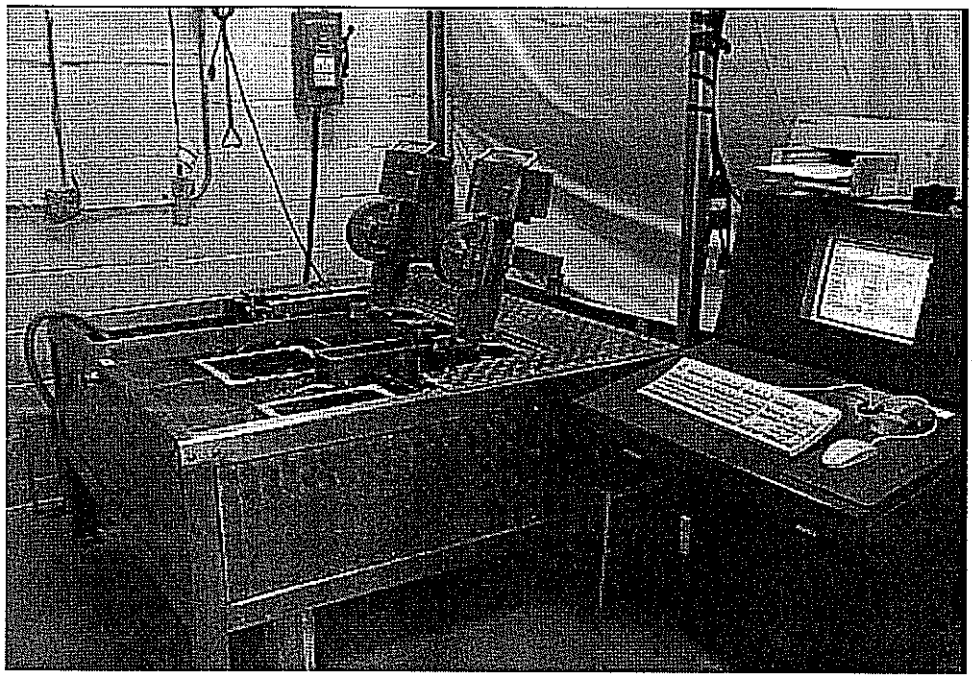

Figure 8.9 - Hamburg Wheel Tracking Device

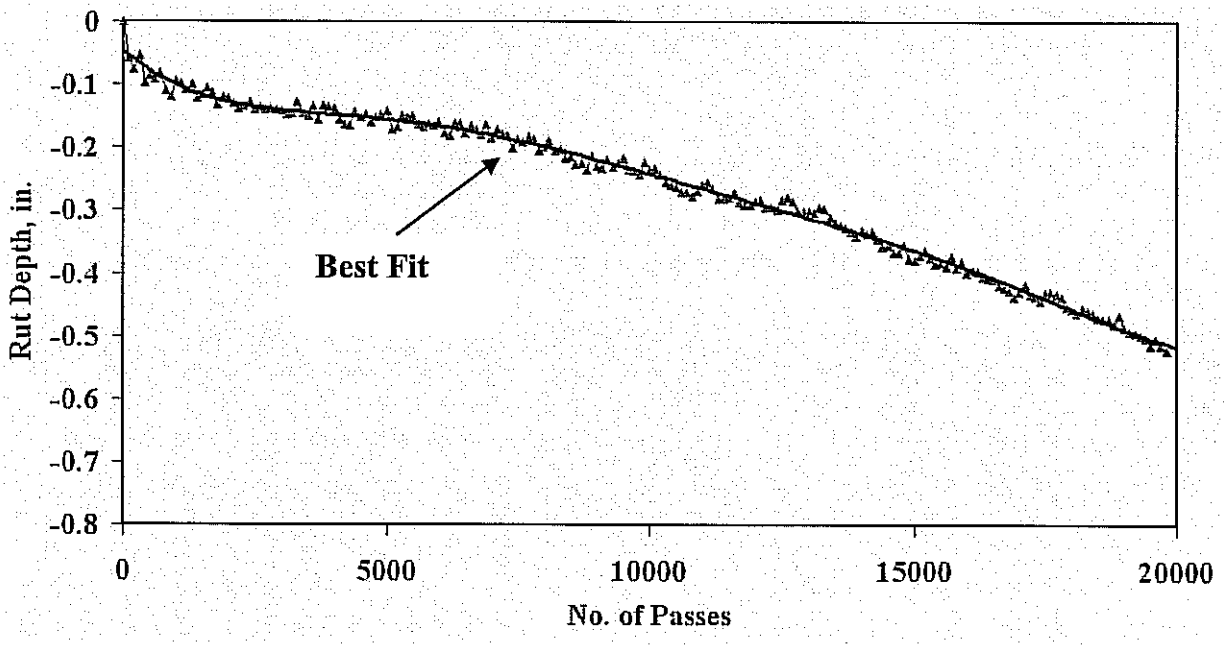

Figure 8.10 - Hamburg Wheel Tracking Device Test Results

Table 8.3 - HWTD Summary Results for Specimens Prepared at both Levels of Compaction

Material	Type	Maximum Rut Depth, in. (Condition)	
		Nominal 7% Air Voids	250 Gyrations
Hard Limestone	CMHB-C	0.49 (passed)	0.38 (passed)
	Superpave-C	0.40 (passed)	0.73 (failed) @ 14,500 passes
Granite	CMHB-C	0.30 (passed)	0.40 (passed)
	Superpave-C	0.22 (passed)	0.63 (failed) @ 19,000 cycles
Soft Limestone	CMHB-C	0.53 (marginally failed) @ 20,000 cycles	0.70 (failed) @ 16,000 cycles
	Superpave-C	0.52 (marginally failed) @ 20,000 cycles	0.70 (failed) @ 11,000 cycles

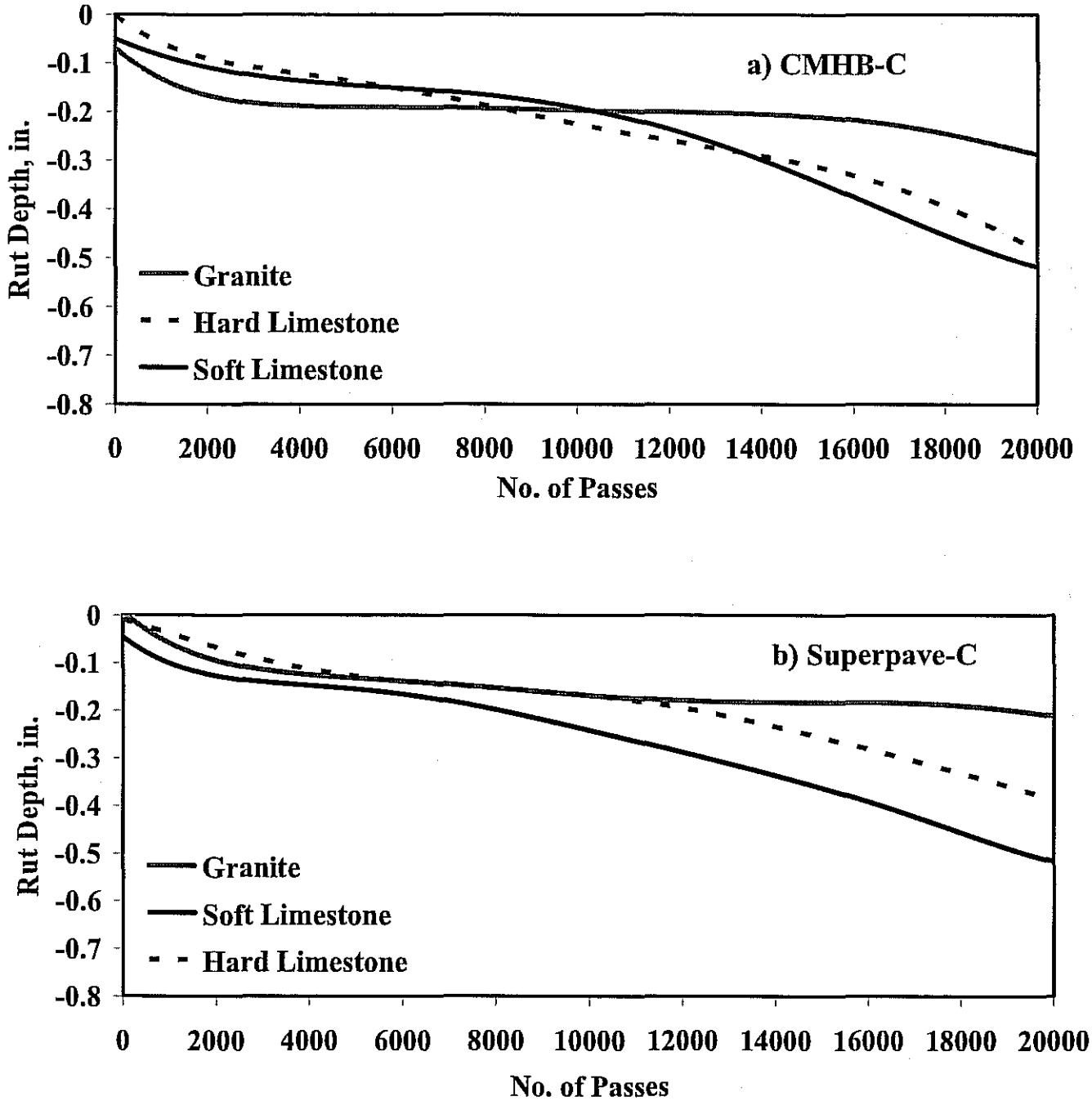

Figure 8.11 - Hamburg Wheel Tracking Device Results for Nominal 7% Air Void Mixes

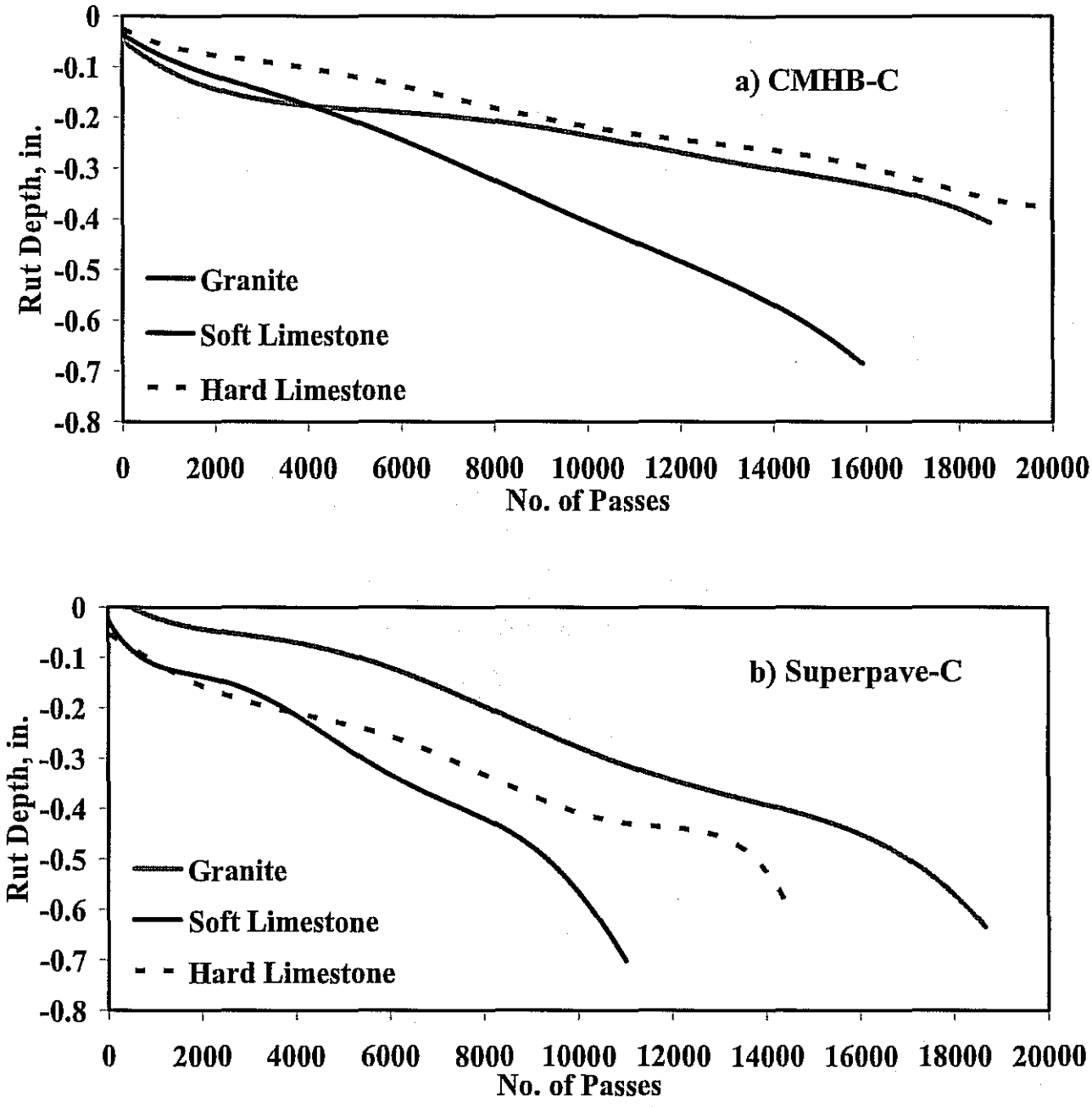

Figure 8.12 - Hamburg Wheel Tracking Device Results for 250 Gyration Level Mixes

INDIRECT TENSILE TEST

The indirect tensile test (IDT, Tex-226-F) is conducted by applying a compressive load to a cylindrical specimen through two diametrically opposed, arc shaped rigid platens as illustrated in Figure 8.13. The loading configuration described develops a relatively uniform state of tensile stresses perpendicular to the load direction, which results in splitting of the specimen.

The IDT device has four components: the testing apparatus, the test control unit and data acquisition system, load measuring device, and the environmental control chamber. The specimens are compacted to a relative density of 93 ± 1%. The specimens are nominally 4 inch in diameter and 2 inch thick and are loaded at a rate of 2 inch/min.

Three replicate specimens of each mix at both compaction levels were tested at a temperature of 77°F as specified by Tex-226-F. To ensure that the specimens achieved the desired test temperatures, they were placed in a temperature-controlled chamber maintained at 77°F overnight prior to the start of the tests.

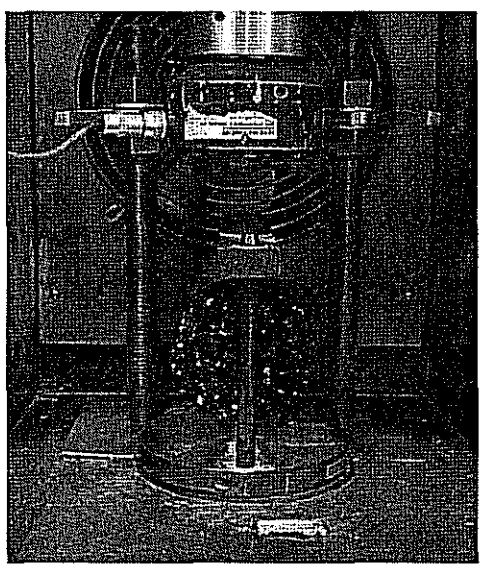

Figure 8.13 - Indirect Tensile Test

Typical variations of the load with deformation for the CMHB-C, Superpave-C, and PFC mixes compacted to achieve the nominal in-place air void contents are shown in Figure 8.14. The peak strengths and coefficient of variations are summarized in Table 8.4 for all three aggregates. For each aggregate type, the Superpave-C mixes were the strongest and the PFC the weakest. For the Superpave-C mixes, with the finest gradation, samples from the three coarse aggregates exhibited more or less similar strengths (from 116 psi to 125 psi). For the CMHB-C mixes with a gap-graded gradation, the hard limestone mixes exhibited the highest tensile strength (106 psi), while the granite ones exhibited the lowest (83 psi). For the PFC mixes with coarse but uniform gradations, the granite aggregates exhibited the highest strength, followed by the soft limestone and the hard limestone. The data presented in this table suggests that this test is reasonably repeatable with COVs of less than 11%.

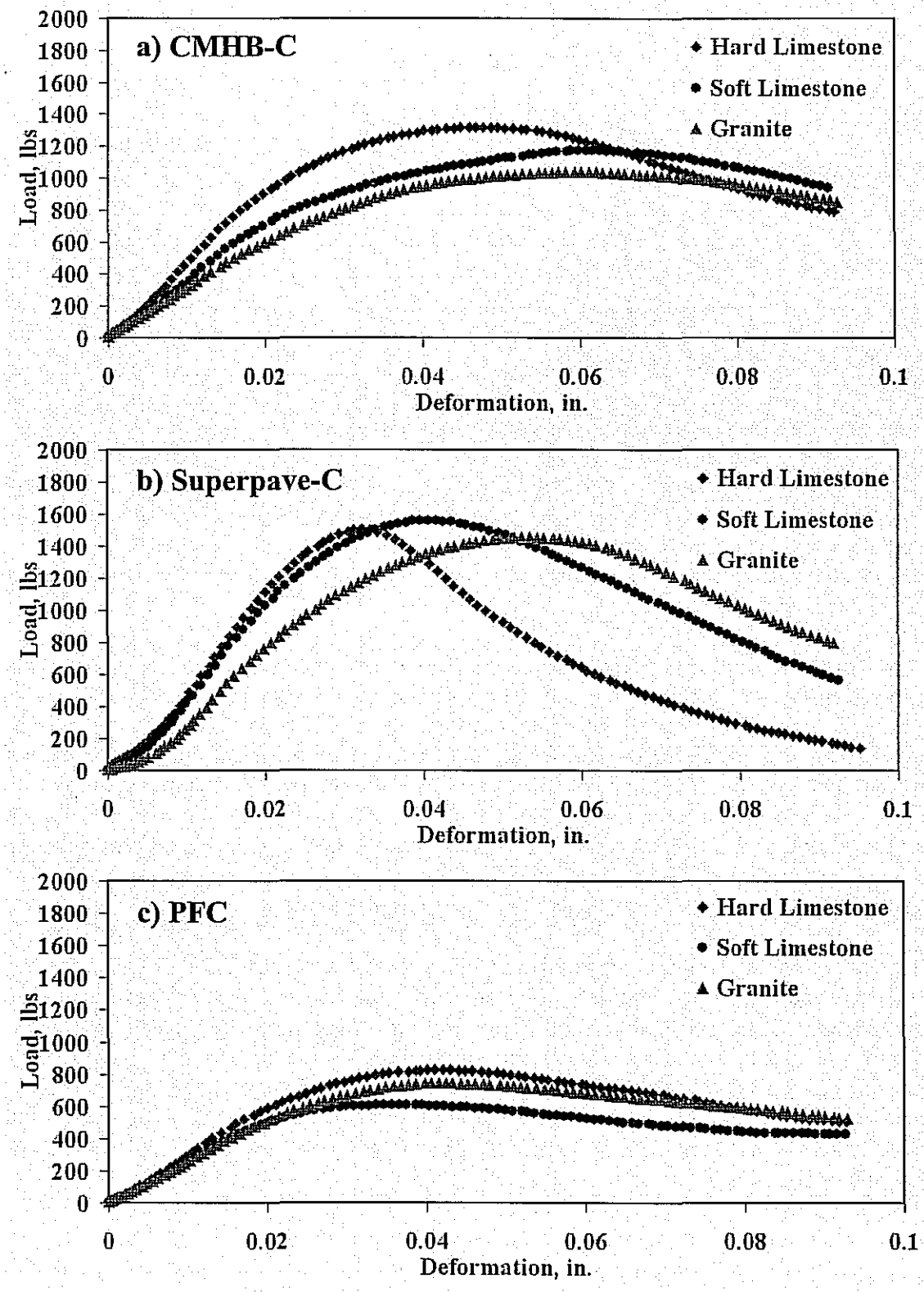

Figure 8.14 - Indirect Tensile Strength Test Results for Nominal In-place Air Void Mixes

Table 8.4 - Summary Results for IDT Mixes

Material	Mix Type	Tensile Strength, psi	
		Nominal In-place Air Voids	250 Gyrations
Hard Limestone	CMHB-C	106 *(1%)**	103 *(1%)**
	Superpave-C	120 *(9%)**	112 *(6%)**
	PFC	39 (11%)*	46 (2%)*
Granite	CMHB-C	83 *(7%)**	116 *(5%)**
	Superpave-C	116 *(7%)**	132 *(1%)**
	PFC	61 *(0%)**	50 *(1%)**
Soft Limestone	CMHB-C	94 *(5%)**	142 *(2%)**
	Superpave-C	125 *(1%)**	165 *(1%)**
	PFC	50 *(7%)**	68 *(9%)**

** - Numbers in the parentheses are the coefficient of variation from triplicate tests.*

Figure 8.15 shows the typical variations of the load with deformation for the CMHB-C, Superpave-C, and PFC mixes for the 250 gyrations compaction level. The peak strengths and coefficient of variances at both compactive efforts are summarized in Table 8.4. When the specimens were prepared with 250 gyrations, the Superpave-C mixes were again the strongest mixes while the PFC the weakest.

For the hard limestone, the differences in the tensile strengths with the two compactive efforts are less than 8% for the CMHB-C and Superpave-C mixes. For the PFC specimens with hard limestone, the tensile strength of the mix increased by about 17% when the number of gyrations increased. This trend makes sense since for mixes with hard aggregates the failure plane during the indirect tensile test is essentially through the binder and around the individual aggregates. As such, the tensile strengths are controlled primarily by the strength of the binder and to a lesser extent by the packing of aggregates. As reflected in Table 8.2, the gradations of the three mixes from the two compactive efforts are similar, i.e. the extra number of gyrations during compactions did not cause any appreciable breakage of aggregates.

The tensile strengths for the three mixes with soft limestone increased by 30% to 50% due to the additional compaction efforts. For the soft limestone, the failure plane may not be primarily through the binder. The failure plane may also go through some of the aggregates. The increase in the number of gyrations during compaction would break some of the weak aggregates that would have been broken during the indirect tensile tests. As demonstrated in Table 8.2, the gradations for specimens compacted to 250 gyrations are usually finer than those specimens prepared for the nominal air voids, indicating further breakage of aggregates as the number of gyrations increases.

The tensile strengths with granite demonstrate trends that are closer to the soft limestone for the CMHB-C, and closer to the hard limestone for the Superpave-C. The reasons for the lower tensile strength after 250 gyrations as compared to the nominal in-place air voids, is not known at this time.

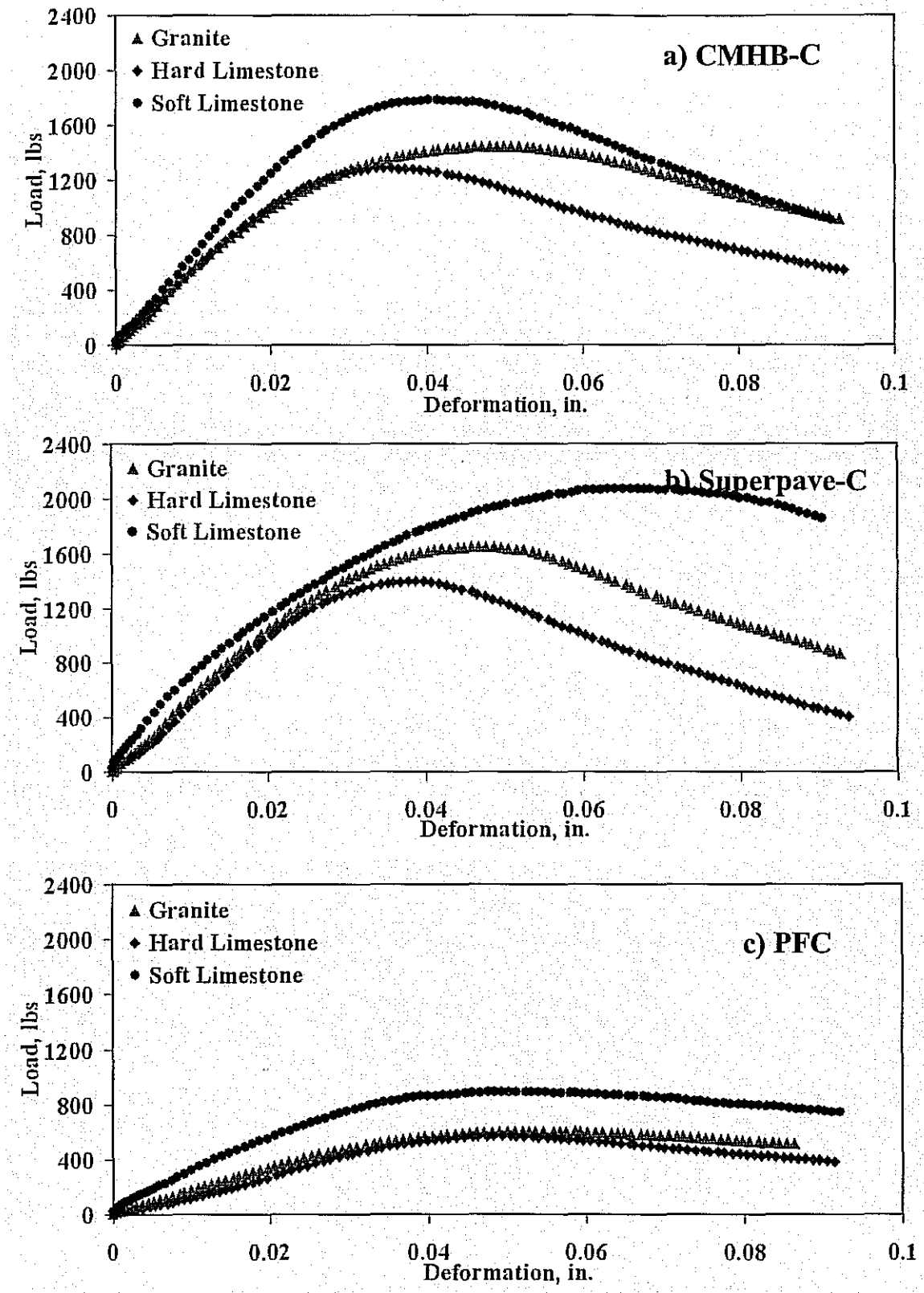

Figure 8.15 - Indirect Tensile Strength Results for 250 Gyration Level Mixes

DYNAMIC MODULUS TEST

The dynamic modulus test protocol is being advocated for characterizing bituminous mixtures. Briefly described, a sinusoidal axial compressive stress is applied to the specimen at a given temperature and loading frequency. The applied stress and the resulting recoverable axial strain response of the specimen are measured and used to calculate a dynamic modulus and a phase angle. A total of about fifty combinations of load regimes at different frequencies and temperatures are applied to each specimen. The specimen's stress-strain time histories under each continuous sinusoidal loading are measured.

A schematic of a typical dynamic modulus test set up is shown in Figure 8.16. The specimens are 4 in. in diameter and 6 in. in height with target air void contents of 7 ± 1 %. The specimen is placed on the bottom end platen, which is tightly attached to a steel base plate through a stainless steel cylinder. Two linear variable differential transformers (LVDT's) are used to measure the deformation of the specimen. Two targets are fixed on one side of the specimen with a gauge length of 4 in. and two other targets are fixed exactly on the opposite side of the specimen. The strain experienced by the specimen is the average of the deformations on the two opposite sides of the specimen divided by the gauge length.

The complex modulus of the material, which is the ratio of the applied stress and the measured strain, can be defined as:

$$E^* = E_0 e^{j\phi} \tag{8.2}$$

where E^* is the complex modulus of the material, E_0 is the ratio of σ_0 (maximum applied stress) and ε_0 (maximum measured strain), and j is the identity number. The phase angle, ϕ, is measured from the time difference between the occurrences of the maximum stress and maximum strain. The absolute value of $|E^*|$ is termed as dynamic modulus.

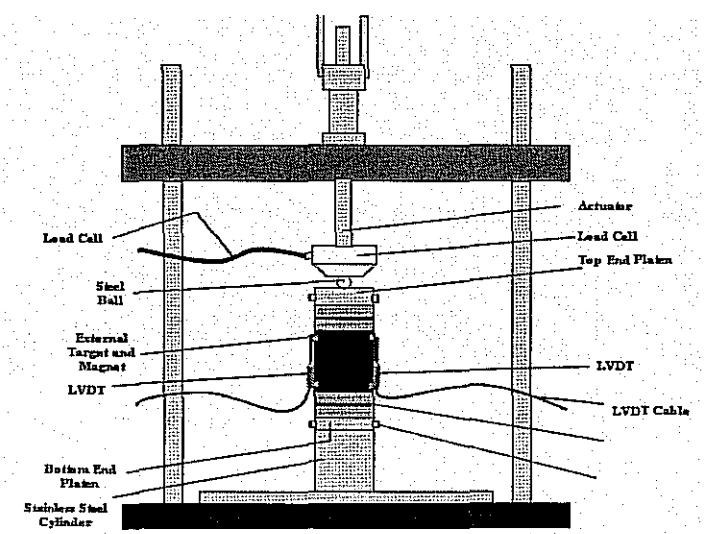

Figure 8.16 - Schematic of the Dynamic Modulus Test Setup

Each specimen is tested at five temperatures: 14, 40, 73, 100 and 130°F. To perform the test at each temperature, the specimen is initially subjected to 200 conditioning cycles at 20 Hz. After the initial conditioning, the specimen is subjected to 50 loading cycles at 10 Hz and 5 Hz. In the end, the specimen is subjected to 7 loading cycles at frequencies of 10, 5, 2 and 1 Hz. This sequence of testing results in a total of 50 dynamic modulus tests on each specimen. The measured moduli are then converted to a variation in modulus with frequency (called a master curve) at a reference temperature of 77°F using the principles of visco-elasticity.

The master curves for the three mixes prepared at nominal in-place air void contents are shown in Figure 8.17. The moduli at 10 Hz, which are representative of those measured with a Falling Weight Deflectometer, are summarized in Table 8.5. For all three mixes, the PFC blends are the softest of the three blends simply because of the higher air void contents of PFC mixes (about 20%). For the hard limestone and granite, the CMHB-C mixes are stiffer than the Superpave-C mixes. One the other hand, for the soft limestone, the Superpave-C mix is stiffer than the CMHB-C. The reason for this is not quite known at this time. One speculation is that the breakage of the soft limestone aggregates during mixing for the coarser CMHB-C mix might have impacted the quality of these specimens. This pattern will be investigated with the micro-mechanical models in the future.

Table 8.5 - Summary Results for Dynamic Modulus Tests for the Two Compaction Levels

Material	Type	Dynamic Modulus at 10 Hz, ksi	
		Nominal In-place Air Voids	250 Gyrations
Hard Limestone	CMHB-C	909	1164
	Superpave-C	827	690
	PFC	239	661
Granite	CMHB-C	847	1041
	Superpave-C	694	665
	PFC	193	319
Soft Limestone	CMHB-C	664	1513
	Superpave-C	765	724
	PFC	198	690

The master curves for the three mixes at 250 gyrations are shown in Figure 8.18. The moduli at 10 Hz for the two different compactive efforts are summarized in Table 8.5. Unlike the samples prepared at the nominal in-place air void contents where the hard limestone appeared to have the highest dynamic modulus, the mixes with the soft limestone at the 250 compaction effort exhibited the highest stiffness. This may indicate that a better packing of aggregates is obtained with breakage of the soft aggregates during compaction.

For the CMHB-C mixes, the specimens prepared at 250 gyrations exhibited higher stiffness as compared to those compacted to the nominal in-place air void contents for all three mixes. The most significant increase in modulus is associated with the soft limestone.

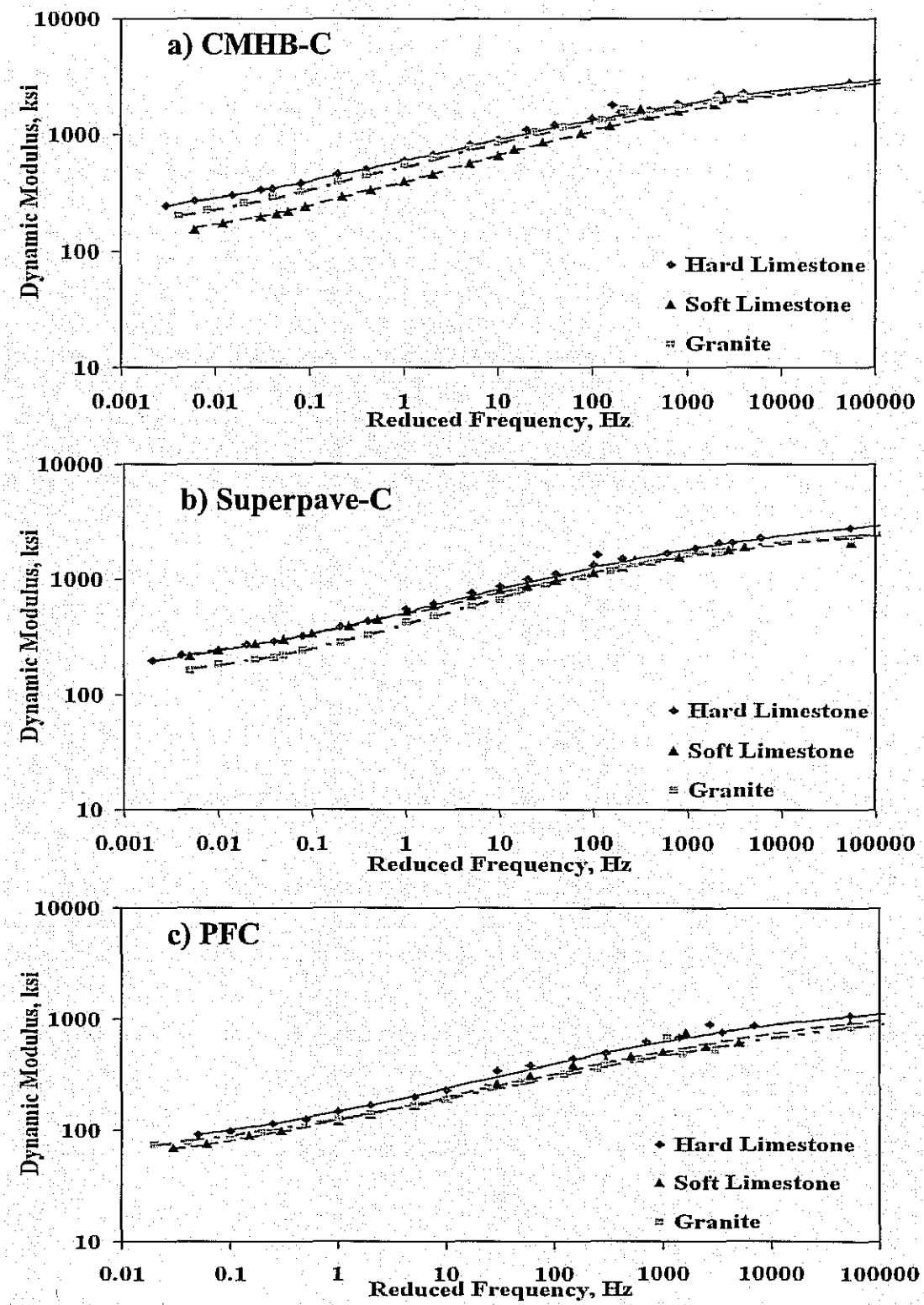

Figure 8.17 - Dynamic Modulus Master Curves for Nominal In-place Air Void Mixes

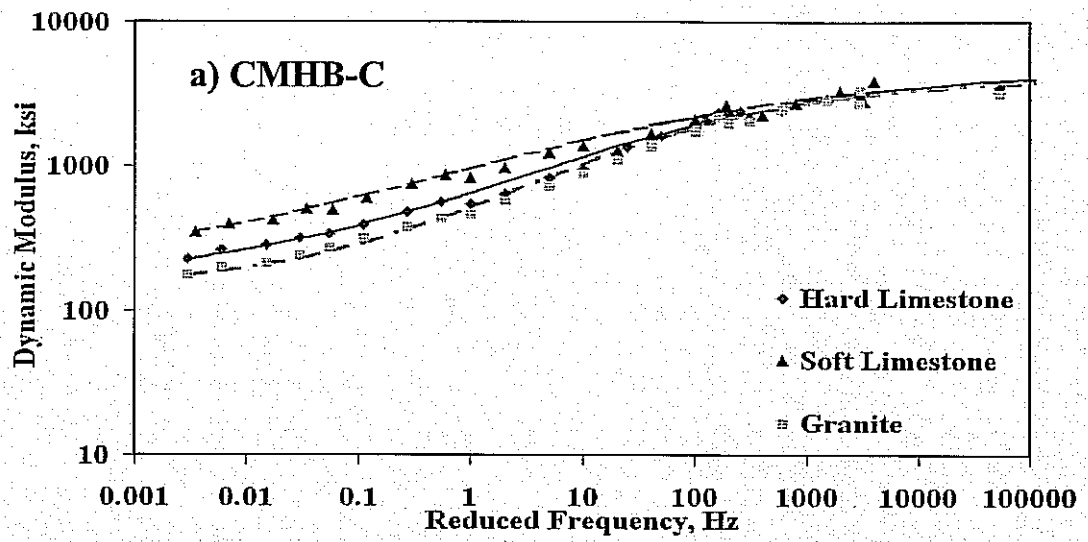

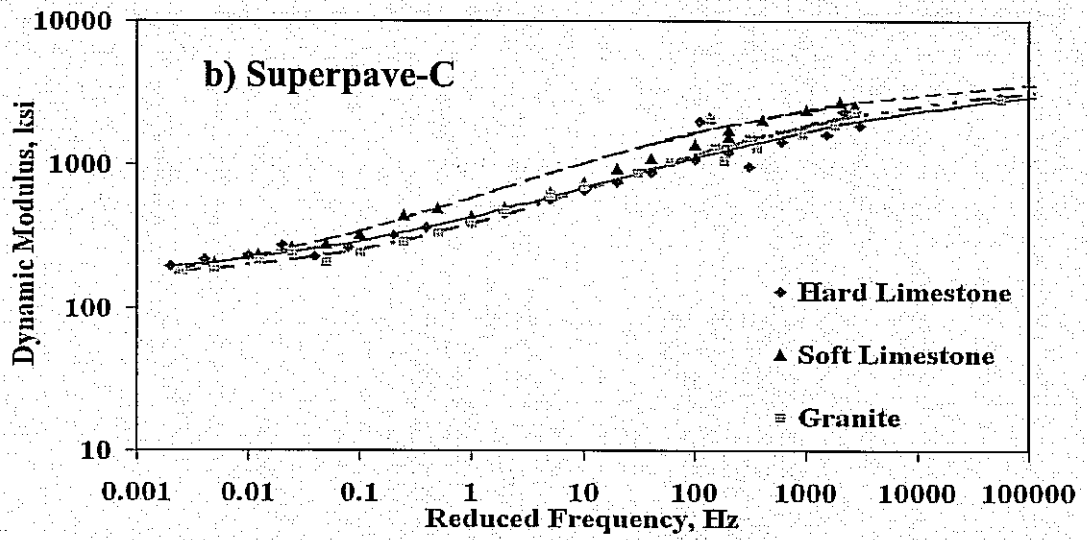

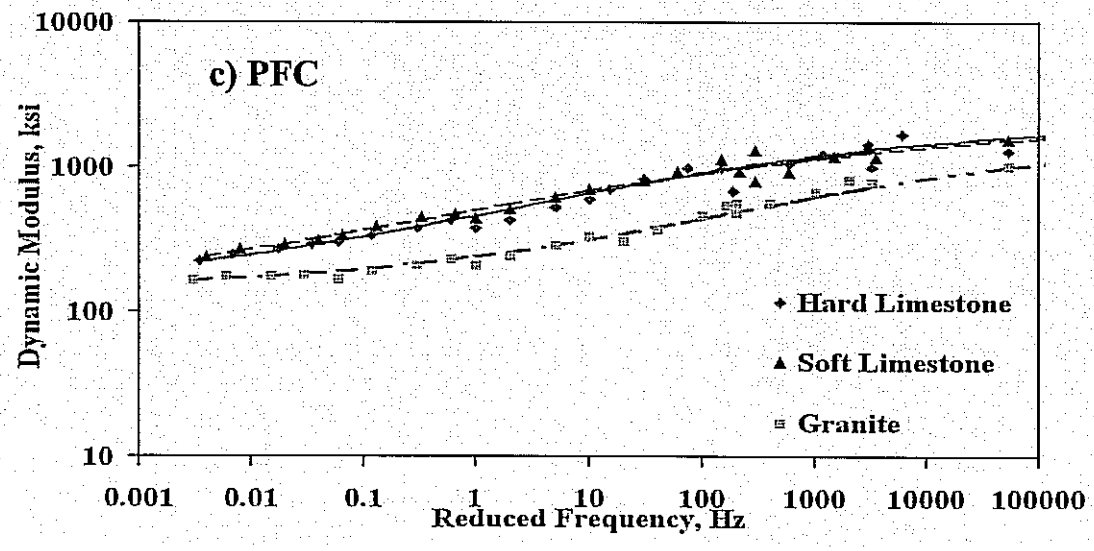

Figure 8.18 - Dynamic Modulus Master Curves for 250 Gyration Level Mixes

For the Superpave-C mixes, the moduli of the specimens with 250 gyrations are less than those prepared at the in-place air voids, especially for the hard limestone. However, the moduli of the PFC mixes are substantially (1.6 times to 3.5 times) greater than those measured on the specimens prepared at a nominal air void content of 20%.

SIMPLE PERFORMANCE TEST

The flow time test, which is one of the so-called simple performance tests, is a variation of the static creep test (Tex-231-F) commonly performed by TxDOT to assess the rutting potential of HMAC. In this test, a static load is applied to the specimen, and the resulting strains are recorded as a function of time (see Figure 8.19). The flow time is defined as the time when the minimum rate of change in strain occurs during the creep test. The flow time is determined by differentiating the strain versus time curve.

The flow time test is quite appealing as a simple performance test because the equipment is simple and the training required for its implementation is minimal. One major difference between the flow time test and Tex-231-F procedure is the specimen size. While a 4 in. by 6 in. specimen is used in the flow test, a 4 in. by 2 in. specimen is used in the Tex-231-F procedure. The larger specimen may be one factor that reduces the variability of the flow time test results as compared to the Tex-231-F procedure. This test is performed at a temperature of 140°F and a stress level of 30 psi which is maintained for three hours. The applied load and the resulting displacement of the specimen are continuously recorded.

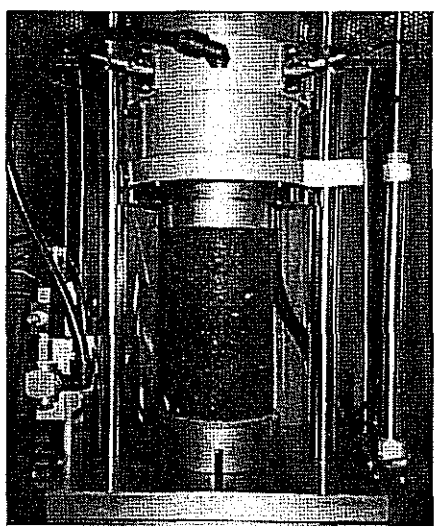

Figure 8.19 - Simple Performance Test

Three replicate specimens of each mix at the two compaction levels were tested. The average axial strains with time for the CMHB-C, Superpave-C, and PFC mixes prepared to achieve the nominal air void content are plotted in Figure 8.20, and the results are summarized in Table 8.6. For the three CMHB-C mixes, the hard limestone specimens deformed the least, and the soft limestone specimens deformed the most. The same trend was observed for the Superpave-C mixes. The strains measured on the PFC specimens from the three aggregates vary between 7150 and 7860 μstrain. Considering the COVs of the experiments, these values are quite similar.

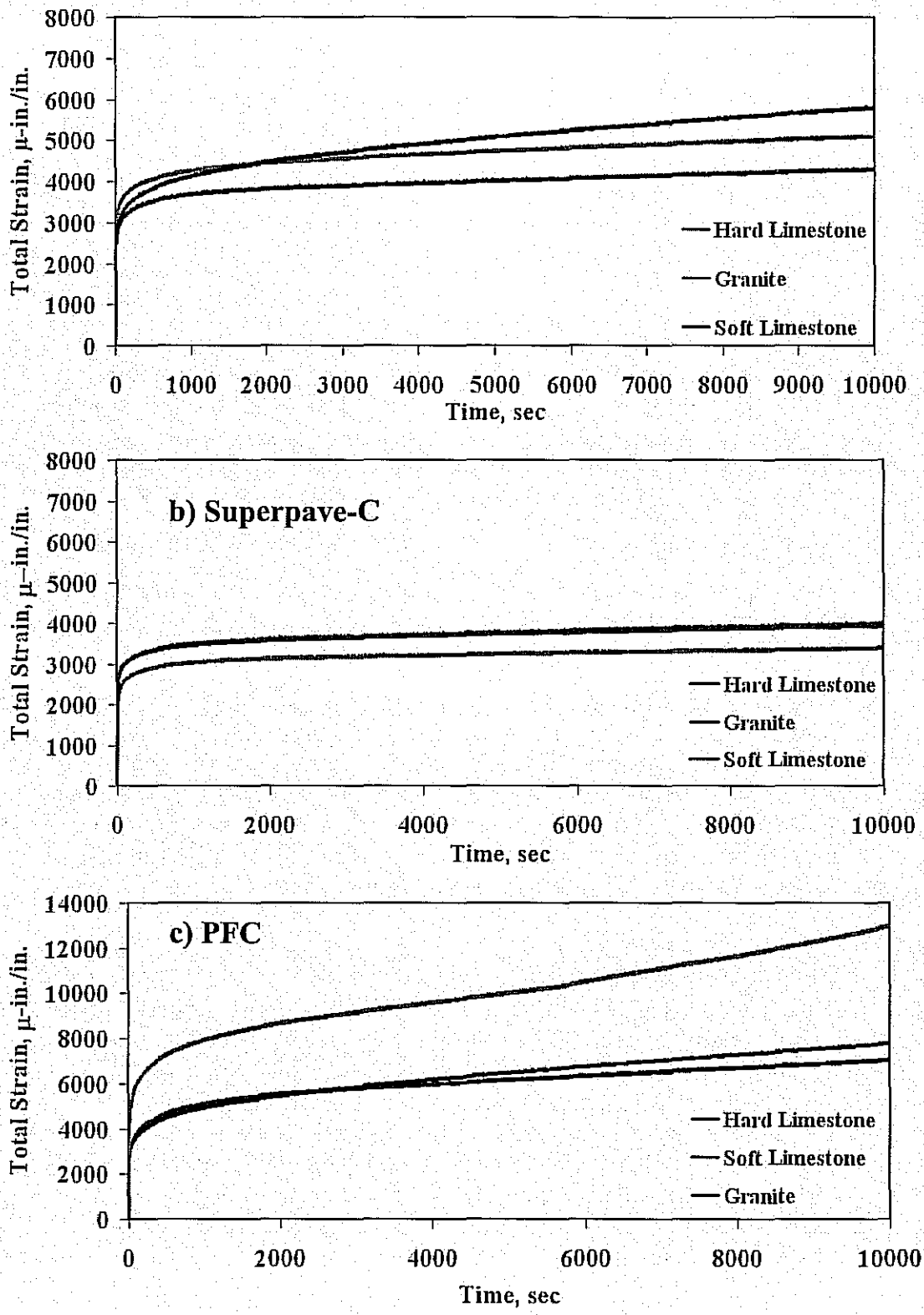

Figure 8.20 - Flow Time Results for Nominal In-place Air Void Mixes

Table 8.6 - Summary Results of the Flow Time Test for both Compactive Efforts

Material	Type	Maximum Strain after 10,000 sec, μ-in./in.	
		Nominal In-Place Air Voids	250 Gyrations
Hard Limestone	CMHB-C	3820 *(6%)**	4280 *(16%)**
	Superpave-C	3175 *(0%)**	3980 *(11%)**
	PFC	7860 *(5%)**	7020 *(10%)**
Granite	CMHB-C	4860 *(7%)**	5100 *(15%)**
	Superpave-C	5280 *(3%)**	3380 *(14%)**
	PFC	7150 *(22%*)*	12980 *(24%)**
Soft Limestone	CMHB-C	6750 *(7%)**	5790 *(3%)**
	Superpave-C	6910 *(1%)**	3980 *(11%)**
	PFC	7320 *(10%)**	7780 *(11%)**

** - Numbers in the parentheses are the coefficient of variation from triplicate tests*

The average strains with time for the CMHB-C, Superpave-C, and PFC mixes prepared to the 250 gyration level are plotted in Figures 8.21. The maximum strains for the 250 gyration compactive effort are also summarized in Table 8.6. A clear pattern in changes between the maximum strains for each mix prepared at the two compactive efforts cannot be observed. Even though the samples for the two compactive efforts were prepared and tested by the same group, the variability in test results for the specimens prepared with 250 gyrations in many cases are greater than those prepared at the nominal in-place air voids.

ULTRASONIC TESTING OF MIXES

The same ultrasonic device (v-meter) used to test the rock masses was also used to measure the seismic moduli of the mixes. The seismic modulus test was performed on the samples prepared for the dynamic modulus tests at room temperature. The test results for seismic modulus of the nominal in-place air voids and 250 gyration samples are summarized in Table 8.7. The seismic moduli of all hard limestone mixes are greater than the moduli measured on the other materials. The moduli for the mixes prepared with a compactive effort of 250 gyrations increased by approximately 35% with respect to the samples tested at the nominal in-place air void contents. Once again, the modulus of the three hard limestone mixes was greater than the moduli measured on the soft limestone and granite materials.

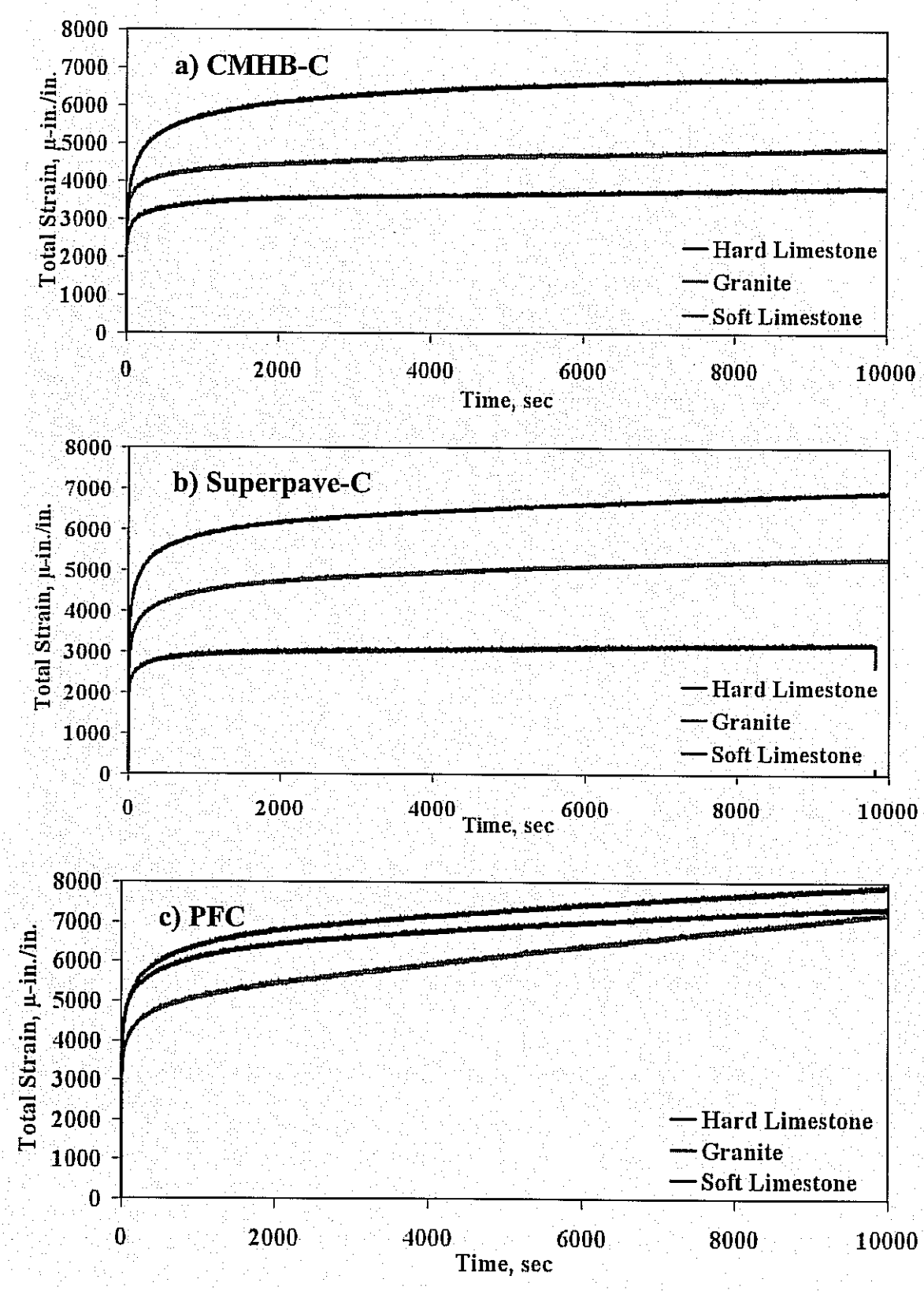

Figure 8.21 - Flow Time Results for 250 Gyration Level Mixes

Table 8.7 - Summary Results for the V-Meter Test for both Compactive Efforts

Material	Type	Seismic Modulus, ksi	
		Nominal In-place Air Voids	250 Gyrations
Hard Limestone	CMHB-C	2826 (*2%*)*	3803 (*10%*)*
	Superpave-C	2800 (*1%*)*	3062 (*1%*)*
	PFC	1074 (*0%*)*	1716 (*14%*)*
Granite	CMHB-C	2740 (*6%*)*	3385 (*8%*)*
	Superpave-C	2276 (*5%*)*	3029 (*1%*)*
	PFC	856 (*0%*)*	1302 (*21%*)*
Soft Limestone	CMHB-C	2662 (*1%*)*	3445 (*18%*)*
	Superpave-C	2101 (*7%*)*	3102 (*3%*)*
	PFC	922 (*0%*)*	1556 (*8%*)*

** - Numbers in the parentheses are the coefficient of variation from triplicate tests.*

CHAPTER NINE - MICROMECHANICAL MODELING

INTRODUCTION

The DEM has been mainly utilized as a research tool in many studies in the last few years. In this study a commercially available DEM code called *Particle Flow Code in 2-Dimensions* (PFC2D Version 3.1), developed by Itasca Consulting Group is used. This code includes a user-friendly graphical interface, linear and non-linear contact models, linear and curvilinear boundary conditions, in addition to the ability of the objects to slide due to shear stresses and detach once the bond strength has been exceeded.

The modeling of HMA cannot be accomplished using simple geometry assignment because of the irregular shape of aggregates and the fact that there are two major phases (mastic and aggregates) in the mix. The HMA model geometry is captured using X-ray computed tomography (CT) and then transferred to PFC2D.

The X-Ray computed tomography is a nondestructive procedure that captures the interior structure of materials. Studies conducted by Masad (2004) have found that the X-Ray CT is a valuable tool to analyze the internal structure of bituminous mixtures. Masad (2004) discussed the various applications for the X-Ray CT. Some of these applications included the determination of air void distribution, and measurements of stone-on-stone contacts within the bituminous mixtures. X-ray CT images are stacked to form the three dimensional representation of the HMA internal structure. An example of an image taken by the X-ray CT is illustrated in Figure 9.1.

The image is transferred to a binary format (i.e., 0 for mastic and 255 for aggregate) as shown in Figure 9.2. The image pixels become the particles in the PFC2D model. The *Image-Pro Plus* (IPP) image analysis package is used to identify the outline pixels of each aggregate particle, and a FORTRAN code is used to group the elements of each aggregate particle in one group, and so is the case for the mastic phase. The FORTRAN code checks in all four directions (up, down, right, and left) whether the adjacent pixel is aggregate or mastic (Abbas 2004). Figure 9.3 shows the discrete element model after differentiating between mastic and aggregate. Each of the model phases can be assigned specific properties, such as bond strength and type, friction coefficient, and density.

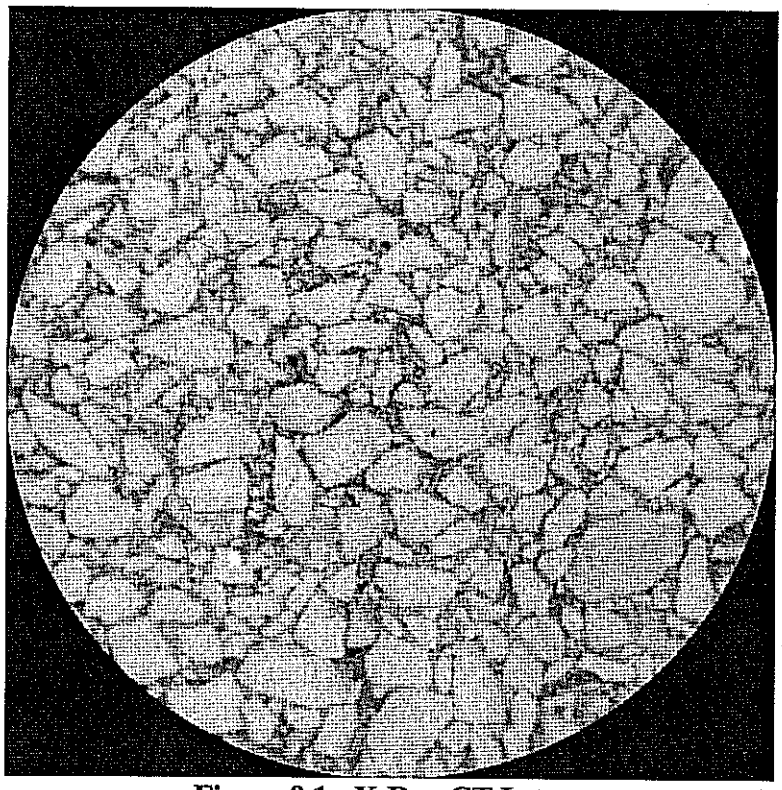

Figure 9.1 - X-Ray CT Image

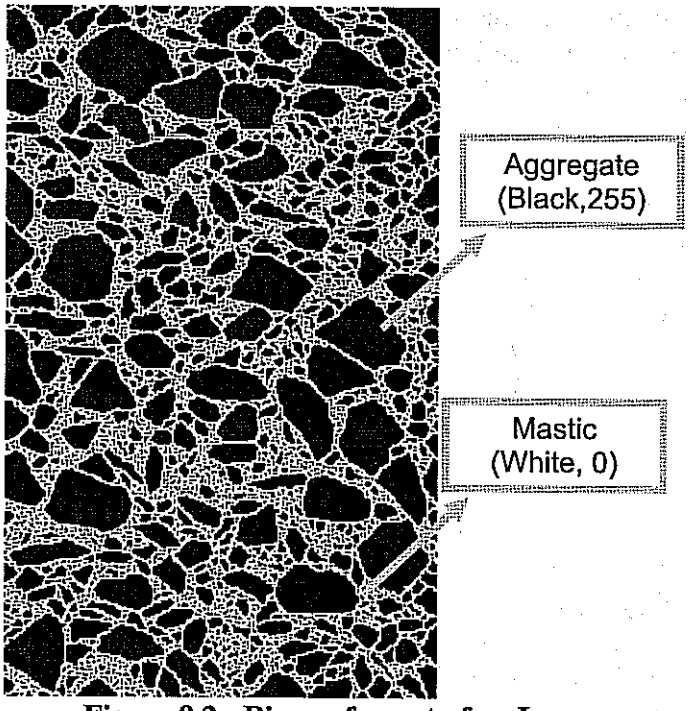

Figure 9.2 - Binary format of an Image

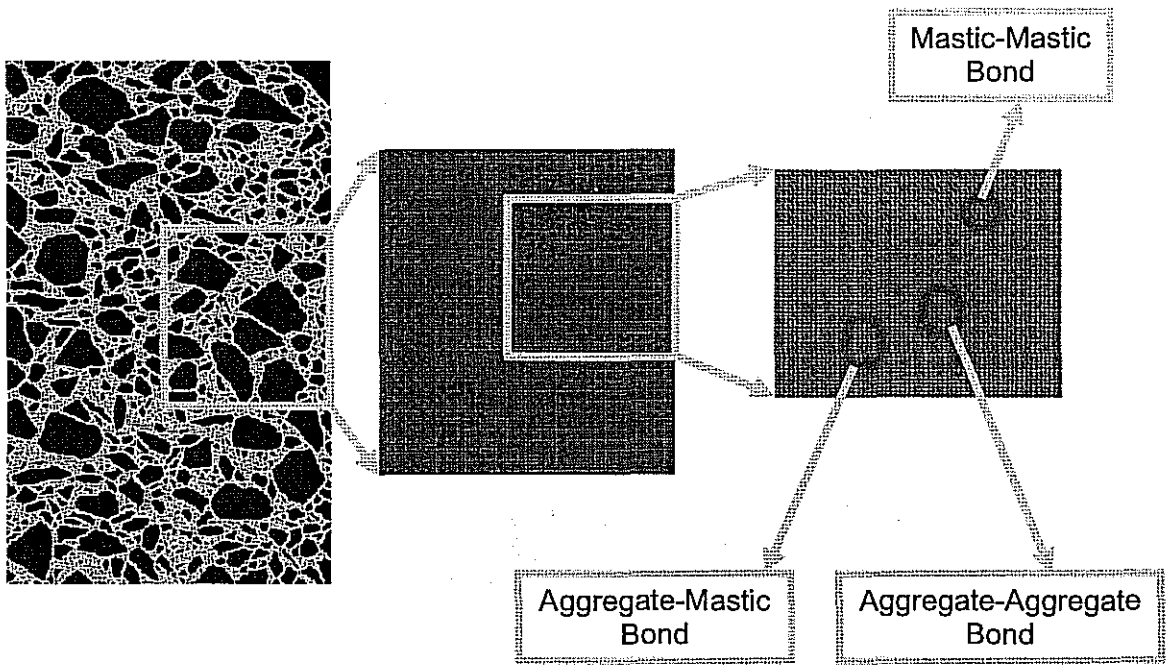

Figure 9.3 - Discrete Element Model for Aggregate and Mastic

DEM of Aggregate Tests

The PFC2D software was used to model the modulus test, compressive strength test and indirect tensile strength of rock samples representing the three aggregates used in this study. The aggregate contact stiffness and strength in the model were determined such that the model results matched the experimental measurements. The parameters determined from this calibration step are then used to represent the aggregates in a model of HMA.

Model Calibration Based on Aggregate Test Results

Aggregate samples of a diameter of about 2 in. and a height of about 2 in. were tested under compression and indirect tension loading. The PFC2D was used to model these tests. The model consisted of particles or balls with a diameter of 14.2 mm and a density of 160 pcf (Figures 9.4 and 9.5). Following the work that was conducted by McDowell and Harireche (2002) and Cheng (2004), the simulation was conducted using a value of unity for the ratio normal stiffness to shear stiffness.

Considerable analysis was conducted to determine the appropriate value for the approaching velocity used in loading. A higher velocity means less loading time and reduction in the simulation time. However, there is a limit on the maximum velocity that can be used after which the DEM becomes unstable numerically. This maximum velocity should be determined for the compressive and indirect tension strength tests.

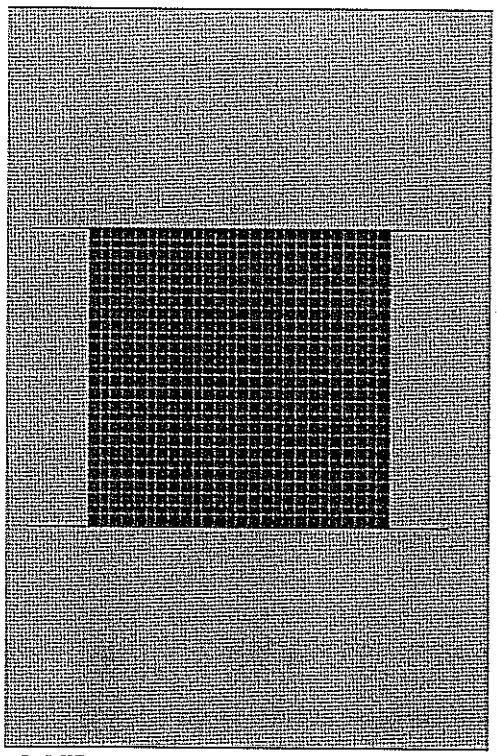

Figure 9.4 - Model Used in Simulating Compressive Strength Test

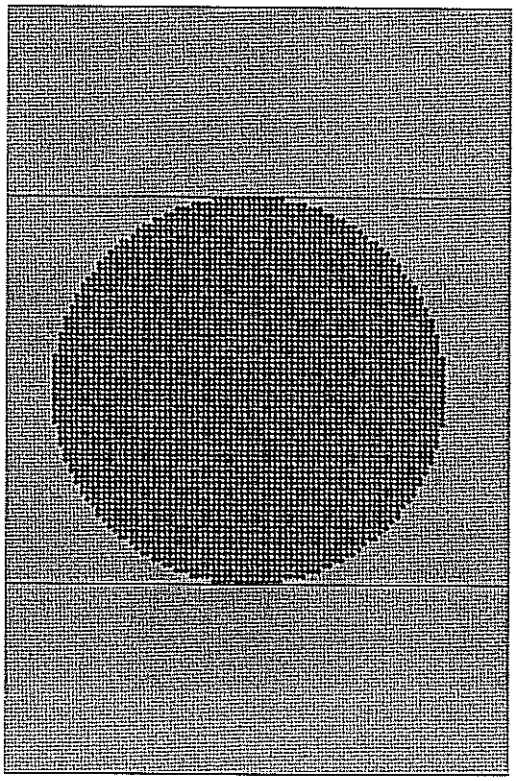

Figure 9.5 - Model Used in Simulating Indirect Tension Strength Test

Several rates of loading were evaluated in the uniaxial compression test as shown in Figure 9.6. The curves for the rate of loading of 19.7 in./s and 39.4 in./s differed from the remaining curves. The rate of loading where the stress-strain curve does not vary was also evaluated for the indirect tensile strength test (see Figure 9.7). Based on the results in Figures 9.6 and 9.7, a rate of loading of 1.2 in./s was selected for the modulus and compressive strength tests, and 2 in./s for the tensile strength test. These two rates of loading limit numerical errors and could be run within reasonable computational time. The contact stiffness among the model balls was varied until the model stiffness matched the experimental stiffness measurements.

The normal and shear bond strengths were varied until the numerical results matched the experimental strength measurements. This required conducting iterative analysis to determine the parameters that had the best match with both tests. The coefficient of friction between the model elements was set to a low value such that sliding occurs after the bond breaks. The friction between the loading walls and the model elements was set to 0.5 as recommended by Cheng (2004). The results of the compressive strength were more dependent on the shear strength, while the indirect tensile strength was more dependent on the tensile normal strength.

Although the previous model was able to calibrate the aggregate properties in a very good manner, the researchers decided to investigate the effect of changing the packing scheme of particles in the model. Many researchers recommended the use of hexagonal packing instead of regular cubic packing (Figure 9.8).

The same procedure described above was repeated for the three aggregates. A comparison between the experimental and modeling results are shown in Figures 9.9 through 9.11, while the model parameters used for each of the aggregates are shown in Table 9.1.Figure 9.12 shows an example of the progress of loss of bond in the indirect tensile test. The failure started in the middle of the specimen and progressed outwards.

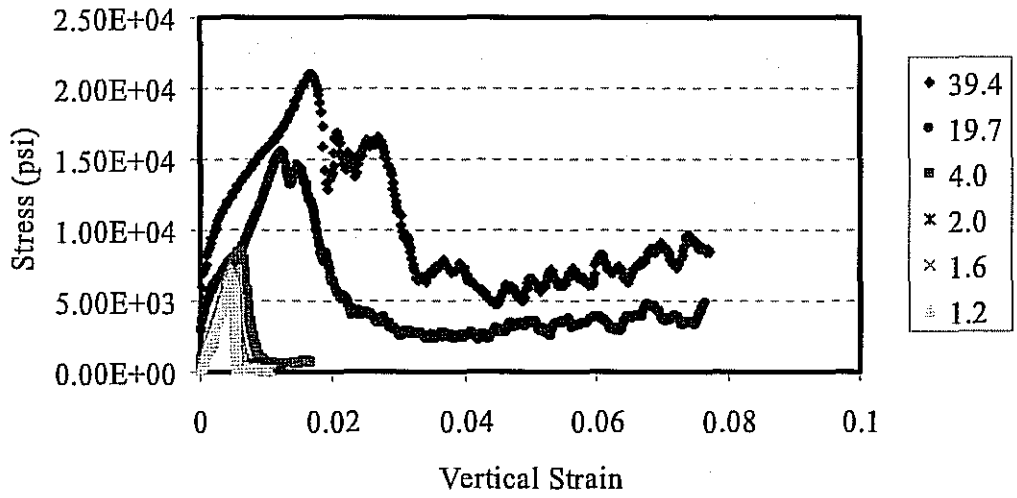

Figure 9.6 - Evaluating Different Rates of Loading in Uniaxial Compression Test

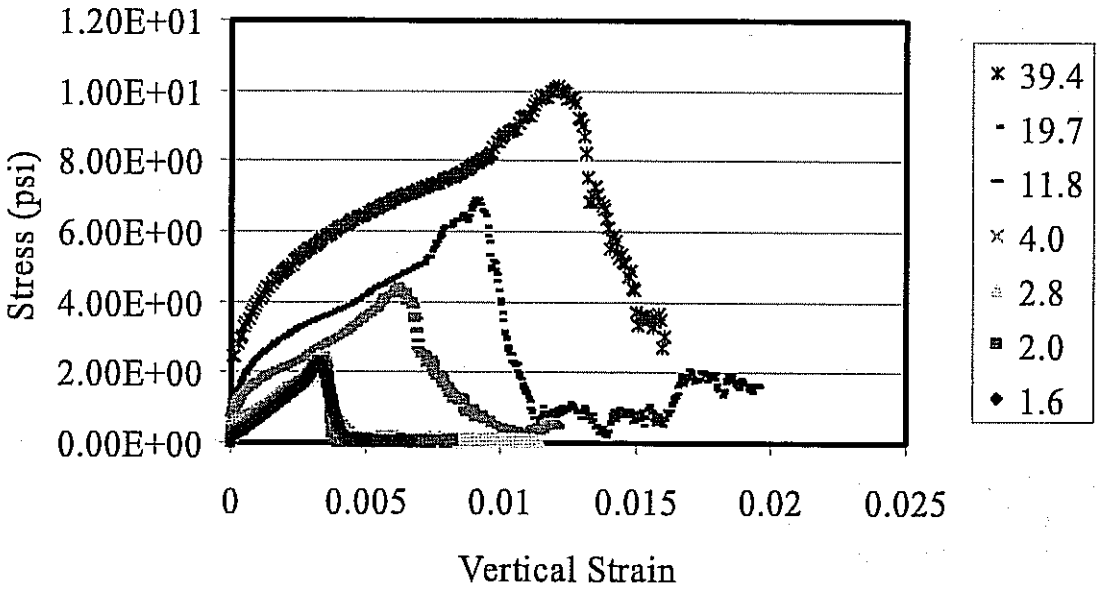

Figure 9.7 - Evaluating Different Rates of Loading for Indirect Tensile Strength Test

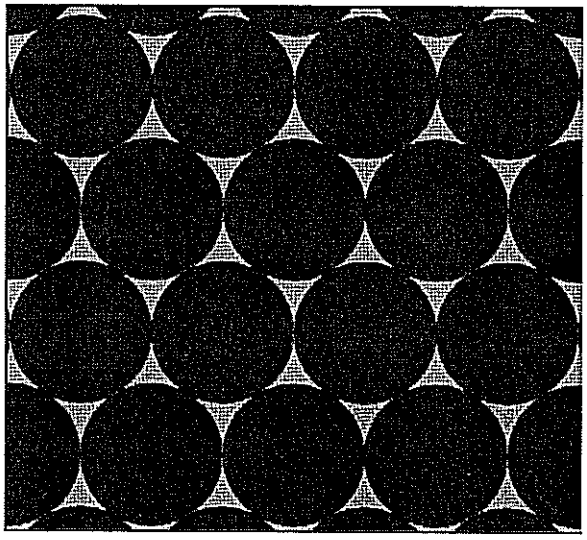

Figure 9.8 - Hexagonal Packing

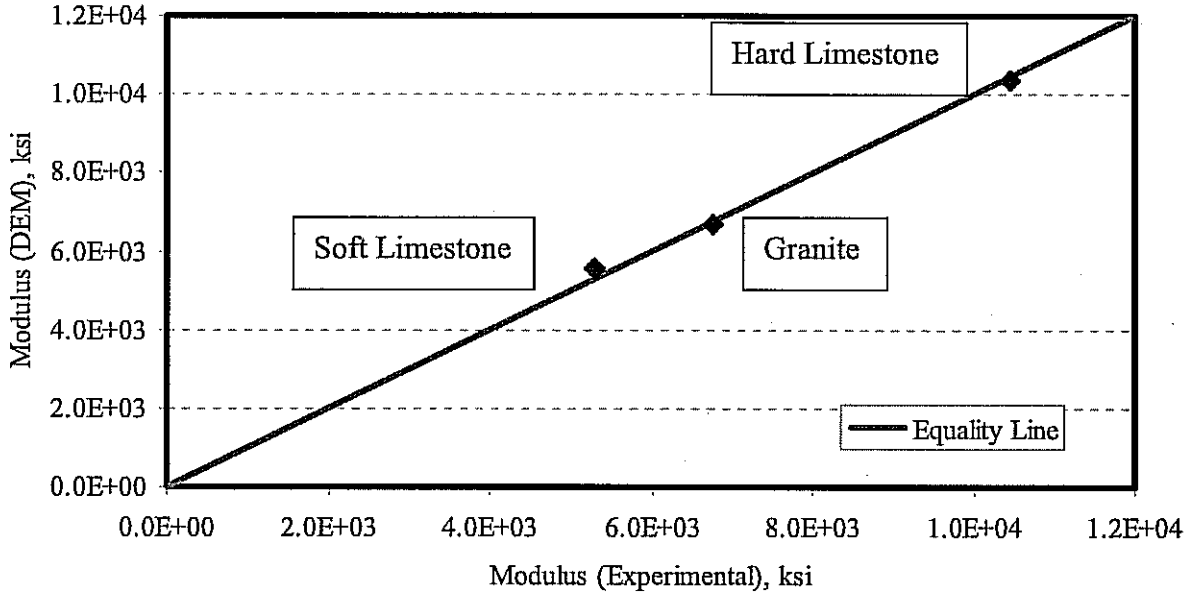

Figure 9.9 - Comparison of Numerical and Experimental Results for Modulus (hexagonal packing)

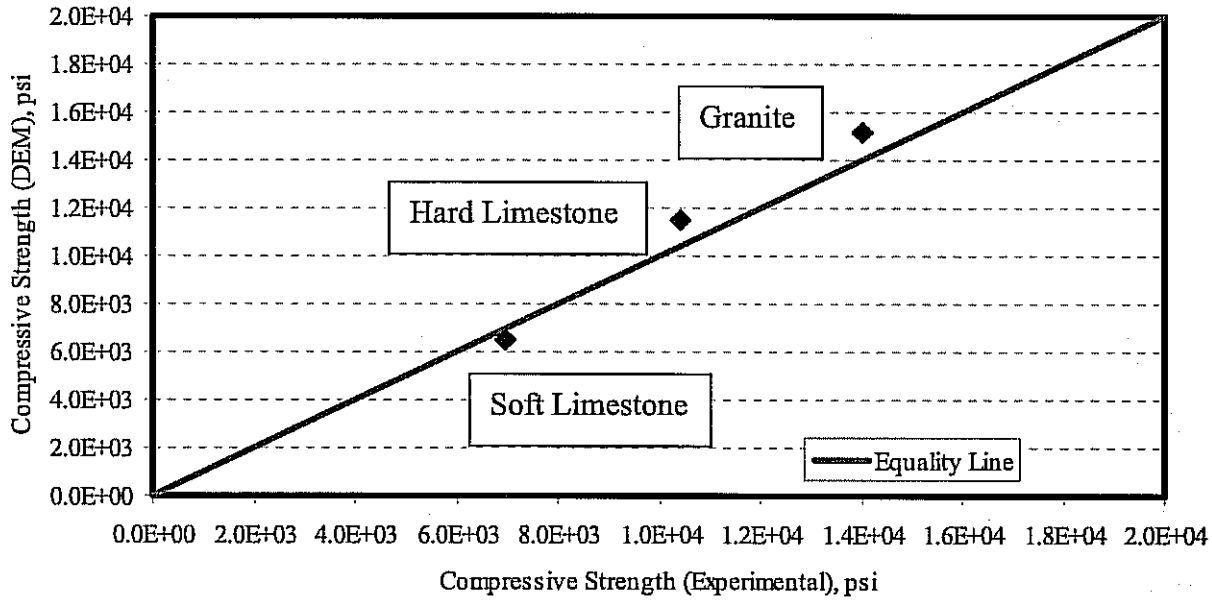

Figure 9.10 - Comparison of Numerical and Experimental Results for Compressive Strength (hexagonal packing)

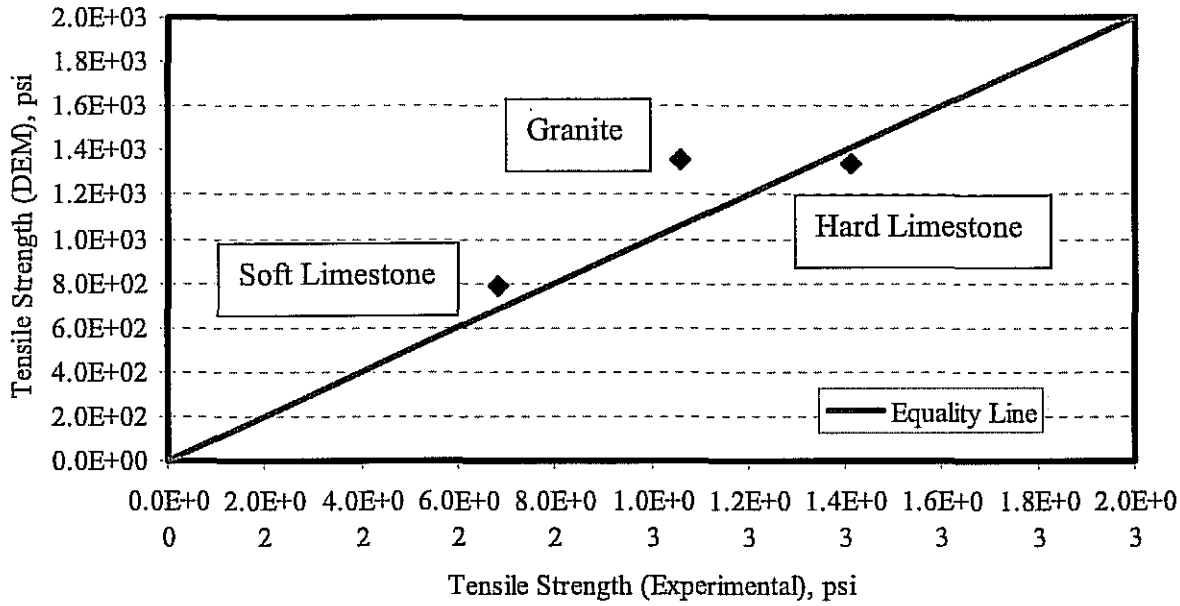

Figure 9.11 - Comparison of Numerical and Experimental Results for Tensile Strength (hexagonal packing)

Table 9.1 - Model Parameters used in DEM

Parameter	Granite	Hard Limestone	Soft Limestone
Bond Strength, lb	45.86	33.72	19.78
Stiffness, ksi	75.42	145.04	65.27

Modeling HMA Response

The contact stiffness and strength parameters obtained from the calibration were used to model the aggregates in the HMA. Figure 9.13 shows a model of a HMA specimen subjected to a vertical compressive stress. The bonds after about 2% vertical strain are shown in Figure 9.14. As this strain level, one of the aggregate particles experienced high stresses which caused the loss of bond strength within the aggregate. However, there was no separation within this aggregate particle probably due to the confinement of the aggregate particle under the compressive forces from the surrounding materials within the specimen. Upon further loading, more fracture occurred at an aggregate particle located towards the top of the specimen. The aggregate particle experienced high tensile and shear stresses that caused loss of the bonds and separation within the aggregate sample. These results demonstrate the ability of PFC2D to model the response of HMA and capture aggregate fracture under different loading conditions.

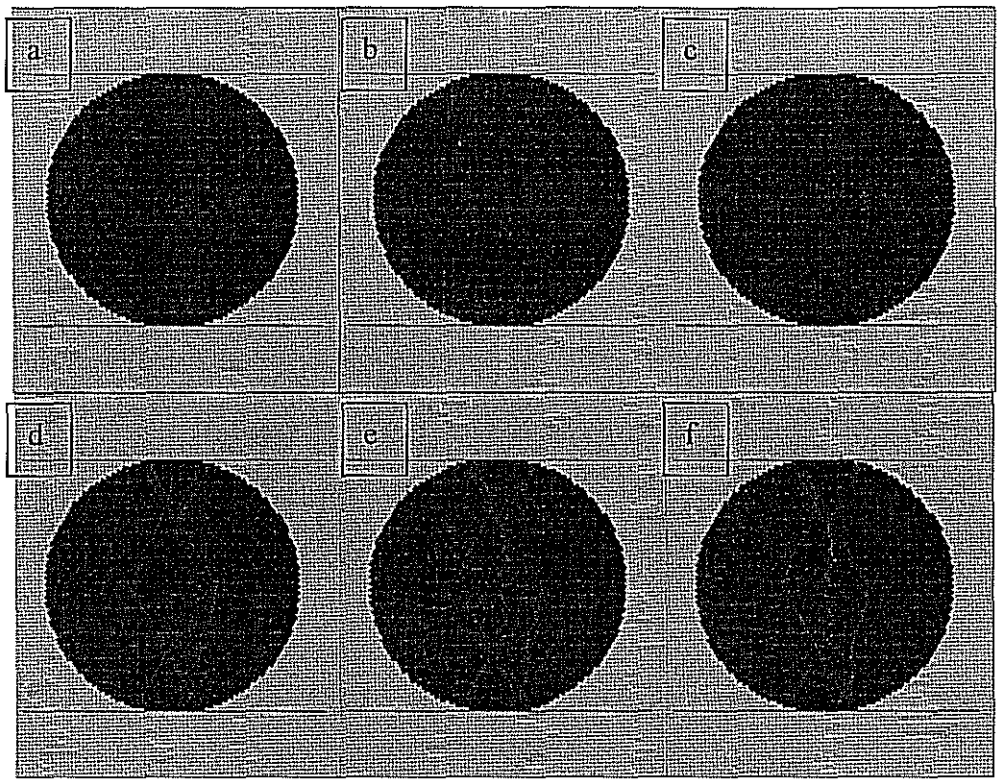

Figure 9.12 - Loss of Bond Progress in IDT

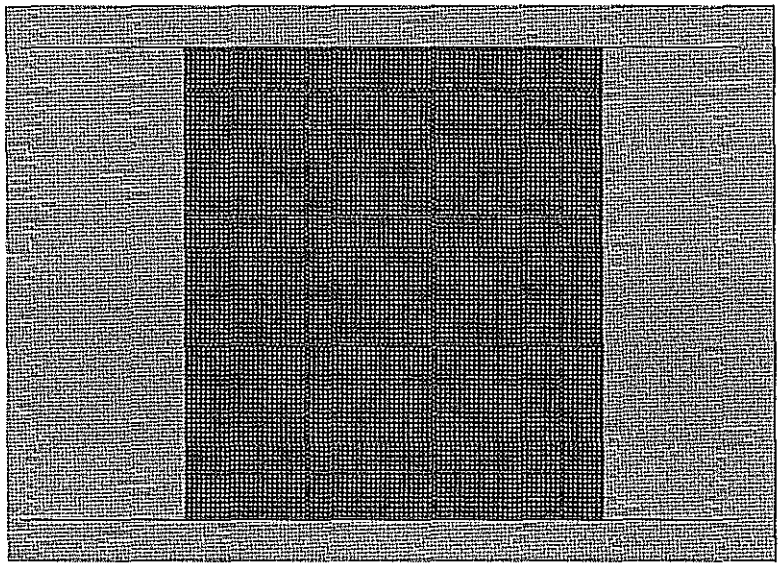

Figure 9.13 - HMA Model used in PFC2D

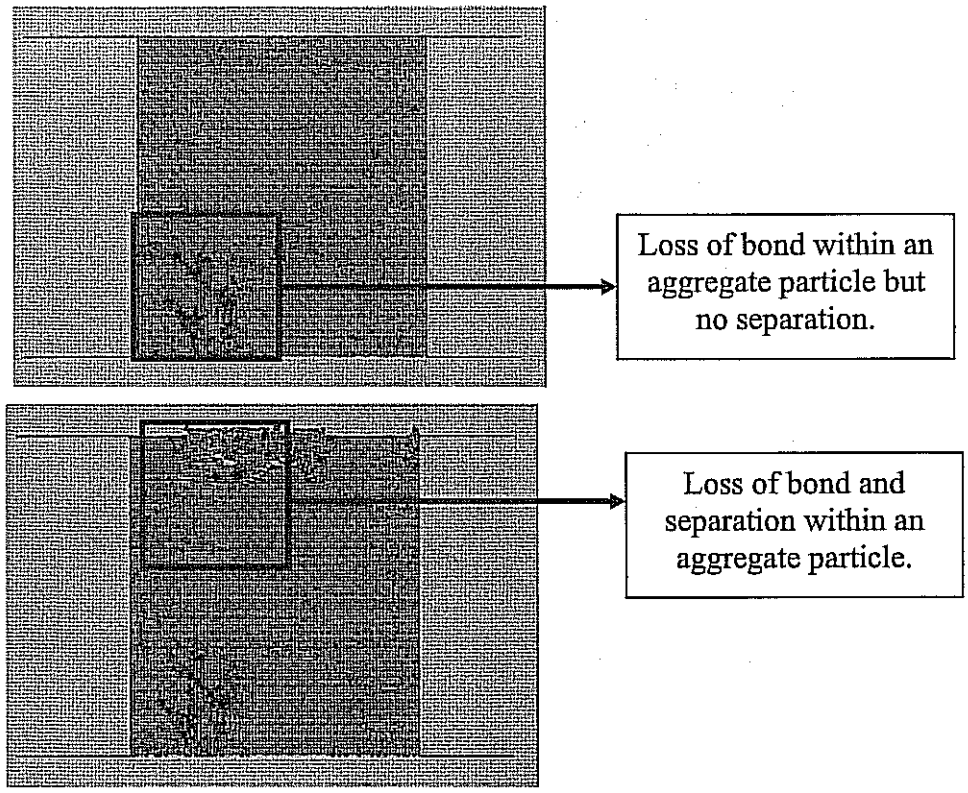

Figure 9.14 - Demonstration of Loss of Bonds in HMA at Different Loading Increments

Indirect Tension of Bituminous Mixes

Figures 9.15 through 9.17 show the PFC2D models for Superpave-C, CMHB-C, and PFC, respectively. The aggregate stiffness and strength determined in the calibration step were used to represent the properties of the aggregate phase in HMA. The mastic properties were determined such that the model results match the indirect tensile strength of the mixes. The mastic strength was determined for the nine mixtures (three different aggregates and three different mixes).

The results plotted in Figures 9.18 and 9.19 show the comparison between the DEM results and the experimental results mix-wise and aggregate type-wise, respectively. The mastic properties used in this model are presented in Table 9.2 for the three different mixes.

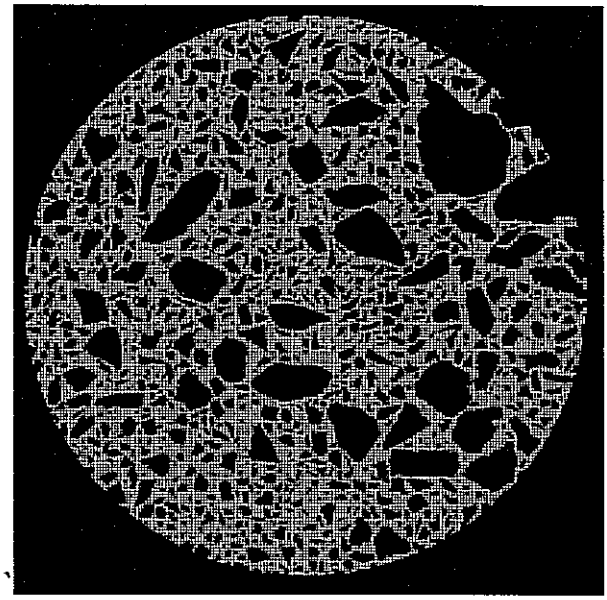

Figure 9.15 - Superpave-C Indirect Tensile Strength Model

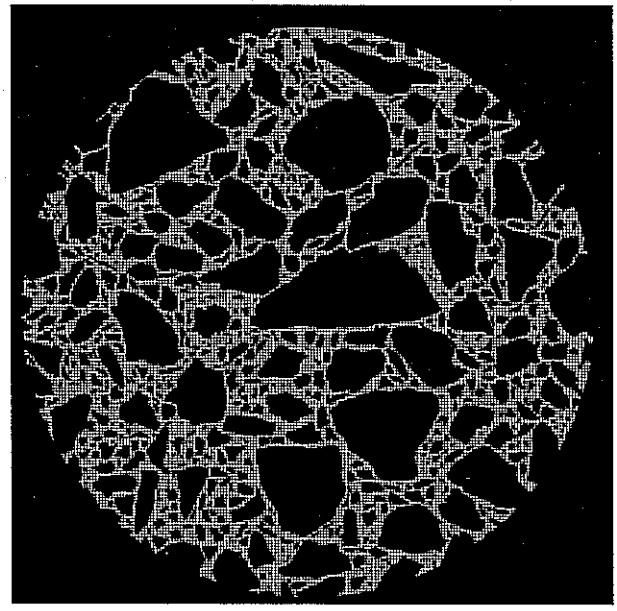

Figure 9.16 - CMHB-C Indirect Tensile Strength Model

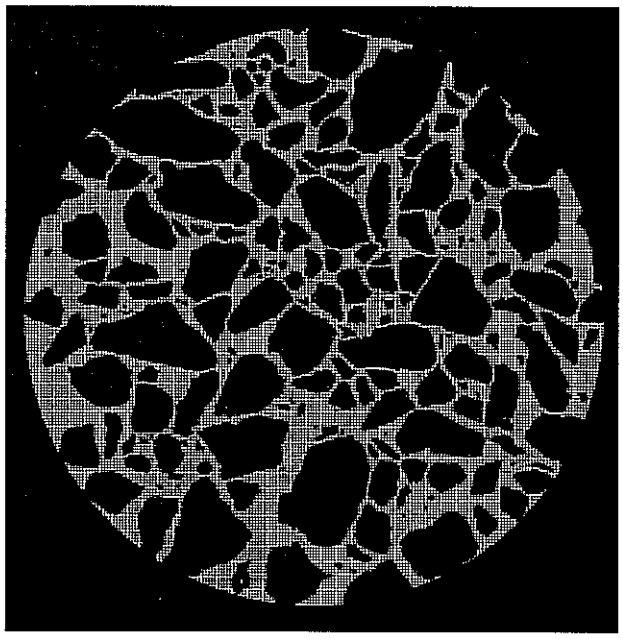

Figure 9.17 - PFC Indirect Tensile Strength Model

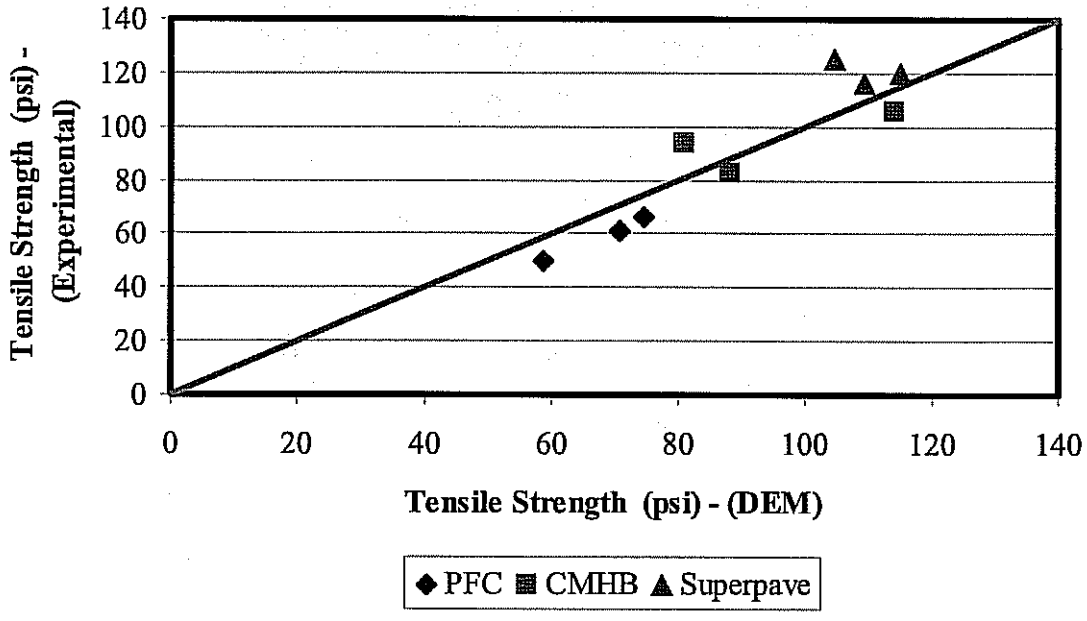

Figure 9.18 - Indirect Tensile Strength Model (Mixes)

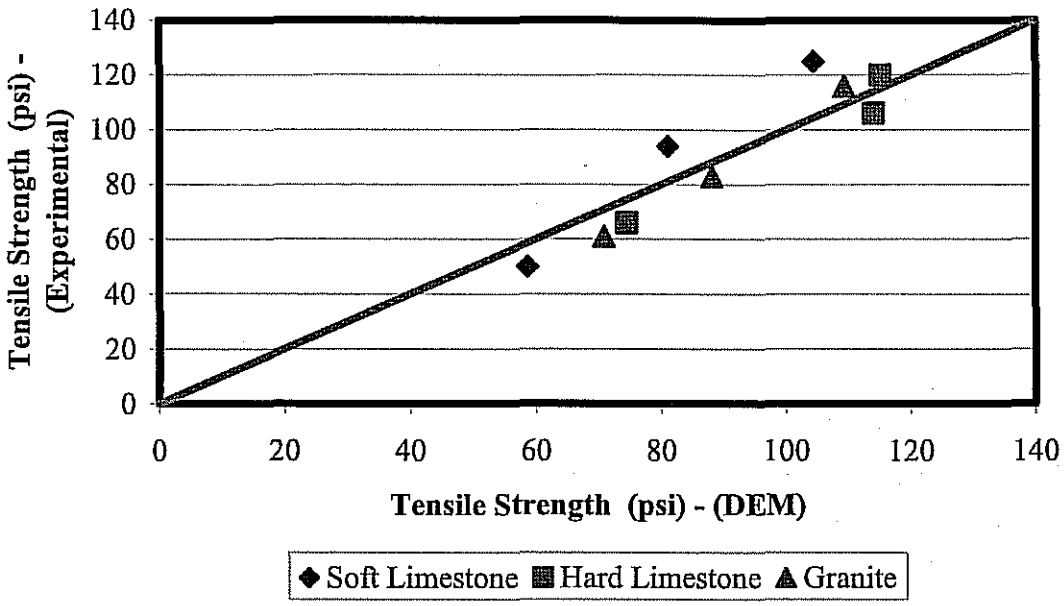

Figure 9.19 - Indirect Tensile Strength Model (Aggregate Type)

Table 9.2 - Mastic Model Parameters used in DEM

a) CMHB-C

Parameter	Granite	Hard Limestone	Soft Limestone
Bond Strength, lb	7.87	9.22	7.87
Stiffness, ksi	43.51	43.51	43.51

b) PFC

Parameter	Granite	Hard Limestone	Soft Limestone
Bond Strength, lb	2.92	2.92	2.70
Stiffness, ksi	43.51	43.51	43.51

c) Superpave-C

Parameter	Granite	Hard Limestone	Soft Limestone
Bond Strength, lb	8.99	10.57	14.61
Stiffness, ksi	43.51	43.51	43.51

The indirect tensile model for the bituminous mixes compared very well with the experimental data, except for the San Antonio soft limestone in the Superpave mix. It was possible to match the experimental measurements for this aggregate, but this required mastic strength much higher than the other two aggregates. As shown in Table 8.4, the soft limestone mixes exhibited, in general, a higher tensile strength than the other two aggregates. It is possible that the aggregate crushing of the soft limestone was higher than the other two aggregates, which caused more fines to be produced within the mastic. The addition of more fines to the mastic increases its tensile strength. The mastic properties play a major role in the mix resistance to tensile stresses such as those applied in the indirect tension test.

The generated model results were examined to determine the points at which the mix lost its bond strength. It was found that the soft limestone mixes experienced loss of bond within the aggregate particles, while the majority of the failure in the hard limestone and granite mixes was within the mastic phase. An example of the loss of bond in the soft limestone Superpave-C mix is shown in Figure 9.20.

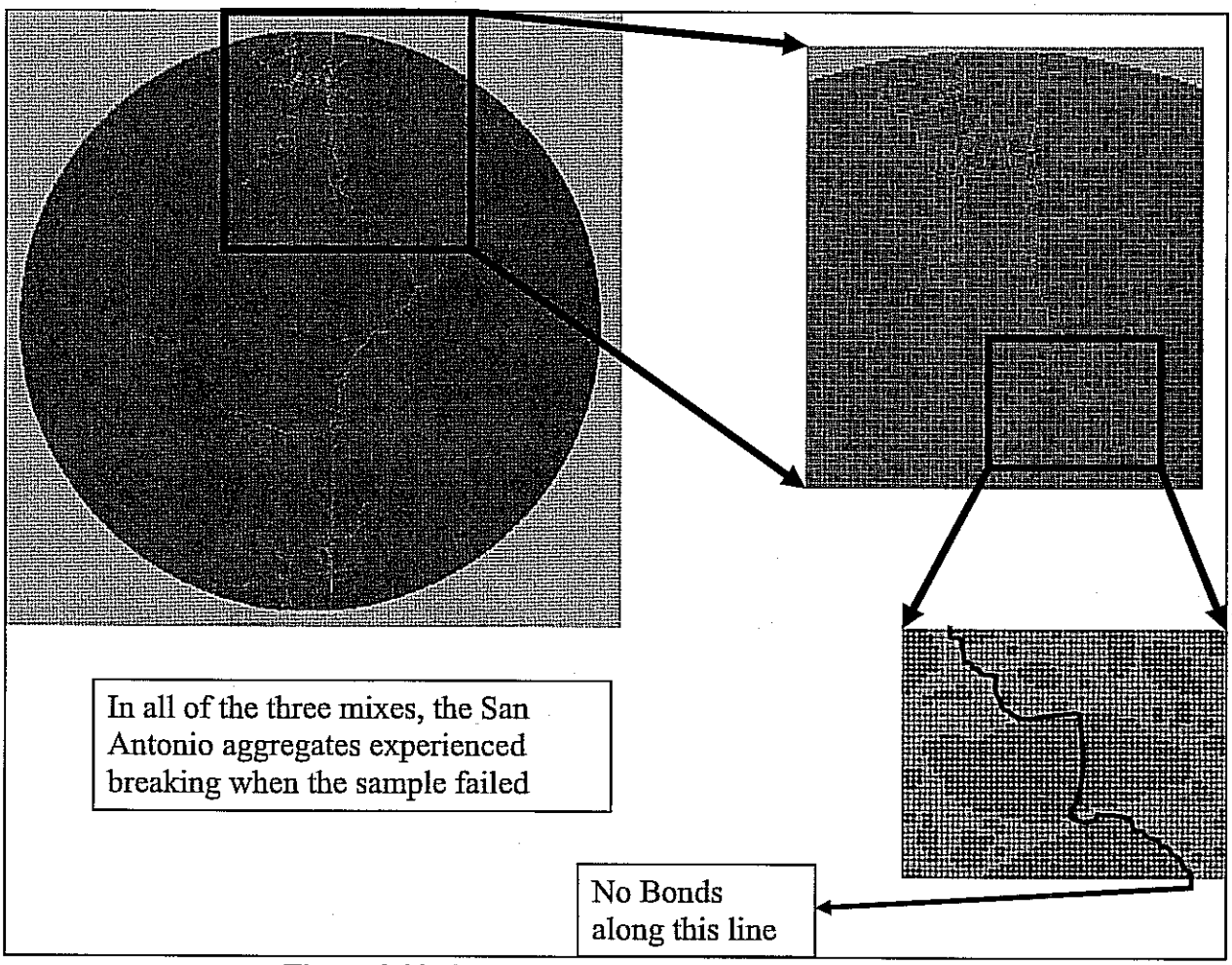

Figure 9.20 - Bond Loss (Indirect Tensile Strength)

Compressive Strength of Bituminous Mixes

The compressive strength of the bituminous mixes was investigated by performing a simulation of axial loading on a rectangular cross section of cylindrical samples. Figures 9.21 through 9.23 present the models used in the compressive strength simulations for the three different mixes. The mastic properties and aggregate properties were used based on the previous two models results. The stiffness of the samples was selected to be the same as the stiffness of the dynamic modulus test results at 1 Hz. A comparison between the model stiffness and measurements is shown in Figure 9.24 for the Superpave-C mix.

Figure 9.25 presents the stress strain curves for the Superpave-C mix for the three different aggregates. The granite mix has the highest compressive strength, followed by the hard limestone and then the soft limestone. This ranking is in agreement with the compressive strength measurements of the rock specimens shown in Figure 9.10.

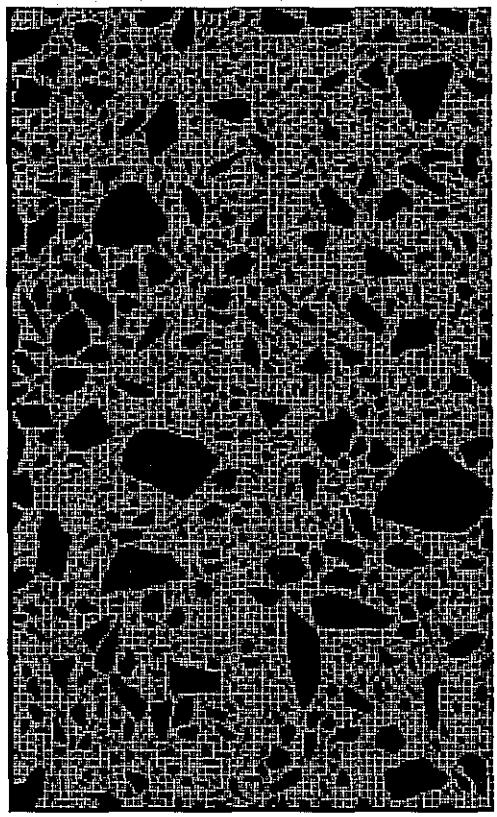

Figure 9.21 - Superpave-C Compressive Strength Model

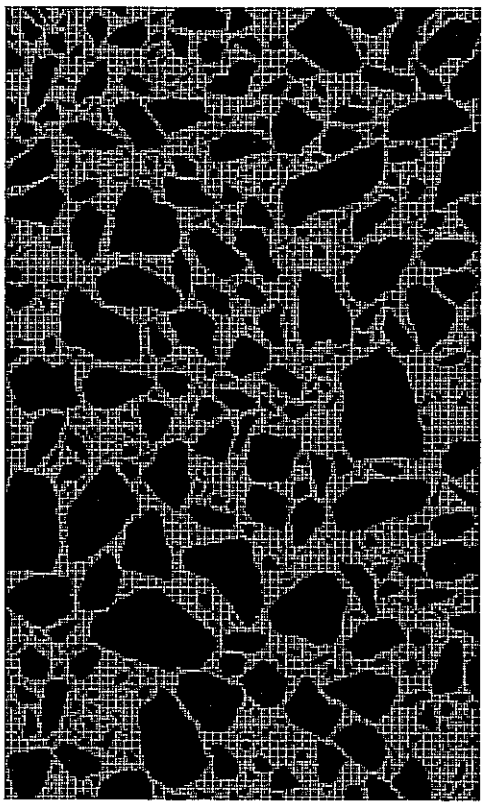

Figure 9.22 - CMHB-C Compressive Strength Model

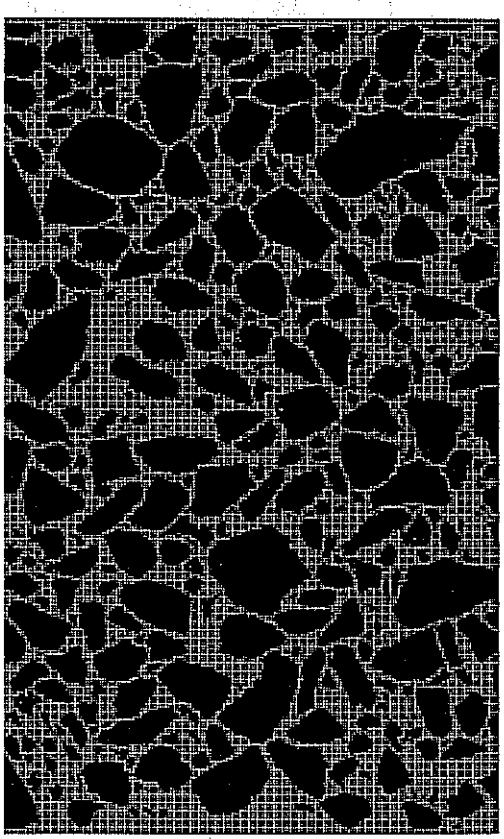

Figure 9.23 - PFC Compressive Strength Model

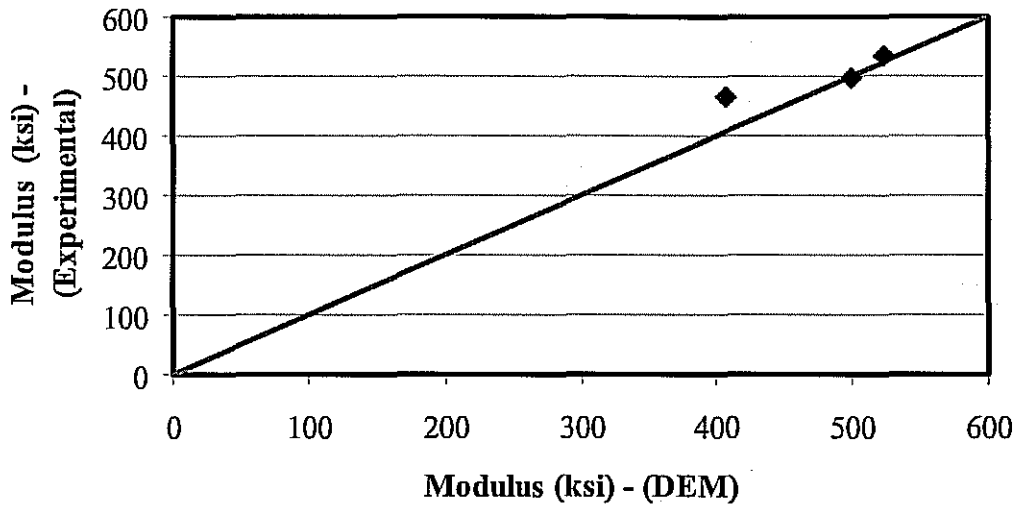

Figure 9.24 - Mixes Stiffness at 1HZ

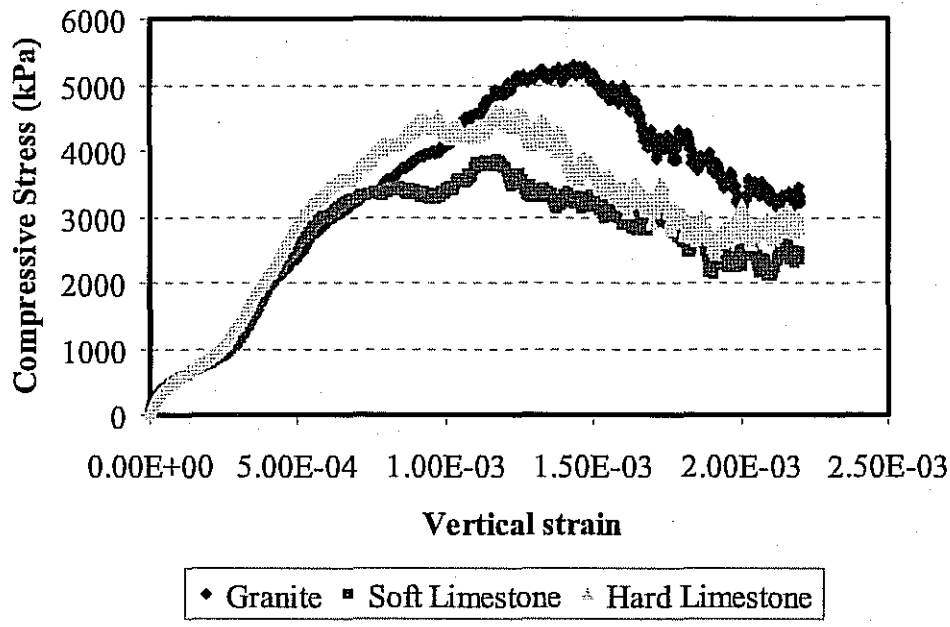

Figure 9.25 - Stress Strain Curves for Superpave-C Mix

Figure 9.26 presents the simulation for the soft limestone sample. The aggregate breakage can occur with separation or without separation. Breakage without separation is a result of losing the bond along a specific plane inside the aggregate, but the crack surface has enough compression to keep the two faces in contact.

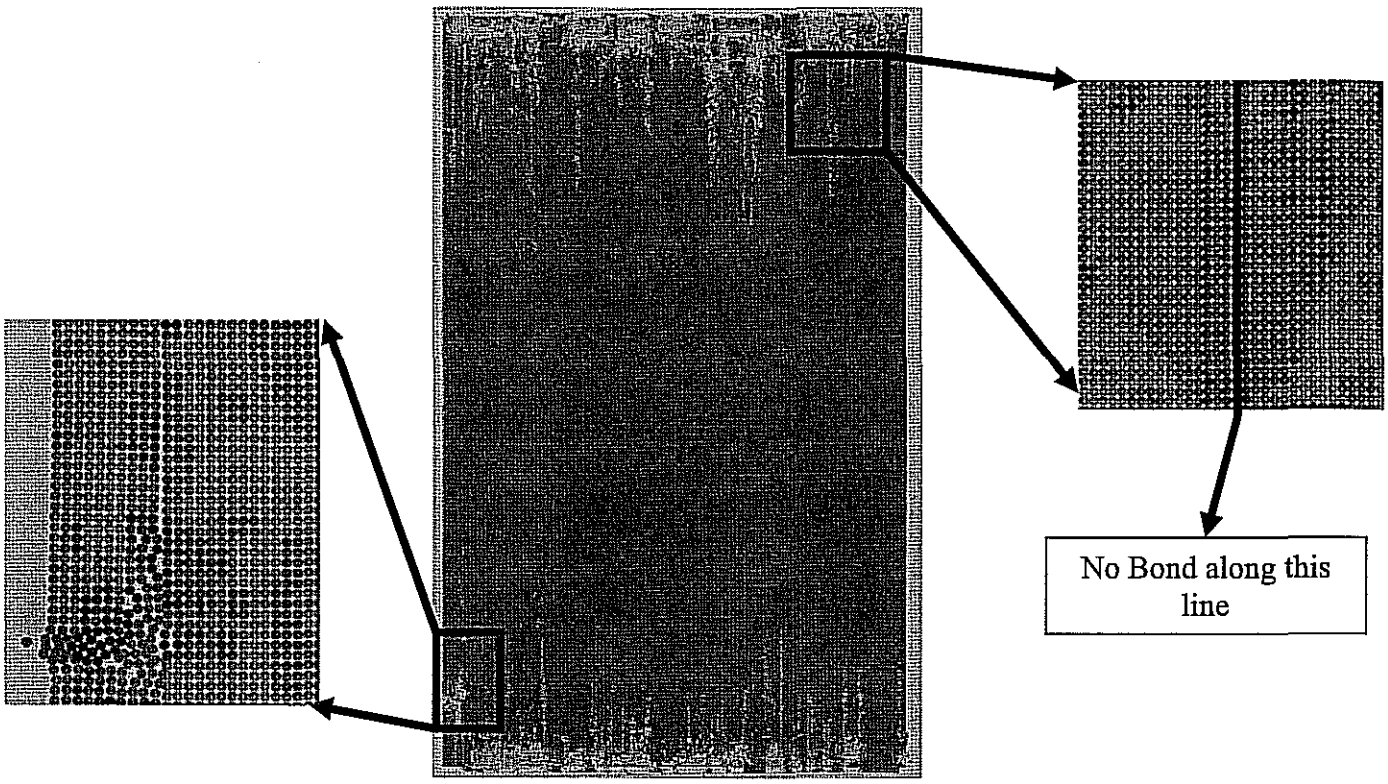

Figure 9.26 - Bond Loss (Compressive Strength)

Stress Distribution

Stress distribution within the indirect tensile test samples was investigated as shown in Figures 9.27 through 9.29 for the hard limestone, soft limestone, and granite, respectively. Each figure presents the stress distribution for the three mixes for one type of aggregates and at two stress levels. All these figures are plotted to the same scale. The contact forces are distributed more uniformly in the Superpave-C mix compared with the other mixes. The PFC mix experienced the highest concentration of contact forces within the aggregate structure at low and high stress levels. The CMHB-C mix showed results close to the Superpave-C mix; and in all cases, the CMHB-C has a more uniform distribution than the PFC mix. As the low stress levels (a, b and c in the figures), the maximum internal chain force within the PFC mix is about 127 kN (granite), about 91 kN in the Superpave mix (granite), and 88 kN in the CMHB-C mix (granite). At the high stress levels (d, e, and f in the figures), the maximum internal force within the PFC mix is about 589 kN, while it is only 393 kN in the Superpave and around 400 kN in the CMHB-C. A higher maximum value in the PFC is another indication of less uniformity in force distribution compared with the Superpave-C and CMHB-C mixes.

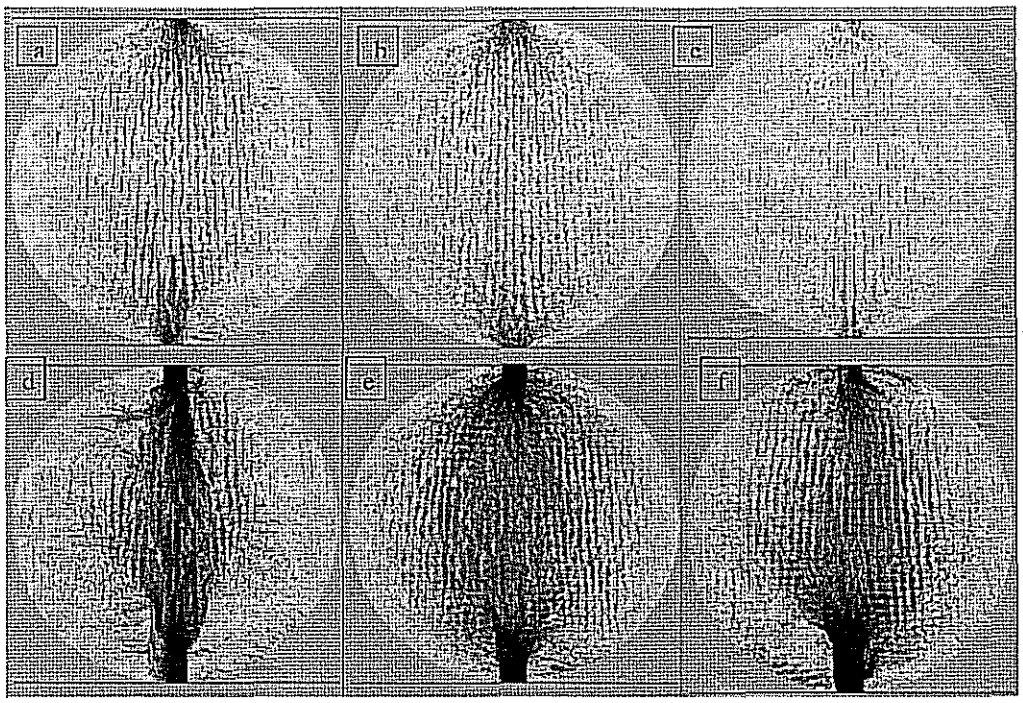

Figure 9.27 - Stress Distribution for Hard Limestone
a) low stress PFC, b) low stress Superpave-C, c) low stress CMHB-C, d) high stress PFC, e) high stress Superpave-C, f) high stress CMHB-C

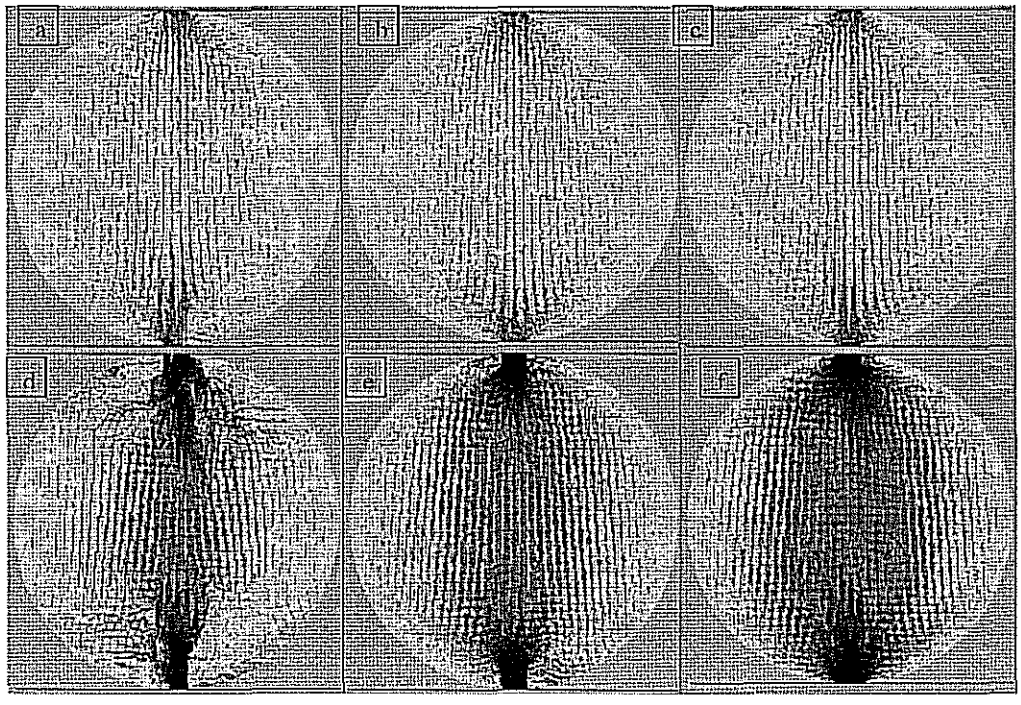

Figure 9.28 - Stress Distribution for Soft Limestone
a) low stress PFC, b) low stress Superpave-C, c) low stress CMHB-C, d) high stress PFC, e) high stress Superpave-C, f) high stress CMHB-C

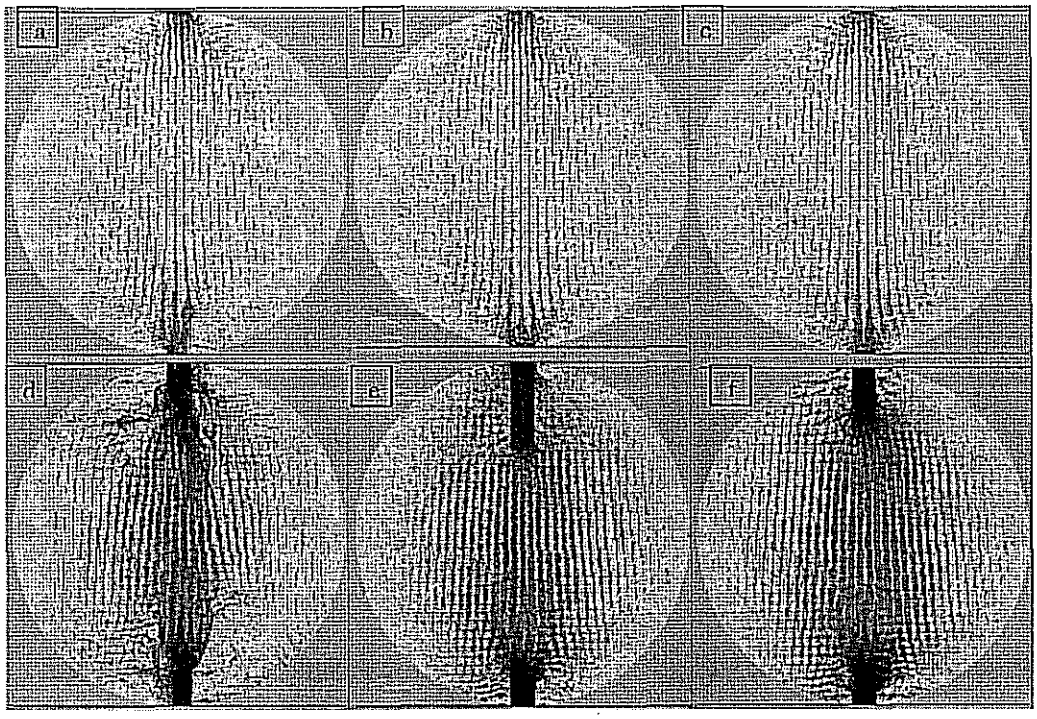

Figure 9.29 - Stress Distribution for Granite
a) low stress PFC, b) low stress Superpave-C, c) low stress CMHB-C,
d) high stress PFC, e) high stress Superpave-C, f) high stress CMHB-C

CHAPTER TEN - ANALYSIS OF RESULTS

INTRODUCTION

The experimental and modeling results were presented in the previous chapters for three aggregates and three mixes. Chapters 3 through 6 include the test procedures and results of experiments regarding the aggregates and rock properties. Chapters 7 and 8 cover the performance of the mixes estimated from a number of laboratory tests. In Chapter 9, the results from micro-mechanical models were presented. In this chapter, the results from these tests are analyzed to draw a number of preliminary observations with regard to the applicability of tests used in this study to estimate the impact of point and mass strength on the performance of the mixes. It should be emphasized that the goal of the activities reported in this chapter is to mainly demonstrate the process to be followed in the final report. Given that only three aggregates were tested, and given the variability inherent in each test, the results from more than three aggregates are needed. The Phase II report will contain a more comprehensive database that can be used for drawing more concrete conclusions.

The first section of this chapter includes a study on the ranking of the aggregates from a number of diverse points of view. Correlation analysis among all of aggregate tests is then carried out to identify the redundant, complementary and inconclusive aggregate tests.

The second part of this chapter focuses on the material characterization tests for the mixes. A correlation analysis among the test methods for the characterization of mixes is carried out to once again identify the redundant, complementary and inconclusive mix tests. Finally, a process for developing relationships between individual aggregate tests and tests related to HMA performance is discussed.

AGGREGATE RANKING

Table 10.1 includes the results from all aggregate-related tests. The results are categorized in the following three groups:

1. Aggregate properties from tests that may contribute to the identification of point and mass strength,
2. Rock properties of the bulk specimens used to identify the strength and stiffness of rocks before crushing, and
3. Shape and texture properties from the traditional tests commonly carried out by TxDOT for defining the quality of aggregates.

Two processes were used to rank the aggregates. This ranking is either based on the maximum likelihood or based on a composite score. All aggregate characterization tests were assigned equal weight in both approaches. This translates to the hypothesis that all tests are equally appropriate. The validity of this assumption will be further explored toward the end of this chapter.

Maximum Likelihood Approach

The results in Table 10.1 were first used to rank the aggregates from each test. The rankings of aggregates for each test are included in Table 10.2. A value of one signifies that the aggregate is the strongest or the best from that particular test. On the other hand, a value of three means the aggregate is the weakest or worst. When the results for two aggregates were similar, the same ranking was assigned to both.

Figure 10.1 shows the frequency of rankings for each material when all tests are considered. Of the 23 tests that were carried out on the aggregates and rock samples, the hard limestone is ranked the best (ranking of 1) with a frequency of 16, and ranked second best (ranking of 2) seven times. The hard limestone can therefore be ranked the best among the aggregates. Following that logic, granite is ranked the second best and the soft limestone the worst.

To further understand the impact of the three categories of tests enumerated above (aggregate properties, rock properties, and shape and texture), the ranking is broken done by the category of tests. These results are summarized in Figure 10.2. From the aggregate properties, the hard limestone clearly ranks the best, granite the second best and the soft limestone the worst. From the rock properties, however, it would be difficult to judge whether the hard limestone or the granite can be categorized as the best; but again the soft limestone is clearly the worst. From traditional shape and texture, the granite is slightly better than the hard limestone, with once again soft limestone being the worst.

Composite Score

A more objective way for ranking the aggregates is based on a composite score. This method, which is used in Multiple Attribute Decision Making (MADM), is routinely used in evaluating competing alternatives objectively. Over the years, several methods have been developed depending on the type of information available to the decision maker. Hobbs (1980) and Hwang and Yoon (1981) provide a good review and explanation of numerous weight assessment techniques for MADM. The main idea behind the MADM methodology is to obtain a meaningful set of attributes than can be used to measure a set of alternatives. Part of this process is to have a homogeneous data type by transformation or normalization of the raw data.

To implement the process, the aggregate tests are first separated into two groups: (1) those tests on where a higher value indicates a better aggregate, and (2) those that a lower value signifies a

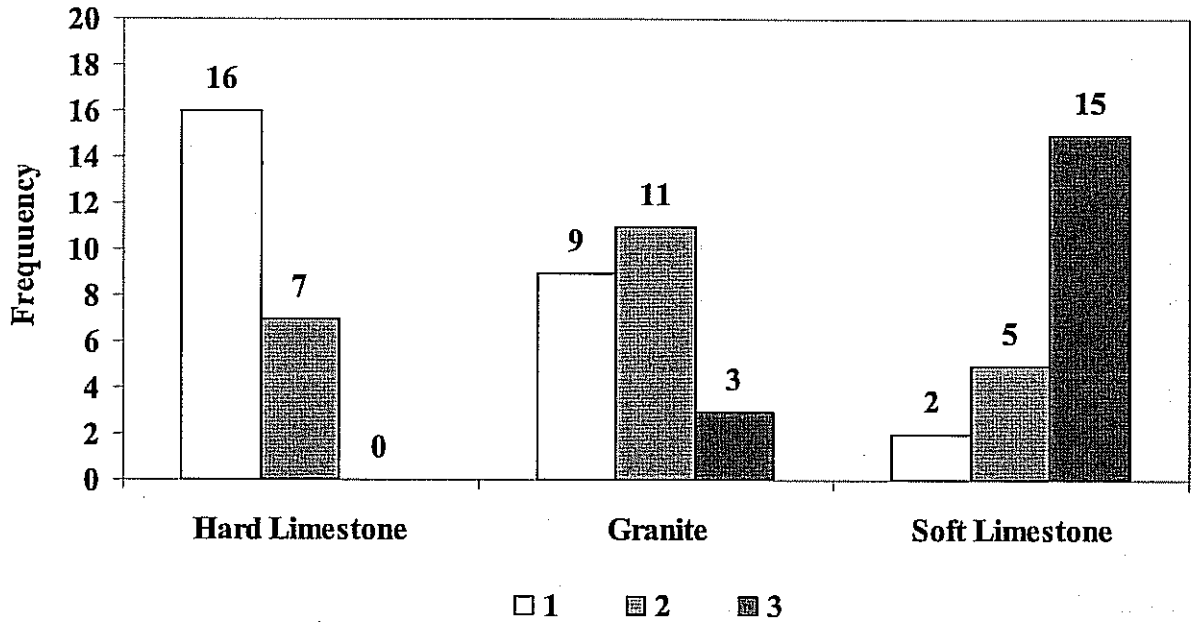

Figure 10.1 - Ranking of Aggregates Based on All Tests

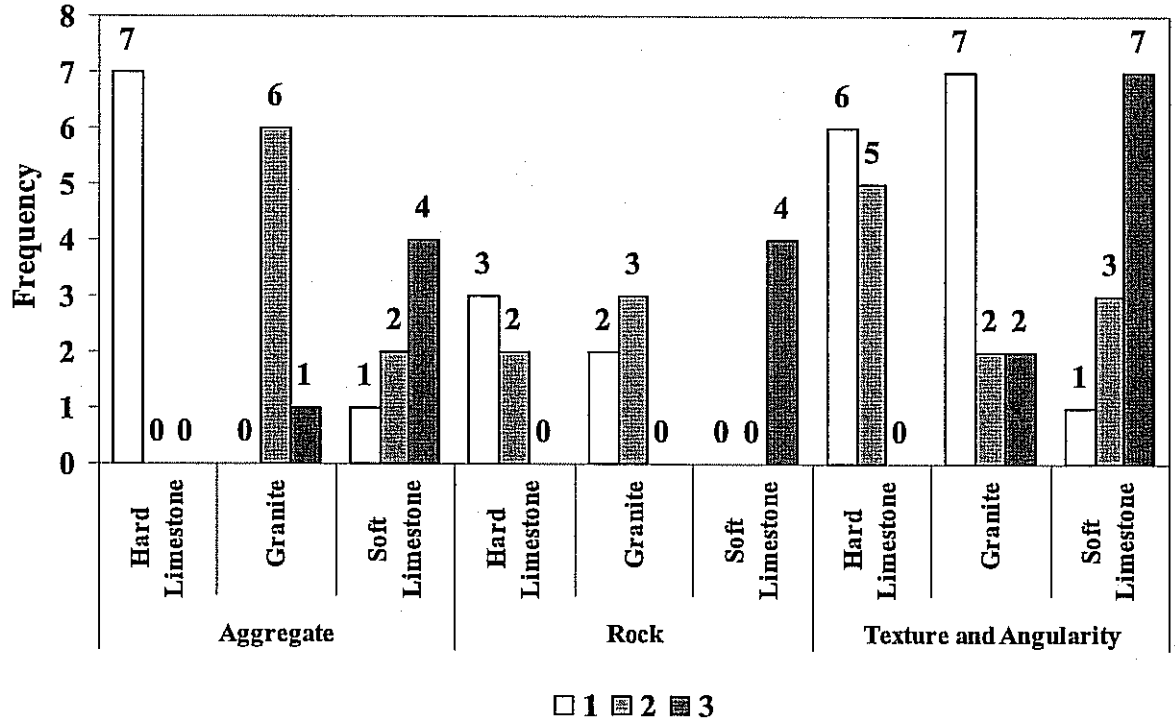

Figure 10.2 - Ranking of Aggregates Delineated by Type of Tests

Table 10.1 - Results of Aggregate Characterization Tests

Material	Aggregate							Rock					Shape and Texture										
	ACV	Compacting Modulus, ksi	Crushing Modulus, ksi	Max. Compacting Stress, psi	AIV-dry	AIV-wet	TFV	Compressive Strength, psi	Tensile Strength, psi	Compressive Strength from Schmidt Hammer, psi	Seismic Modulus from V-meter, ksi	Seismic Modulus from FFRC, ksi	Los Angeles Abrasion % Wt. Loss - Bituminous	Mg Soundness Test - Bituminous	Mg Soundness Test - Stone	Polish Value	Micro Deval % Wt. Loss - Bituminous	Aggregate Acid Insolubility	Micro Deval % Wt. Loss - Stone	Texture Before Micro Deval	Texture After Micro Deval	Angularity Before Micro Deval	Angularity After Micro Deval
Hard Limestone	22%	6.8	26	1371	13%	31%	9%	10427	1412	9719	10328	10299	22	5	4	22	11	3	15	193	95	2323	1730
Granite	27%	4.9	27.2	1008	29%	35%	12%	14034	1062	12034	6686	7440	33	9	7	29	10	97	9	221	187	2791	2491
Soft Limestone	32%	4.1	32	988	28%	34%	10%	6970	682	6994	5473	--	29	18	14	25	23	2	20	80	36	2195	1671

Table 10.2 - Ranking of Aggregates from Characterization Test

Material	Aggregate							Rock					Shape and Texture											Final Ranking
	ACV	Compacting Modulus	Crushing Modulus	Max. Compacting Stress	AIV-dry	AIV-wet	TFV	Compressive Strength	Tensile Strength	Compressive Strength from Schmidt Hammer	Seismic Modulus from V-Meter-	Seismic Modulus from FFRC	Los Angeles Abrasion % Wt. Loss-BIT	Mg Soundness Test - BIT	Mg Soundness Test - Stone	Polish Value	Micro-Deval % Wt. Loss - BIT	Aggregate Acid Insolubility	Micro-Deval % Wt. Loss - Stone	Texture Before Micro-Deval	Texture After Micro-Deval	Angularity Before Micro-Deval	Angularity After Micro-Deval	
Hard Limestone	1	1	1	1	1	1	1	2	1	2	1	1	1	1	1	1	1	1	2	2	2	2	2	1
Granite	2	2	2	2	2	2	3	1	2	1	2	2	3	2	2	3	1	1	1	1	1	1	1	2
Soft Limestone	3	3	3	3	2	2	1	3	3	3	3	3	2	3	3	2	2	1	3	3	3	3	3	3

better aggregate. For the first group of tests (higher values signify a better aggregate) the results from each test are normalized using:

$$r_{ij} = \frac{min\{x_j\}}{x_{ij}} \tag{10.1}$$

where $min\{x_j\}$ is the minimum value measured from test method j for the three aggregates; x_{ij} is the result from test j for aggregate i (for i = 1 to 3); and r_{ij} is the normalized value from test j for aggregate i. On the other hand, if a lower value signifies a better aggregate, Equation 10.2 is used to obtain r_{ij}:

$$r_{ij} = \frac{x_{ij}}{max\{x_j\}} \tag{10.2}$$

where $max\{x_j\}$ is the maximum value measured from test j. Based on the measured values reported in Table 10.1, the normalized values from each test for the three aggregates are shown in Table 10.3.

The final step is to sum the normalized values from all tests for each aggregate to obtain the composite score. The aggregate with the highest score is considered as the best aggregate.

Table 10.4 shows the composite score and the ranking from all tests. With composite scores of 19.8 and 19.2, the hard limestone and granite rank similarly with the hard limestone being slightly better. However, the soft limestone is significantly worse than the other two aggregates. This ranking is similar to that from the maximum likelihood method.

Table 10.4 also contains the rankings by the test categories as well. Based on all three tests, the soft limestone is the worst aggregate. However, the granite and hard limestone exhibit mixed trends in terms of which one is better. Based on the aggregate mechanical properties, the hard limestone is ranked significantly higher than the granite. Based on the rock properties, the hard limestone is marginally better than the granite. Based on the texture and angularity tests, the granite is ranked higher than the hard limestone. To interpret the impact of each category of tests on the final performance, further analysis was carried out as included later in this chapter.

CORRELATION OF TEST METHODS

One of the objectives of this study was to determine which tests are most representative of the aggregate point and bulk strength, shape and texture, and performance of the HMA mixtures. Since some tests may provide redundant information, a correlation analysis among the tests was performed to eliminate the redundant tests and to select complimentary tests. Based on the correlation analysis, tests that provide similar results or are highly correlated can be isolated so that one of them can be selected. At this point, little consideration was given to the selection process in terms of cost, test time, and impact on the TxDOT operation. These items will be considered by the end of Phase II of the project.

The preliminary correlations between the three categories of tests (aggregate properties, rock properties and shape and texture) are included in Table 10.5. Preliminary, two parameters are considered correlated when the absolute value of their correlation coefficient (CC) is greater than

Table 10.3 - Normalized Score for Aggregate Characterization Tests

Material		Aggregate Type		
		Hard Limestone	Granite	Soft Limestone
Aggregate	ACV	1.0	0.8	0.7
	Compacting Modulus, ksi	1.0	0.7	0.6
	Crushing Modulus, ksi	1.0	1.0	0.8
	Max. Compacting Stress, psi	1.0	0.7	0.7
	AIV-dry	1.0	0.4	0.5
	AIV-wet	1.0	0.9	0.9
	TFV	1.0	0.8	0.9
Rock	Compressive Strength, psi	0.7	1.0	0.5
	Tensile Strength, psi	1.0	0.8	0.5
	Schmidt Hammer, psi	0.8	1.0	0.6
	V-meter, ksi	1.0	0.6	0.5
	FFRC, ksi	1.0	0.7	-
Texture and Angularity	Los Angeles Abrasion % Wt. Loss	1.0	0.7	0.8
	Mg Soundness Test - Bituminous	1.0	0.6	0.3
	Mg Soundness Test - Stone	1.0	0.6	0.3
	Polish Value	0.8	1.0	0.9
	Micro-Deval % Wt. Loss - Bituminous	0.9	1.0	0.4
	Fine Aggregate Acid Insolubility	0.0	1.0	0.0
	Micro-Deval % Wt. Loss - Stone	0.6	1.0	0.5
	Texture Before Micro-Deval	0.9	1.0	0.4
	Texture After Micro-Deval	0.5	1.0	0.2
	Angularity Before Micro-Deval	0.8	1.0	0.8
	Angularity After Micro-Deval	0.7	1.0	0.7

Table 10.4 - Ranking of Aggregates based on Composite Score

Test Category	Hard Limestone		Granite		Soft Limestone	
	Score	Rank	Score	Rank	Score	Rank
All Tests	19.8	1	19.2	2	12.3	3
Aggregate Tests Only	7.0	1	5.3	2	5.1	3
Rock Tests Only	4.6	1	4.1	2	2.1	3
Texture and Angularity Tests Only	8.2	2	9.8	1	5.1	3

0.6. As a reminder, a CC of 1 corresponds to a perfect correlation and a CC of zero to no correlation. A negative sign for CC indicated that when one parameter is increasing, the other one is decreasing.

As shown in Table 10.5a, the ACV test results and its surrogate parameters (compacting and crushing modulus and maximum compacting stress) correlate well with one another and with the AIV test results. The TFV seems to correlate reasonably well with maximum compacting stress, as expected. As such, the ACV test would be an appropriate test to use for characterizing the aggregates, especially since several parameters can be readily determined from the same test. Furthermore, the cost of implementing these tests in Districts that own a concrete compressive test machine is rather small.

Table 10.5b illustrates the correlation analysis for the tests carried out on rock specimens retrieved from quarries. From micro-mechanical modeling, three parameters are necessary: compressive strength, tensile strength and the modulus. Since the compressive strength test results and those from the Schmidt hammer are well-correlated, the Schmidt hammer can be used for assessing the compressive strength of the rock. This eliminates the need for coring the rock, and requires minimal training.

The tensile strength seems to be well-correlated to the moduli from either FFRC or V-meter tests. This trend makes sense since both the modulus and the tensile strength are to a great extent controlled by the size of the grains composing the rock. If micro-mechanical modeling is not required, it seems that the V-meter will be a great tool for estimating the quality of the aggregates in tension. The V-meter is recommended over the FFRC since the V-meter tests can be carried out on the rock samples that are faced without coring. This test also provided the third important property of the aggregates, i.e. modulus.

A strong relationship between the compressive strength and modulus has been reported for many geo-materials and concrete. However, in Table 10.5b, these two parameters either show very weak or counterintuitive correlations. The size of the grains within the rock mass may not impact the compressive strength, but it greatly impacts the modulus.

The third set of correlation analyses performed was for the shape and texture characterization tests. This is shown in Table 10.5c. The test results for the aggregate abrasion and soundness resistance, polishing, and physical characteristics such as shape, angularity and texture are included in this Table. The test method conducted by TTI for the characterization of the angularity of the aggregate revealed a fair correlation with most of the tests except for the soundness characterization tests. On the other hand, the LA abrasion resistance test showed a poor relationship with almost all the other tests while the Micro-Deval correlated better.

Table 10.5 - Correlation Analysis among Different Aggregate Tests

a) Aggregate Tests

Test	ACV	Compacting Modulus	Crushing Modulus	Max. Compacting Stress	AIV-dry	AIV-wet	TFV
ACV	1.00						
Compacting Modulus	-0.97	1.00					
Crushing Modulus	0.94	-0.84	1.00				
Max. Compacting Stress	-0.89	0.97	-0.69	1.00			
AIV-dry	0.84	-0.94	0.61	-0.99	1.00		
AIV-wet	0.72	-0.86	0.45	-0.96	0.98	1.00	
TFV	0.33	-0.53	0.00	-0.72	0.79	0.89	1.00

b) Rock Tests

Test	Compressive Strength	Tensile Strength	Compressive Strength from Schmidt Hammer	Seismic Modulus from V-meter	Seismic Modulus from FFRC
Compressive Strength	1.00				
Tensile Strength	0.51	1.00			
Schmidt Hammer	1.00	0.56	1.00		
V-meter	0.23	0.95	0.29	1.00	
FFRC	**-1.00**	1.00	**-1.00**	1.00	1.00

Note: values that are bold and underlined demonstrate high correlations that are seemed counterintuitive

c) Shape and Texture Tests

Test	LA BIT	MG BIT (HMAC)	MG BIT (ST)	PV	MD BIT	CA AI	MD	Texture BMD	Texture AMD	Angularity BMD	Angularity AMD
Los Angeles Abrasion % Wt.	1.00										
Mg Soundness Test- BIT	0.45	1.00									
Mg Soundness Test- Stone	0.44	1.00	1.00								
Polish Value	0.97	0.22	0.21	1.00							
Micro-Deval % Wt. Loss- BIT	0.06	0.92	0.92	-	1.00	-					
Fine Aggregate Acid Insolubility	0.77	-	-	0.90	-	1.00					
Micro-Deval % Wt. Loss- Stone	-	0.65	0.65	-	0.90	-	1.00				
Texture Before Micro-Deval	0.03	-	-	0.27	-	0.66	-	1.00			
Texture After Micro-Deval	0.47	-	-	0.67	-	0.93	-	0.90	1.00		
Angularity Before Micro-Deval	0.63	-	-	0.80	-	0.98	-	0.79	0.98	1.00	
Angularity After Micro-Deval	0.74	-	-	0.87	-	1.00	-	0.70	0.94	0.99	1.00

Table 10.6 shows the results obtained for the mixture performance characterization tests. Correlation analysis was also carried out on these tests to identify the relationship between performance tests on HMA specimens and geotechnical tests carried out on specimens prepared with aggregates alone (see Table 10.7). The HWTD only correlates with the shear strength from direct shear tests on aggregates. The correlation is counterintuitive since one expects that with the increase in shear strength of aggregate skeleton, the rutting potential should decrease (not increase as reflected in Table 10.7). The IDT strength of the HMA seems to correlate well with the seismic and dynamic moduli, flow time, and to some extent to the triaxial strength of the aggregates. The seismic and dynamic moduli are well correlated. In general in most cases, the results from aggregate strength tests do not correlate to the results from HMA tests. In light of this analysis, the indirect tensile tests and the seismic modulus with the V-meter can be the two candidates to provide information about the strength and stiffness of the HMA.

CORRELATION OF TESTS WITH PERFORMANCE

Finally, the performance tests are correlated to the aggregate tests in Table 10.8 independent of the mix gradation (Superpave, CMHB and PFC). The goal of this correlation analysis is to determine which of the aggregate tests, rock tests, or shape and texture tests relate to the performance tests. The rut depth from HWTD is correlated well with the compressive strength of the rock (either measured directly or through the Schmidt hammer) and the shape and texture of the aggregates. Surprisingly, the correlation indicates that as the potential for crushing increases, the potential for rutting increases. This pattern is counterintuitive, perhaps due to limited data available.

The other HMA test results do not seem to be strongly correlated to any of the aggregate properties. Table 10.9, a correlation analysis between gradation and the performance tests, may shed some light on the reasons for this lack of correlation. As reflected in the Table, the results from all tests except the HWTD are well-correlated to the change in gradation. This implies that the results from different mixes (PFC, CMHB-C and Superpave-C) should be considered separately.

As an example, the results of correlation analysis for modulus of the mix with V-meter, one of the performance tests recommended in the previous section, is shown in Figure 10.10. A strong or reasonable correlation between the ACV test results and the modulus of the bulk rock with V-meter are obtained for all three mixes, despite the fact that the global relationship did not yield any correlation. Once again, this process will be followed as soon as the data from Phase II tests are obtained.

Table 10.6 - Results for Mixture Characterization Tests

Mixture	Aggregate Type	Rut Depth from HWDT, in.	Indirect Tensile Strength, psi	Seismic Modulus from V-Meter, ksi	Dynamic Modulus, ksi	Max. Strain from Flow Time, μ-in./in.	Strength from Triaxial Test, psi	Strength from Direct Shear Test, psi
CMHB-C	Hard Limestone	0.49	106	2826	909.4	4280	149	55
	Granite	0.30	83	2740	847	5100	186	44
	Soft Limestone	0.53	94	2662	663.6	5790	198	46
Superpave-C	Hard Limestone	0.40	120	2800	827	3980	241	45
	Granite	0.22	116	2276	693.8	3380	208	40
	Soft Limestone	0.52	125	2101	764.9	3980	226	45
PFC	Hard Limestone	--	39	1074	239	7020	--	50
	Granite	--	61	856	193	12980	--	43
	Soft Limestone	--	50	922	198	7780	--	48

Table 10.7 - Correlation Results for Mixture Characterization Tests

Test		HMA					Aggregate	
		Rut Depth from HWDT	Indirect Tensile Strength	Seismic Modulus from V-Meter	Dynamic Modulus	Max. Strain from Flow Time	Strength from Triaxial Test	Strength from Direct Shear Test-
HMA	HWDT	1.00						
	IDT- Tensile Strength	0.11	1.00					
	V-Meter	0.08	0.78	1.00				
	Dynamic Modulus	0.05	0.85	0.97	1.00			
	Flow Time	0.42	-0.71	-0.77	-0.81	1.00		
Aggregate	Triaxial- Strength	-0.09	0.56	-0.42	-0.43	-0.30	1.00	
	Direct Shear Test	**0.63**	-0.23	0.03	0.03	-0.07	**-0.68**	1.00

Note: values that are bold and underlined demonstrate high correlations that seem counterintuitive

Table 10.8 - Correlation Analysis between HMA Performance Tests and Aggregate Properties

Aggregate Parameters \ Performance Tests		Correlation Coefficients				
		Rut Depth from HWDT	Indirect Tensile Strength	Seismic Modulus from V-Meter	Dynamic Modulus	Max. Strain from Flow Time
Aggregate	ACV	0.28	0.01	-0.17	-0.17	0.11
	Compacting Modulus	-0.06	-0.01	0.18	0.17	-0.17
	Crushing Modulus	0.56	0.03	-0.14	-0.15	0.01
	Max. Compacting Stress	0.17	0.00	0.18	0.17	-0.23
	AIV-dry	-0.26	-0.01	-0.18	-0.16	0.25
	AIV-wet	-0.43	-0.01	-0.17	-0.15	0.27
	TFV	-0.77	-0.03	-0.12	-0.09	0.30
Rock	Compressive Strength	-0.93	-0.04	0.03	0.05	0.19
	Tensile Strength	-0.30	-0.02	0.17	0.17	-0.10
	Compressive Strength from Schmidt Hammer	-0.92	-0.04	0.04	0.06	0.18
	Seismic Modulus from V-meter	-0.02	0.00	0.18	0.17	-0.18
Shape and Texture	LA BIT	-0.53	-0.02	-0.16	-0.14	0.29
	MG BIT (HMAC)	0.47	0.02	-0.16	-0.16	0.05
	MG BIT (ST)	0.48	0.02	-0.15	-0.16	0.04
	PV	-0.70	-0.03	-0.13	-0.11	0.30
	MD BIT	0.76	0.03	-0.10	-0.12	-0.07
	CA AI	-0.91	-0.04	-0.06	-0.04	0.28
	MD	0.94	0.04	-0.03	-0.05	-0.20
	Texture BMD	-0.81	-0.03	0.09	0.10	0.10
	Texture AMD	-0.95	-0.04	0.01	0.03	0.22
	Angularity BMD	-0.95	-0.04	-0.03	0.00	0.25
	Angularity AMD	-0.93	-0.04	-0.05	-0.03	0.27

Table 10.9 - Correlation Analysis between HMA Performance Tests and Aggregate Gradation

Sieve No. (Percent Passing) \ Performance Tests	Rut Depth from HWDT	Indirect Tensile Strength	Seismic Modulus from V-Meter	Dynamic Modulus	Max. Strain from Flow Time
1/2"	-0.26	0.15	-0.39	-0.28	0.00
3/8"	-0.26	0.90	0.59	0.67	-0.72
#8	-0.26	0.94	0.69	0.77	-0.77
#200	0.26	0.80	0.97	0.96	-0.75

Table 10.10 - Correlation Analysis between HMA Modulus from V-meter and Aggregate Properties for Each Individual Mix

Aggregate Parameter		Correlation			
		Global	Superpave-C	CMHB-C	PFC
Aggregate	ACV	-0.17	-0.96	-1.00	-0.68
	Compacting Modulus	0.18	1.00	0.98	0.83
	Crushing Modulus	-0.14	-0.82	-0.94	-0.40
	Max. Compacting Stress	0.18	0.98	0.90	0.94
	AIV-dry	-0.18	-0.96	-0.85	-0.97
	AIV-wet	-0.17	-0.88	-0.74	-1.00
	TFV	-0.12	-0.58	-0.35	-0.92
Rock	Compressive Strength	0.03	0.23	0.46	-0.31
	Tensile Strength	0.17	0.95	1.00	0.66
	Compressive Strength from Schmidt Hammer	0.04	0.29	0.52	-0.25
	Seismic Modulus from V-meter	0.18	1.00	0.97	0.86
	Seismic Modulus from FFRC	0.17	1.00	1.00	1.00
Shape and Texture	Los Angeles Abrasion % Wt. Loss-Bituminous	-0.16	**-0.82**	**-0.65**	**-1.00**
	Mg Soundness Test- Bituminous	-0.16	-0.88	-0.97	-0.50
	Mg Soundness Test- Stone	-0.15	-0.87	-0.97	-0.50
	Polish Value	-0.13	**-0.66**	-0.45	**-0.95**
	Micro-Deval % Wt. Loss-Bituminous	-0.10	-0.62	-0.80	-0.12
	Fine Aggregate Acid Insolubility	-0.06	-0.27	-0.02	**-0.73**
	Micro-Deval % Wt. Loss- Stone	-0.03	-0.20	-0.44	0.33
	Texture Before Micro-Deval	0.09	0.55	0.74	0.04
	Texture After Micro-Deval	0.01	0.12	0.36	-0.41
	Angularity Before Micro-Deval	-0.03	-0.07	0.18	-0.58
	Angularity After Micro-Deval	-0.05	-0.21	0.04	**-0.69**

CHAPTER ELEVEN - CLOSURE AND RECOMMENDATIONS

SUMMARY

The performance of the new generation of HMA mixtures relying more on a stone-on-stone contact is greatly influenced by the properties of the aggregate blends such as gradation and strength. As a result, aggregates have a significant and direct effect on the performance of bituminous pavements and it is important to maximize the quality of aggregates to ensure a proper performance of roadways. Several methods are available to determine the aggregate characteristics but their relationship to filed performance, aggregate structure in HMA and traffic loading needs to be further investigated and defined.

The objective of this research is to evaluate the effect of stress concentrations at contact points on coarse aggregates that could cause aggregate fracture. The validation effort involved subjecting individual aggregates as well as HMA mixtures prepared with different aggregates to full-scale testing in order to correlate the performance of particles and blends to their respective characterization test methods.

CONCLUSIONS

Aggregates were ranked according to their performance when subjected to numerous characterization test methods. The ranking was based on three categories of tests (aggregate properties, rock properties, and shape and texture) in order to further understand the impact of each. From such ranking, the following conclusions were drawn:

- From the aggregate properties, the hard limestone clearly ranked as the best (ranking of 1), granite the second best and the soft limestone the worst.
- From the rock properties, the hard limestone and granite ranked similarly with the hard limestone being slightly better and the soft limestone ranked the worst.
- As per the traditional shape and texture tests, the granite is ranked higher than the hard limestone, with once again soft limestone being the worst.
- In general, from the 23 tests that were carried out on the aggregates and rock samples, the hard limestone ranked the best followed by the granite ranked second best and the soft limestone ranking the worst.

In order to determine which of the tests are the most representative for the characterization of the aggregates and mixtures, correlation analysis amongst the tests was performed. From this analysis, the following observations are provided:

- From the correlation analysis conducted on the tests characterizing the aggregate point and bulk strength results, the ACV test and its surrogate parameters were found to correlate well with most of the tests. As a result, the ACV test seems to be the most appropriate test for characterizing the aggregates, especially since several parameters can be readily determined from the same test and the cost of implementing this test in Districts owning a concrete compressive test machine would be insignificant.
- The compressive strength obtained using the Schmidt hammer seems to be the most appropriate test for characterizing this parameter. This test is not only easier and faster than the compressive strength test, but also eliminates the need for coring the rock and requires minimal training.
- The V-meter seems to be a great tool for estimating the modulus as well as the quality of the aggregates in tension. In addition, no coring is necessary to perform this test on the rock samples. Therefore, the V-meter is recommended over the FFRC.
- For the performance characterization of the mixtures the indirect tensile test and the modulus with the V-meter test seem to be the two test methods that best provide information about the strength and stiffness of the HMA.
- An approach for modeling the response of HMA bituminous was developed in this study. The aggregate properties (stiffness, compressive strength and tensile strength) were determined by matching the model results to experimental measurements conducted on aggregate samples. The model can be used to predict the mix response under different loading conditions. The results show that the failure in the soft limestone mixes occur primarily within the aggregate phase, while the failure in the mixes with the other two aggregates occur in the mastic phase. The model was used to investigate the stress or load distributions within the different mixes. The PFC mixes are shown to have more localized high stresses within the aggregates than the Superpave and CMHB mixes. This finding indicates that aggregates with higher resistance to fracture need to be used in PFC mixes. The current model uses average aggregate properties. We are currently working on modifying the model to include the distribution of aggregate properties, which will provide more realistic representation of the mix behavior.

In general, the tests proposed on aggregates and rock specimens are rather simple, for the most part low-cost, and simple to perform.

RECOMMENDATIONS

It should be emphasized that these observations are preliminary since the database is rather small. As a result, it is proposed to further study these tests in the second phase where more materials will be tested. Phase II of this project will contain a more comprehensive database that can be used for drawing more concrete conclusions.

In addition, more consideration should be given to the selection process in terms of cost, test time, and impact on TxDOT operation at the end of Phase II of the project.

REFERENCE

1. Abbas, A. R. (2004), "Simulation of the Micromechanical Behavior of Asphaltic Mixtures Using the Discrete Element Method," PhD Dissertation, Washington State University.
2. Aho, B.D., W.R. Vavrik, and S.H. Carpenter (2001), "Effect of Flat and Elongated Coarse Aggregate on Field Compaction of Hot-Mix Asphalt," Transportation Research Record 1761, Transportation Research Board, National Research Council, Washington, DC; pp. 26–31.
3. Al-Rousan, T. M. (2004), "Characterization of aggregate shape properties using a computer automated system," PhD Dissertation, Texas A&M University, College Station, Tex.
4. Brown, E. M, and M. S. Buchanan (2001), "Literature Review: Verification of Gyration Levels in the Superpave Ndesign Table," NCHRP Web Document 34, Transportation Research Board, National Research Council, Washington, DC
5. Brown, E.R, and J.E. Haddock (1997), "A Method to Ensure Stone-on-Stone Contact in Stone Matrix Asphalt Paving Mixtures," National Center for Asphalt Technology, Auburn University. NCAT Report No. 97-2.
6. Chandan, C., Sivakumar, K., Masad, E., and Fletcher, T. (2004), "Application of imaging techniques to geometry analysis of aggregate particles," Journal of computing in civil engineering, 75-82.
7. Cheng, Yi P. H. (2004), "Micromechanical investigation of soil plasticity," PhD Dissertation, Churchill College, University of Cambridge.
8. Cheung, L.W, and A.R. Dawson (2002), "Effects of Particle and Mix Characteristics on Performance of Some Granular Materials," Transportation Research Record 1787, Transportation Research Board, National Research Council, Washington, DC; pp. 90-98.
9. Chowdhury, A., J.W. Button, and J.D. Grau (2001), "Effects of Superpave Restricted Zone on Permanent Deformation," Research Report ICAR 201-2, International Center for Aggregate Research, College Station, TX.
10. Cooley, L. Jr., and James, R. (2003), "Micro-Deval testing of aggregates in the southeast," Transportation Research Record 1837, Transportation Research Board, Washington, D.C., 73-79.
11. Cundall, P. A. (1971), "A Computer Model for Simulating Progressive Large Scale Movements in Blocky Rock Systems," in Proceedings of the Symposium of the International Society of Rock Mechanics (Nancy, France, 1971), Vol. 1, Paper No. II-8.
12. Cundall, P. A., and R. Hart (1992), "Numerical Modeling of Discontinua," J. Engr. Comp., 9, 101-113.

13. Cundall, P. A., and O. D. L. Strack (1979), "A Discrete Numerical Model for Granular Assemblies," Geotechnique, 29(1), 47-65.
14. Hand, A.J., J.L. Stiady, T.D. White, A.S. Noureldin, and K. Galal (2002),"Gradation Effects on Hot-Mix Asphalt Performance," Association of Asphalt Paving Technologists, Vol. 70, pp. 132-175.
15. Holmgeirsdottir, T., and P.R. Thomas (1998), "Use of the D-762 Shore Hardness Scleroscope for Testing Small Rock Volumes," International Journal of Rock Mechanics and Mining Sciences, Vol. 35, No.1, pp. 85-89.
16. Hobbs, B.F. (1980), "A Comparison of Weighting Methods in Power Plant Citing," Decision Sciences 11, pp. 725-737.
17. Hwang, C.L., and K. Yoon (1981), "Multiple Attribute Decision Making: Methods and Applications," Berlin/Heidelberg/New York: Springer-Verlag.
18. Gilson Company website, http://www.globalgilson.com/
19. Kandhal, P.S., and L.A. Cooley, Jr. (2001), "The Restricted Zone in the Superpave Aggregate Gradation Specification," NCHRP Report 464, Transportation Research Board, National Research Council, Washington, DC.
20. Kandhal, P.S., J.B. Motter, and M.A. Khatri (1991), "Evaluation of Particle Shape and Texture: Manufactured Versus Natural Sands," Transportation Research Record 1301, Transportation Research Board, National Research Council, Washington, DC, pp. 48–56.
21. Karakouzian, M. (1996), "Performance of Hot Mix Asphalt Using Coarse and Skip Graded Aggregates," Journal of Materials in Civil Engineering, Vol. 8, No. 2, pp. 101-107.
22. Mahmoud, E. M. (2005), "Development of Experimental Methods for The Evaluation of Aggregate Resistance to Polishing, Abrasion, and Breakage," Master of Science Thesis, Texas A&M University, College Station, Tex.
23. Masad E., J.W. Button, and T. Papagiannakis (2000), "Fine-Aggregate Angularity: Automated Image Analysis Approach," Transportation Research Record 1721, Transportation Research Board, National Research Council, Washington, DC; pp. 66-73.
24. Masad, E., D. N. Little, L. Tashman, S. Saadeh, T. Al-Rousan, and R. Sukhwani (2003), "Evaluation of Aggregate Characteristics Affecting HMA Concrete Performance," Research Report ICAR 203-1, The Aggregate Foundation of Technology, Research, and Education, Arlington, VA.
25. Masad, E. (2004), "X-Ray Computed Tomography of Aggregates and Asphalt Mixes," in Materials Evaluations Journal, Vol. 62, No. 7, 2004, pp.775 – 783.
26. Meininger, R. (2004), "Micro-Deval vs. L.A. Abrasion," Rock Products 107, 33-35.
27. McDowell, G. R., and O. Harireche (2002), "Discrete Element Modeling of Soil Particle Fracture," Geotechnique 52, No 2, pp 131-135.
28. Öztas, T., K. Sönmez, and M.Y. Canbolat (1999), "Strength of Individual Soil Aggregates Against Crushing Forces. I. Influence of Aggregate Characteristics," Journal of Agriculture and Forestry, Vol. 23; pp. 567-57.
29. Prowell, B.D., J. Zhang., and E.R. Brown (2005), "Aggregate Properties and the Performance of Superpave Designed Hot Mix Asphalt," NCHRP Report 539, Transportation Research Board, National Research Council, Washington, DC.
30. Rogers, C.A., M.L. Bailey, and B. Price (1991), "Micro-Deval Test for Evaluating the Quality of Fine Aggregate for Concrete and Asphalt," Transportation Research Record 1301, Transportation Research Board, National Research Council, Washington, DC; pp. 68–76.

31. Rogers, C. (1998), "Canadian experience with the Micro-Deval test for aggregates," Advances in Aggregates and Armourstone Evaluation 13, 139-147.
32. Schmiedlin, R.B., and D.L. Bischoff (2002), "Stone Matrix Asphalt the Wisconsin Experience," Transportation Research Record. 1616; Transportation Research Board, National Research Council, Washington, DC; pp. 34-41.
33. Senior, S.A., and C.A. Rogers (1991), "Laboratory Tests for Predicting Coarse Aggregate Performance in Ontario," Transportation Research Record 1301, Transportation Research Board, National Research Council, Washington, DC; pp. 97–106.
34. Vallejo, L.E, and Z. Chik (2002), "The Evolution of Crushing in Granular Materials and its Effect on their Mechanical Properties," Section 2: Infrastructure and Mobility, National Science Foundation, Pittsburgh, PA.
35. Vavrik, W.R, S.H. Carpenter (1998), "Calculating Air Voids at Specified Number of Gyrations in Superpave Gyratory Compactor," Transportation Research Record 1630, Transportation Record Board, National Research Council, Washington, D.C., 1998, pp. 117-125.
36. Wang, L.B., and L.N. Mohammad (2003), "Quantification of Morphology Characteristics of Aggregate Profile Images," Preprint: Papers Presented at the 82nd Annual Meeting of the Transportation Research Board, Washington, DC.
37. West, R.C., and R. S. James (2005), "Determining Ndesign for SMA Mixtures in Alabama," NCAT Report No. 05-xx, Alabama Department of Transportation, Auburn University, AL.
38. Wilson, J.D., and L.D. Klotz (1996), "Quantitative Analysis of Aggregate Based on Hough Transform," Transportation Research Record 1530, Transportation Research Board, National Research Council, Washington, DC; pp. 111–115.
39. Wu, Y., F. Parker, and P.S. Kandhal (1998), "Aggregate Toughness/Abrasion Resistance and Durability/Soundness Tests Related to Asphalt Concrete Performance in Pavements," Transportation Research Record 1638, Transportation Research Board, National Research Council, Washington, DC. pp. 85–93.
40. Wylde, L.J. (1976), "Degradation of Road Aggregates," Australian Road Research, Vol. 6, No. 1, pp. 22-29.
41. Yiping, W., F. Parker, and K. Kandhal (1998), "Aggregate Toughness/Abrasion Resistance and Durability/Soundness Tests Related to Asphalt Concrete Performance in Pavements," NCAT Report No. 98-4, National Center for Asphalt Technology, Highway Research Center, Auburn University, AL.